Biochimica et Biophysica Acta, 1057 (1991) 1–41

ADONIS 000527289100082N

BBABIO 43340

The chlorophyll triplet state as a probe of structure and function in photosynthesis

David E. Budil [1] and Marion C. Thurnauer [2]

[1] *Baker Laboratory of Chemistry, Cornell University, Ithaca, NY 14850 (U.S.A.) and* [2] *Chemistry Division, Argonne National Laboratory, Argonne, IL 60439 (U.S.A.)*

(Received 22 August 1990)

Key words: Chlorophyll; Triplet state; Photosynthesis

Contents

Correspondence: M.C. Thurnauer, Chemistry Division, Argonne National Laboratory, Argonne, IL 60439, U.S.A.

I. Introduction

Since the first observation of a photoexcited molecular triplet state by electron paramagnetic resonance (EPR) 30 years ago [1], the triplet state * has provided an important tool for investigating molecular structure and dynamics in a wide diversity of photochemical systems. Perhaps nowhere is its utility better illustrated than by the central role triplet state studies have played in the elucidation of structure and dynamics in photosynthesis. Photosynthetic systems are eminently suited for such studies by virtue of their extremely efficient photochemistry and the nature of the organic dye molecules which carry out the reactions. In addition, the unique photochemical properties of such systems have made them in many ways an ideal proving ground for new experimental approaches to magnetic resonance.

The intense research effort in photosynthesis shows no signs of abating, despite recent major breakthroughs in the field. Indeed, the availability of single protein crystals of the bacterial photosynthetic apparatus [2,3] and the structural details provided by X-ray crystallography [4–9] has stimulated interest in many new types of triplet investigation that would have been impossible only a few years ago. The advent of single crystals thus marks a new stage in the investigation of triplet states in photosynthesis.

In this review, we have tried to emphasize work on the triplet state of chlorophyll (^{3}Chl) in photosynthetic and related systems which has appeared since previous reviews were published, and to demonstrate the impact that the newly available crystal structure has had on many of these studies. Although we have aimed at completeness, it is an impossible task to include all the studies in this very active field, particularly since there are relevant publications appearing as this is being written.

* In general, when we discuss 'the triplet state' of a molecule, we mean the first, or lowest, excited triplet state.

I-A. The light reactions of photosynthesis

The basic light reaction of photosynthesis, in which light energy is converted into useful chemical energy, is formally the same in all photosynthetic organisms, which include some bacteria, algae, and green plants. Photosynthetic cells contain a complement of light-harvesting or 'antenna' pigments consisting mainly of some form of chlorophyll (Chl) or bacteriochlorophyll (BChl) bound to proteins associated with the photosynthetic membrane. The absorption of a quantum of light by these pigments creates an electronic excited state that migrates among the antenna chlorophylls until it is trapped by a specialized Chl species contained in a membrane-spanning pigment-protein complex called the reaction center (RC). The primary light reaction is an electron transfer from the excited special Chl (the 'primary electron donor' which we will denote generically by P) to a nearby electron acceptor in the RC. Secondary electron transfer reactions that re-reduce P and re-oxidize the primary acceptor then prevent recombination of the closely spaced charges. Once charge separation across the photosynthetic membrane is stabilized, the cell can use the resultant electrical and chemical potential to drive its metabolic processes.

The specific nature of the RC, the primary donor, and the associated secondary electron transport chains differ among photosynthetic organisms. In oxygenic plants and algae, two RCs known as Photosystems I and II (PS I and PS II) are required to mediate electron transfer from water to nicotinamide adenine dinucleotide phosphate, which is the source of the reducing equivalents needed for carbon fixation and other biosynthesis. Bacteria cannot use water as an electron donor, depending instead upon reduced organic substrates or sulfur compounds as a source of reduction equivalents.

Historically, bacterial photosynthesis has served as a model for the more complicated plant and algae systems. The bacterial RC protein was isolated [10], purified [11] and thoroughly characterized [12] a number of years ago; more recently, bacterial RCs from three

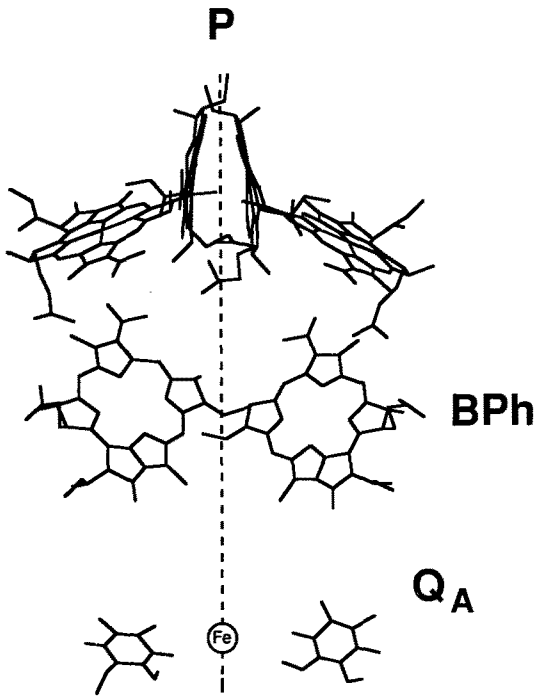

Fig. 1. Pigment structure in the reaction center of *Rb. sphaeroides* R-26. P is the primary electron donor, a dimer of bacteriochlorophyll *a* molecules; BPh is the bacteriopheopytin that serves as primary electron acceptor; Q_A is the secondary electron acceptor, ubiquinone. The dashed line indicates the axis of approximate C_2 symmetry in the structure. Pigments associated with the L-protein appear on the right side of the figure, excepting the L bacteriochlorophyll of the primary donor.

organisms, *Rhodopseudomonas viridis*, and the 2.4.1 and R-26 strains of *Rhodobacter sphaeroides*, have been crystallized [2,3,13] and their electron density maps obtained by X-ray crystallography [4,5,7,14]. A simplified depiction of the structure of the RC pigment molecules revealed in the electron density map is shown in Fig. 1.

The photochemical reactions of the bacterial RC are also the best characterized. Primary electron transfer proceeds from the top to the bottom of Fig. 1, separating charges across the photosynthetic membrane in which the RC is implanted. The primary electron donor P appears as the BChl dimer in the center of the figure. The photoexcited dimer transfers an electron to bacteriopheophytin (BPh) within a few picoseconds [15–17]. Within about 200 ps at room temperature [18,19] the electron is transferred from BPh to a quinone acceptor (denoted Q), the exact identity of which is species-dependent.

The RC pigment structure possesses close to C_2 symmetry about the axis indicated in the figure, including the two halves of the P dimer. Each half of the structure is primarily associated with one of the RC protein subunits; the subunits themselves, called L and M, possess a considerable degree of amino acid sequence homology [20–23] and are quite symmetric in their tertiary structure [4,5]. Surprisingly, stable electron transfer appears to occur along only one of the two acceptor 'chains' appearing in Fig. 1, those pigments primarily associated with the L subunit [6,24,25]. This is frequently referred to as the 'L-chain', despite the fact that Q_A is actually bound to the M subunit; many authors have taken to calling it the 'A-chain' in order to avoid this ambiguity. The active chain appears on the right hand side of Fig. 1, with the exception of the L half of the primary donor, which is at the upper left.

I-B. The chlorophyll triplet state in photosynthesis

Triplet states, first observed by EPR in bacterial RCs over a decade ago [26] and somewhat later in higher plants [27,28], appear when electron transfer to secondary acceptors is 'blocked' by lowering the redox potential of the medium, thus pre-reducing the secondary electron acceptors. Despite initial speculation that the observed triplets were a trapped intermediate of the charge separation process [29–33], it is now clear that they appear instead as side products of photoexcitation in RCs where secondary electron transfer has been blocked.

Nevertheless, the properties of chlorophyll triplet states render them ideal probes of the working photochemistry in RCs. Chlorophylls can be photoexcited into the triplet state either as isolated chemical species in vitro, or as the specialized form in which they perform their photosynthetic function in vivo. Thus, a principal strategy for investigating photosynthetic systems has been to compare the spectroscopic properties of chlorophyll triplets in a controlled medium with those of triplets in vivo. For a more detailed description of the early work on this topic, the reader is referred to several reviews on the subject [34–40].

II. Characterization of the chlorophyll triplet state

The triplet states of chlorophylls have been extensively characterized theoretically, and all of the concepts needed to interpret comparative spectroscopy of chlorophylls in vitro and in vivo have been presented in EPR textbooks and previous reviews. Here we have attempted to assemble the most relevant physical descriptions in one place as a useful reference. Because of our emphasis on triplet magnetic properties we will not discuss the vibrational states of chlorophylls in any depth, although such considerations are likely to be relevant to more detailed magnetic resonance investigations of triplet photochemistry in the future. The molecular framework and axis systems of several relevant chlorophyll pigments are given in Fig. 2.

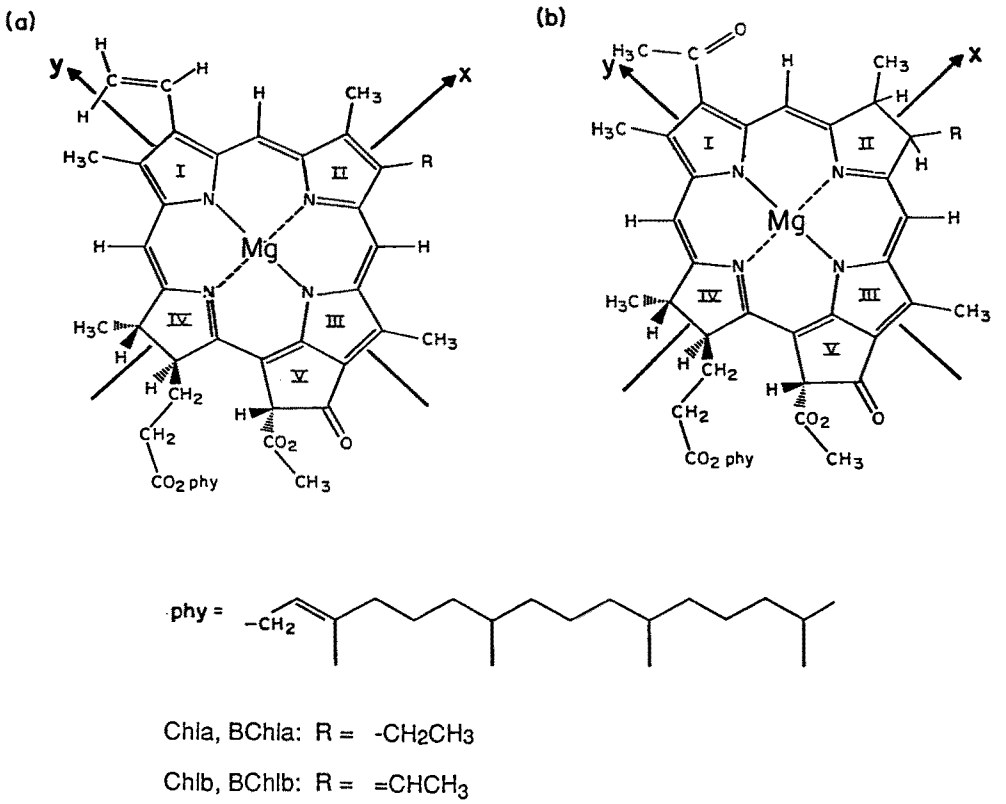

Fig. 2. Molecular structure of (a) chlorophyll *a* and *b* and (b) bacteriochlorophyll *a* and *b*. The axes marked x and y are the approximate directions of the Q_x and Q_y electronic transition dipoles, and also approximately the x and y zero-field axes of the triplet state (see text).

II-A. Monomeric chlorophyll triplets

II-A.1. Electronic states

The electronic structure of chlorophylls has been the subject of considerable theoretical investigation, reviews of which may be found in Refs. 41–45. The general approach has been to start from the simpler, symmetric porphin molecule [46] and describe chlorophyll molecular orbitals (MOs) in terms of deviations from the underlying symmetry. A simple but very useful treatment is the four-orbital model of Gouterman [46], which focuses on the two highest occupied molecular orbitals (HOMOs) and two lowest unoccupied molecular orbitals (LUMOs) earlier calculated by the extended Hückel method [47]. Particular strengths of this model are its success in modeling the visible and near-infrared spectral regions and its useful qualitative description of ring reduction and substituent effects in chlorophylls.

Fig. 3 shows the spatial distributions of the HOMOs, designated b_1 and b_2, and the LUMOs (c_1 and c_2) of the porphin molecule. The lowest-lying excited states are represented as linear combinations of the four singly excited configurations, $|b_1c_1\rangle$, $|b_2c_2\rangle$, $|b_1c_2\rangle$, and $|b_2c_1\rangle$. For a molecule with perfect D_{4h} symmetry, the electric dipole for the transition to each configuration lies along the x or y symmetry axis shown in Fig. 3. Mixing is forbidden between configurations corresponding to the *x*-polarized ($|b_1c_2\rangle$ and $|b_2c_1\rangle$) and those corresponding to the *y*-polarized ($|b_1c_1\rangle$, $|b_2c_2\rangle$) transitions, but the two pairs of configurations with like polarization are mixed to produce two excited states called B and Q, as depicted in the energy level diagram in Fig. 4.

Gouterman postulated that the b_1 and b_2 orbitals are accidentally nearly degenerate in porphin, which, together with the symmetry degeneracy of c_1 and c_2, produces four excited configurations of equal energy [46]. For this case, depicted in Fig. 4a, $B_{x,y}$ and $Q_{x,y}$ are symmetric and antisymmetric combinations of the *x*- and *y*-polarized basis states, and transitions to the lower-lying Q states have zero intensity. The reduction of ring IV in Chl breaks the degeneracies by destabilizing c_1 and b_2, which confers intensity upon transitions to the Q states and increases the splitting between B_y and Q_y, as shown in the energy level diagrams in Fig. 4b. The ring II reduction in BChl further destabilizes c_1 and b_2, leading to an additional shift of the transition to the Q_y state.

According to this simple picture, the Q_x and Q_y transition moments should lie exactly along the symmetry axes in Chl and BChl. To account for asymmetric ring reductions and substituents, more recent calculations have abandoned the early cyclic polyene-extended Hückel approach in favor of semiempirical Pariser-

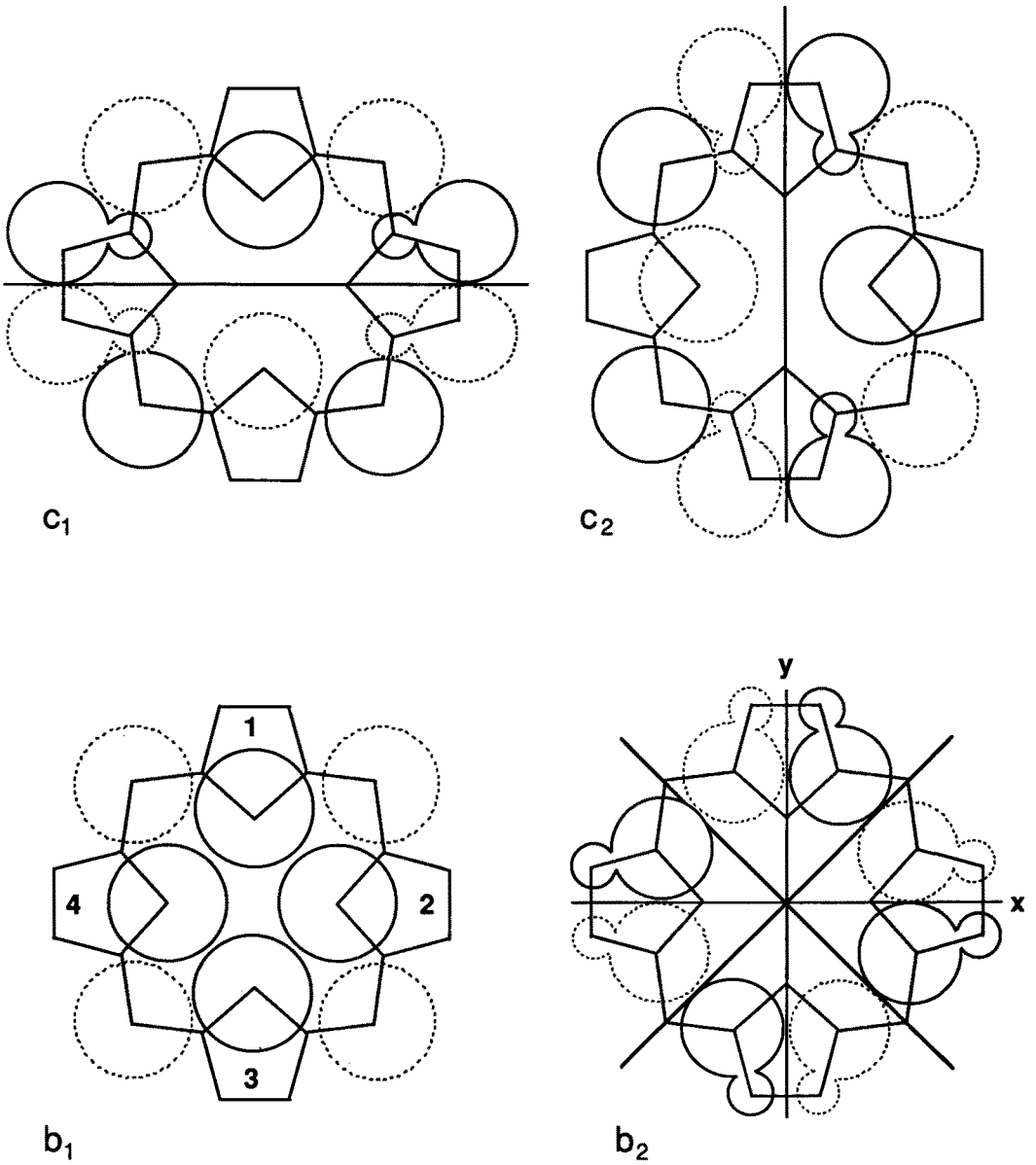

Fig. 3. Electronic distribution of the two LUMOs (c_1 and c_2) and two HOMOs (b_1 and b_2) of porphin in the four-orbital model of Gouterman, showing the directions of x- and y- polarized electronic transitions. Shaded lines indicate negative sign.

Parr-Pople [48,49] and ab initio CNDO calculations [50–52]. When these effects are included, the calculated transition moments [42,49,51–53] do deviate from the x and y directions shown in Fig. 2; however, the difference is usually less than 10°, which is consistent with the experimentally determined Q_y transition of chlorophyllide *a* [54]. Significantly, the more sophisticated calculations have borne out the qualitative four-orbital model for many of the lower excited states of Chl and BChl, which are the states most relevant to their photochemistry.

Different types of calculation are reasonably consistent with regard to the lowest excited triplet states. The lowest excited (T_1) state of both Chl *a* [42,51] and BChl *a* [42,52] consist mainly of the x-polarized $|b_2c_2\rangle$ configuration, while the next highest triplet state (T_2) is primarily a combination of the y-polarized $|b_1c_2\rangle$ and $|b_2c_1\rangle$ configurations. Since the two lowest triplet states appear to consist predominantly of 'four-orbital' configurations, one might reasonably expect their physical properties to be related to the approximate symmetry axes of these configurations, i.e. the x and y axes shown in Fig. 2. We will adopt this axis system and nomenclature as a starting point for a discussion of triplet state properties, bearing in mind that the 'true' triplet axes may depart from this definition owing to deviation of

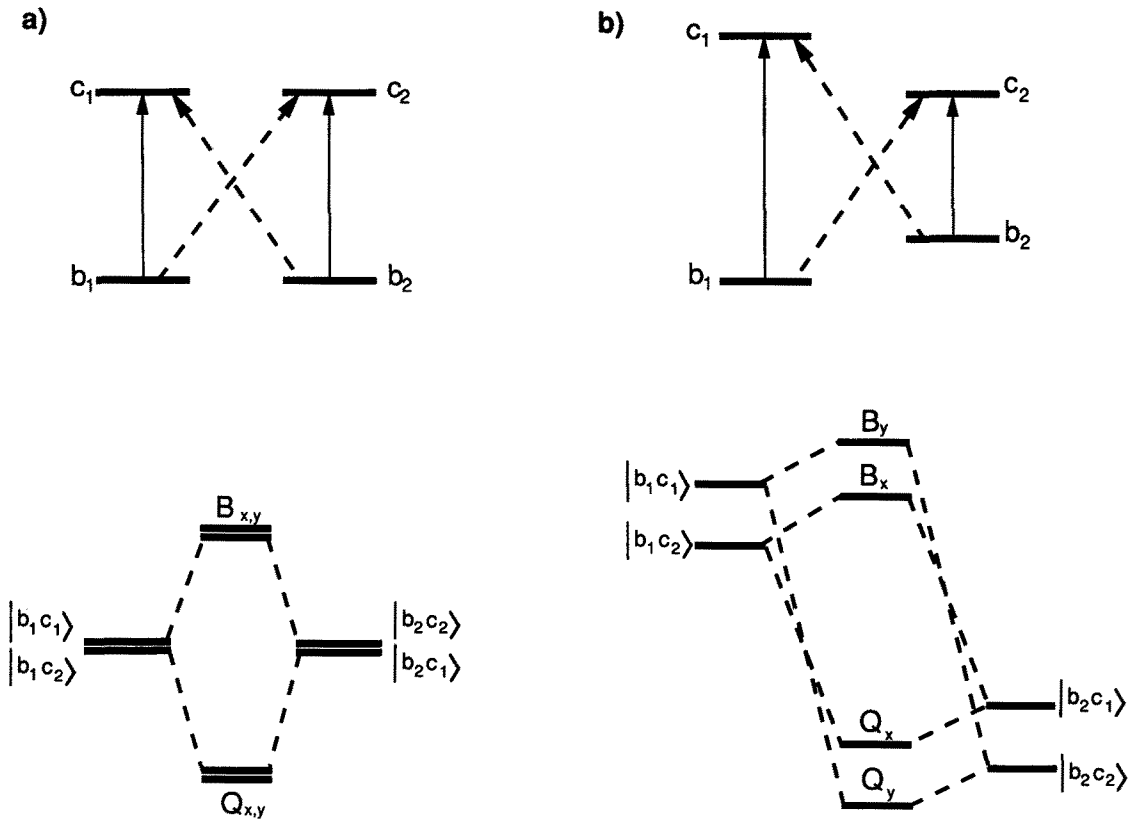

Fig. 4. Mixing of the 'four-orbital' configurations for (a) porphin- and (b) dihydroporphin-like molecules. Upper figures indicate the x-polarized $|b_1c_2\rangle$ and $|b_2c_1\rangle$ configurations (dashed lines) and the y-polarized $|b_1c_1\rangle$ and $|b_2c_2\rangle$ configurations. Lower energy level diagrams illustrate mixing between configurations of like polarization and energies of the resultant excited states.

the chlorophyll 'four orbitals' from rigorous symmetry, as well as other contributions to the excited triplet states.

II-A.2. Spin states

The photochemical behavior of the triplet state is largely dictated by its net electronic spin angular momentum $S = 1$ (in units of $\hbar$). The precise nature of the three associated electron spin sublevels depends upon the magnetic environment of the triplet state. In the absence of an applied magnetic field, the dominant energy term is a magnetic dipolar interaction between the two unpaired spins. * This energy may be described by the spin Hamiltonian

$$\mathbf{H}_D = \mathbf{S}\cdot\mathbf{D}\cdot\mathbf{S} \tag{1}$$

where **S** is the total spin angular momentum operator, and **D** is a tensor describing the angular dependence of the dipolar interaction relative to a molecular frame of reference in which **D** is diagonal. In this reference frame, H_D can be written

$$\mathbf{H}_D = -\left(XS_x^2 + YS_y^2 + ZS_z^2\right) \tag{2}$$

which has three eigenstates, $|t_x\rangle$, $|t_y\rangle$, and $|t_z\rangle$, with energies X, Y and Z. Because $\mathrm{Tr}\{\mathbf{D}\} = -(X+Y+Z) = 0$, the zero-field energies may be expressed in terms of only two quantities, the zero-field splitting (ZFS) parameters D and E:

$$D = -\tfrac{3}{2}Z,$$

$$E = -\tfrac{1}{2}(X-Y) \tag{3}$$

The three zero-field states have their electron spin quantized along the respective principal axes of **D** with zero net spin angular momentum projection on the corresponding axis. Consequently, for a given zero-field state, say $|t_x\rangle$, the spin is constrained to lie in a plane defined by the other two axes, **y** and **z** [55]. We will refer to this axis system as the 'zero-field' axes of the triplet state.

The precise location of the zero-field axes relative to the molecular frame of Chl is not well known. The **z**

* For chlorophylls and porphyrins substituted with a heavy metal, spin-orbit interactions may also have a significant influence on the zero-field spin state energies. This discussion is valid for organic triplet molecules and the Mg-containing chlorphylls found in nature.

axis can be taken as the normal to the molecular plane, a well-established result for planar aromatic organic triplets [56]. The approximate symmetry axes of the spatial wave function of T_1 (x and y in Fig. 2) are reasonable estimates for the directions of the zero-field axes. This assumption has the advantage of maintaining consistency with the optical transition nomenclature; more importantly, it is supported by careful calculations of the dipolar tensor for porphyrin analogues [57,58] and there is abundant evidence from magnetophotoselection studies that in-plane zero-field axes correspond within at least 30° to the optical transition dipoles [59]. Most recently, single crystal triplet studies of bacterial RCs [60–63] offer the strongest experimental evidence for this assignment of zero-field axes, as will be discussed in Section IV.

In an applied magnetic field $\mathbf{B}_0$, the electronic spin Hamiltonian includes the Zeeman interaction:

$$\mathbf{H} = \mathbf{S}\cdot\mathbf{D}\cdot\mathbf{S} + g\beta_e\mathbf{S}\cdot\mathbf{B}_0 \tag{4}$$

where β_e is the Bohr magneton, and g is the g-factor of the triplet electrons, which is nearly orientation-independent for ^{3}Chl at conventional EPR fields. When $g\beta_e B_0$ is much larger than the ZFS parameters, the electron spins are quantized along the field direction into the states $|t_{+1}\rangle$, $|t_0\rangle$, and $|t_{-1}\rangle$. These are simply the eigenfunctions of the total spin $\mathbf{S}^2$ and $\mathbf{S}_z$ operators, with the subscripts referring to the m_s quantum number of the $\mathbf{S}_z$ projection along $\mathbf{B}_0$. If the orientation of $\mathbf{B}_0$ in the zero-field frame is specified by the polar angles (θ, ϕ), the transformation between the low-field and the first-order high-field triplet spin states is the matrix

$$\begin{array}{c} \\ \langle t_{+1}| \\ \langle t_0| \\ \langle t_{-1}| \end{array} \begin{array}{c} \begin{array}{ccc} |t_x\rangle & |t_y\rangle & |t_z\rangle \end{array} \\ \begin{pmatrix} 2^{-1/2}(-\cos\theta\cos\phi + i\sin\phi) & 2^{-1/2}(\cos\theta\sin\phi + i\cos\phi) & -2^{-1/2}\sin\theta \\ -\sin\theta\cos\phi & \sin\theta\sin\phi & \cos\theta \\ -2^{-1/2}(\cos\theta\cos\phi + i\sin\phi) & 2^{-1/2}(-\cos\theta\sin\phi + i\cos\phi) & 2^{-1/2}\sin\theta \end{pmatrix} \end{array} \tag{5}$$

The first-order energies of $|t_{+1}\rangle$, $|t_0\rangle$, and $|t_{-1}\rangle$ are $g\beta B_0 + D_{zz}/2$, $-D_{zz}$, and $-g\beta B_0 + D_{zz}/2$, respectively, where

$$D_{zz} = \frac{D}{3}(3l_z^2 - 1) + E(l_x^2 - l_y^2) \tag{6}$$

and

$$\begin{aligned} l_x &= \sin\theta\cos\phi \\ l_y &= \sin\theta\sin\phi \\ l_z &= \cos\theta \end{aligned} \tag{7}$$

are the direction cosines of $\mathbf{B}_0$ in the zero-field frame. Eqn. 6 provides an adequate description of the ^{3}Chl EPR spectrum at conventional spectrometer fields ($B_0 \sim 3200$ G) where the high-field approximation $|D| \ll g\beta_e B_0$ applies and g-anisotropy is insignificant.

A final important magnetic characteristic of the electron spins is their hyperfine interaction (HFI) with the magnetic nuclei of the Chl macrocycle, particularly ^{1}H, ^{13}C, ^{14}N, and ^{15}N. The HFI is represented by the Hamiltonian

$$\mathbf{H}_{hfi} = \sum_k \mathbf{S}\cdot\mathbf{A}_k\cdot\mathbf{I}_k \tag{8}$$

where the sum is taken over the nuclear spins $\mathbf{I}_k$. The HFI tensors $\mathbf{A}_k$ contain a contribution from the electronic-nuclear dipolar interaction; however, unlike the $\mathbf{D}$ tensor, the $\mathbf{A}_k$ have a nonzero trace that provides information about the electronic spin density at the kth nucleus. Thus, both of these interactions reflect the physical disposition of the electrons in the triplet state.

II-A.3. Spin sublevel kinetics

The electron spins of the triplet state profoundly affects its photochemical behavior, since intersystem crossing (ISC) between the paramagnetic triplet and its diamagnetic precursors or reaction products requires a spin state transition. The most usual mechanisms of ISC in organic triplets involve coupling between the electronic spin and orbital angular momenta [64]. Since the electronic orbital angular momentum is defined relative to the molecular frame, this type of ISC is selective with respect to the zero-field spin states; each spin state will in general have a separate rate of formation or decay. The rate expression for ISC can be written using the 'golden rule' [64]; for example, for ISC to the ground state,

$$k_\mu^{decay} = \frac{2\pi}{\hbar}|\langle\psi_T t_\mu|\mathbf{H}_{ISC}|\psi_S s\rangle|^2\rho(\Delta E) \tag{9}$$

where ψ_S and ψ_T are the spatial MOs of the ground state singlet and lowest triplet, $|s\rangle$ is the singlet spin state, $\mathbf{H}_{ISC}$ represents the perturbation promoting the transition, and $\rho(\Delta E)$ is the density of final states, for $\mu = x, y, z$. Eqn. 9 refers to triplet decay to the ground state; however, a similar expression may be used for the rates of triplet formation from S_1. In fact, the ordering of the relative population rates for each of the spin sublevels generally reflects the ordering of their decay rates to the ground state in monomeric ^{3}Chl [65].

In many planar organic molecules, including Chl, direct spin-orbit coupling between the lowest triplet and nearby singlet states is effectively orbital symmetry-forbidden. Instead, ISC proceeds via a combination of spin-orbit interaction and vibrational coupling in both the singlet and triplet manifolds [66–68]. The standard

theoretical treatment of this mechanism is to construct a Herzberg-Teller expansion of $\mathbf{H}_{ISC}$ in terms of a perturbation in the nuclear coordinates of the electronic states [69] *. $\mathbf{H}_{ISC}$ may then be divided into three contributions, corresponding to different orders of the expansion:

$$\mathbf{H}_{ISC} = \mathbf{H}^{(1)}_{ISC} + \mathbf{H}^{(2)}_{ISC} + \mathbf{H}^{(3)}_{ISC} \tag{10}$$

where $\mathbf{H}^{(1)}_{ISC}$ is the direct spin-orbit coupling, $\mathbf{H}^{(2)}_{ISC}$ represents the Herzberg-Teller spin-vibronic coupling, and $\mathbf{H}^{(3)}_{ISC}$ is a second-order term involving vibronic coupling of the lowest triplet and singlet states to higher triplet and singlet states that are themselves coupled by a direct spin-orbit interaction.

The general features of ISC in Chl can be understood by considering the direct spin-orbit interaction, $\mathbf{H}^{(1)}_{ISC} \equiv \mathbf{H}_{SO}$. For large molecules, we can make the simplifying assumption that only one-center terms are important, so that $\mathbf{H}_{SO}$ may be written as a sum over the k participating atomic orbitals,

$$\mathbf{H}_{SO} = \sum_k \zeta_k \mathbf{L}_k \cdot \mathbf{S}^{(-)} = \sum_k \zeta_k \left(L_{kx} S_x^{(-)} + L_{ky} S_y^{(-)} + L_{kz} S_z^{(-)} \right) \tag{11}$$

Here $\mathbf{L}_k$ is the angular momentum operator defined around atom k with a coupling strength ζ_k, and $\mathbf{S}^{(-)} \equiv \mathbf{S}_1 - \mathbf{S}_2$ so that the $\mathbf{L}_k \cdot \mathbf{S}^{(-)}$ component of the total $\mathbf{L}_k \cdot \mathbf{S}$ operator is antisymmetric with respect to interchange of the two electron spins, permitting singlet-triplet mixing. Since ψ_T is a π orbital consisting mainly of $|\, p_z\rangle$ contributions, we will consider only the individual atomic $|\, p_{kz}\rangle$ orbitals. Then, using the relations [64]

$$\begin{aligned} L_{kx} |\, p_{kz}\rangle &= -i |\, p_{ky}\rangle \\ L_{ky} |\, p_{kz}\rangle &= i |\, p_{kx}\rangle \\ L_{kz} |\, p_{kz}\rangle &= 0 \end{aligned} \tag{12}$$

and

$$\begin{aligned} \mathbf{S}_x^{(-)} |\, t_x\rangle &= 2^{-\frac{1}{2}} |\, s\rangle \\ \mathbf{S}_x^{(-)} |\, t_y\rangle &= \mathbf{S}_x^{(-)} |\, t_z\rangle = 0 \textit{ et cycl.} \end{aligned} \tag{13}$$

it can be shown all $\mathbf{H}_{SO}$ matrix elements vanish except those of the form

$$\begin{aligned} &\langle p_{ky} s |\, \zeta_k L_{kx} S_x^{(-)} |\, p_{kz} t_x \rangle \\ &\langle p_{kx} s |\, \zeta_k L_{ky} S_y^{(-)} |\, p_{kz} t_y \rangle \end{aligned} \tag{14}$$

The relation $L_{kz} \; |\, p_{kz}\rangle = 0$ eliminates all matrix elements connecting $|\, t_z\rangle$ directly with $\pi\pi^*$ singlet states, so that ISC from $|\, t_z\rangle$ must proceed via second-order vibronic coupling with higher states having $|\, p_{kx}\rangle$ and $|\, p_{ky}\rangle$ character; in other words, ISC from $|\, t_z\rangle$ requires the higher-order term $\mathbf{H}^{(3)}_{ISC}$. In contrast, the $|\, t_x\rangle$ and $|\, t_y\rangle$ spin sublevels retain $\mathbf{H}^{(2)}_{ISC}$ matrix elements with $\pi\pi^*$ singlet excited states. Thus, the rates of population and decay of the $|\, t_x\rangle$ and $|\, t_y\rangle$ sublevels are in general faster than those of $|\, t_z\rangle$ in Chls.

II-B. The exciton model for dimeric chlorophyll triplets

The experimental demonstration of the dimeric nature of the bacterial primary donor has stimulated considerable theoretical interest in the excited triplet states of Chl aggregates. The basic description of multimeric triplet states is the exciton model originally used to describe interacting triplets in a crystal matrix [70,71]. We present the model as it may be applied specifically to the lowest triplet states of a pair of closely interacting Chl monomers, M_1 and M_2. Related models have been used to describe Chl dimers in vitro and the bacterial primary donor [72–74].

Using the Born-Oppenheimer approximation, the electronic states of the Chl monomers may be treated separately from their nuclear motions, and we may consider four possible electronic configurations of the pair:

$$\begin{aligned} \psi^{(1)} &= ({}^3M_1^* M_2) \\ \psi^{(2)} &= (M_1 {}^3M_2^*) \\ \psi^{(3)} &= {}^3(M_1^+ M_2^-) \\ \psi^{(4)} &= {}^3(M_1^- M_2^+) \end{aligned} \tag{15}$$

where M_1 and M_2 designate the ground singlet states of each monomer, ${}^3M_1^*$ and ${}^3M_2^*$ their locally excited triplet states, and $M_1^{\pm}$ and $M_2^{\pm}$ their cation and anion states. One important feature of this basis set is that it permits charge-transfer contributions to the dimer triplet state; that is, it allows admixture of a triplet configuration in which one of the unpaired electrons has been transferred from M_1 to M_2, or from M_2 to M_1. Such species are frequently encountered in the triplet states of organic electron donor-acceptor complexes in solution and have been well characterized [75,76].

The configurations $\psi^{(j)}$ are combined to form four dimer triplet states, $\Psi^{(i)}$, according to the relation

$$|\, \Psi^{(i)} t_\mu^{(i)} \rangle = \sum_j \sum_\nu c_{ij} R_{\mu\nu}^{(ij)} |\, \psi^{(j)} t_\nu^{(j)} \rangle \tag{16}$$

where μ and ν index the zero-field axes x, y, z, and the Euler matrices $\mathbf{R}^{(ij)}$ specify the transformation from the

* A concise and exceptionally clear exposition of Herzberg-Teller spin-vibronic coupling is given in Appendix 3 of Ref. 64.

zero-field axis system of configuration $\psi^{(j)}$ into the zero-field axis system of $\Psi^{(i)}$. In general, we will be concerned only with the lowest-energy dimer triplet state.

Eqn. 16 represents a coherent combination of states in the strong coupling limit; that is, interactions between the configurations $\psi^{(j)}$ are assumed to be much larger than the monomeric ZFS. ^{3}P could also be an incoherent combination resulting from fast hopping among the $\psi^{(j)}$. This distinction is potentially of importance in evaluating the intersystem crossing rates of the dimer triplet, as discussed below.

The mixing coefficients c_{ij} and the rotation matrices $\mathbf{R}^{(ij)}$ can be used to predict the ZFS parameters of the dimeric triplet states. Assuming zero differential overlap of the basis wavefunctions $\psi^{(j)}$, each ZFS tensor $\mathbf{D}^{(i)}$ consists of the weighted contributions of the tensors $\mathbf{D}^{(j)}$ from each configuration [70]

$$\mathbf{D}^{(i)} = \sum_j c_{ij}^2 (\mathbf{R}^{(ij)}) \mathbf{D}^{(j)} (\mathbf{R}^{(ij)})^{-1} \tag{17}$$

If the zero-field axes of $\Psi^{(i)}$ are not known, they may be found by defining the $\mathbf{R}$ matrices in a known coordinate system, constructing $\mathbf{D}^{(i)}$, and diagonalizing it. Once the zero-field axes for $\Psi^{(i)}$ are known and the $\mathbf{R}^{(ij)}$ defined for diagonal $\mathbf{D}^{(i)}$ and $\mathbf{D}^{(j)}$, Eqn. 17 simplifies to

$$D_{\mu\mu}^{(i)} = \sum_j c_{ij}^2 \sum_v \left(R_{\mu v}^{(ij)} \right)^2 D_{vv}^{(j)} \tag{18}$$

where the ZFS parameters $-X^{(i)}$, $-Y^{(i)}$, $-Z^{(i)}$ for the state $\Psi^{(i)}$ are given by $D_{\mu\mu}^{(i)}$ for $\mu = x,y,z$.

Intersystem crossing from the zero-field spin states of the triplet state $\Psi^{(i)}$ can also be expressed in terms of the c_{ij} and $\mathbf{R}^{(ij)}$. For example, the decay rates are related to the matrix elements of each configuration $|\psi^{(j)} t_v^{(j)}\rangle$ with the electronic ground state $|M_1 M_2\rangle$ by analogy with Eqn. [9]:

$$k_\mu^{(i)} = \frac{2\pi}{h} \rho(E) |\langle \Psi^{(i)} t_\mu^{(i)} | H_{ISC} | M_1 M_2 \rangle|^2 \tag{19}$$

Substituting Eqn. 16 gives

$$k_\mu^{(i)} = \frac{2\pi}{h} \rho(E) \left| \sum_j \sum_v \langle M_1 M_2 | H_{ISC} | \psi^{(j)} t_v^{(j)} \rangle \right|^2$$

$$= \left| \sum_j \sum_v c_{ij} R_{\mu v}^{(ij)} (k_v^{(j)})^{1/2} \right|^2 \tag{20}$$

The proper application of Eqn. 20 to the kinetics of Chl dimer triplets has been a matter of some debate [39]. Squaring the summations in this equation produces cross-terms of the form $c_{ij} c_{ij}^* R_{\mu v}^{(ij)} R_{\mu v'}^{(ij')} (k_v^{(j)} k_{v'}^{(j')})^{\frac{1}{2}}$ which are frequently discarded in treatments of ISC in dimers [72,74,77]. These terms are important if the ISC occurs to and from a state that is actually a coherent superposition of sublevels $|t_v^{(j)}\rangle$ and $|t_v^{(j')}\rangle$. In such a case, the sublevels share an ISC pathway instead of behaving independently. The terms with $j \neq j'$ refer to coherence between states from different electronic configurations; for example, ISC could be coupled to a superposition of vibrationally excited states of M_1 and M_2[78,79] or a vibrational mode of the dimer structure itself, which have no counterparts in monomeric ^{3}Chl. Another such term is spin-orbit coupling introduced by charge-transfer configurations; this could be particularly significant in cases where the π-electron systems of the radical ions are nonparallel [80,81].

Terms with $j = j'$ and $v \neq v'$ refer to ISC involving a superposition of spin states within a given electronic configuration. This type of coherence has been observed in a molecule where the magnetic zero-field axes differ from the molecular orbital symmetry axes [82]. It should not be important for monomer ^{3}Chl, where the two axis systems coincide at least approximately; however, it is a strong possibility for asymmetric charge-transfer triplet configurations, including intra-dimer charge transfer states as well as those involving one of the accessory pigments. Neglecting all cross-terms reduces Eqn. 20 to

$$k_\mu^{(i)} = \sum_j \sum_v c_{ij}^2 \left(R_{\mu v}^{(ij)} \right)^2 k_v^{(j)} \tag{21}$$

which is the same result obtained for an incoherent hopping mode [74,78] or using the random phase approximation [73].

Some remarks about the limitations of the exciton model are in order, especially regarding its application to the bacterial RC and other in vivo systems where several Chls are rigidly held in proximity. Many possible excited state configurations have been neglected, including all excited singlet states, states involving any of the accessory pigments, or even higher excited triplet states of the constituent monomers. There is some justification for neglecting triplet states of the accessory pigments since their excitonic interactions are much weaker than those among excited singlet states; however, such states have not rigorously been ruled out. In fact, most recent exciton model studies of the RC [83–87] have included all of the pigments and focused on the optical properties of its singlet state manifold.

Even the specialized exciton model given above has required further approximations to reduce the number of parameters in equations [16–21] for practical application to Chl dimers [39,72–74,78]. Typically, (1) the monomers are taken as magnetically equivalent ($D_{vv}^{(1)} = D_{vv}^{(2)}$ for $v = x,y,z$); (2) charge transfer contributions are neglected ($c_{i3} = c_{i4} = 0$); (3) triplet excitation is assumed to be equally shared between the monomers ($|c_{i1}| = |c_{i2}| = 2^{-\frac{1}{2}}$); and (4) the dimer is assumed to have C_2 symmetry ($R_{\mu v}^{(i1)} = \pm R_{\mu v}^{(i2)}$ for $\mu, v = x,y,z$, where the '+'

applies if μ is the dimer C_2 axis). In this restricted form, the exciton model has been useful for defining the dimer geometry using the ZFS parameters and spin sublevel kinetics in many cases. For dimers satisfying approximations (2) through (4), it is possible to write down the zero-field axes of the dimer triplet by inspection: each dimer axis is a bisector of corresponding monomer axes, and one will coincide with the C_2 symmetry axis. In practice, many of the in vitro dimers that have been investigated share these properties. Although the bacterial primary donor is also C_2-symmetric, the more general exciton model is needed in order to evaluate the degree of participation of the configurations $\psi^{(j)}$ from the known geometry.

Finally, it is important to note that the interpretation of a dimeric triplet state 'structure' in terms of the exciton model also depends upon the timescale of the experimental method employed, i.e. the magnitude of the interaction energy measured. For EPR methods, this timescale is on the order of the inverse of the triplet ZFS, or about 300 ps. In contrast, optical spectroscopy probes interactions on the order of 10^{15} s^{-1}; thus, a given Chl pair could exhibit dimeric EPR properties and at the same time the optical properties of its constituent monomers.

II-C. Experimental characterization of chlorophyll triplet states

To summarize the preceding section, the Chl triplet state provides a number of experimentally observable quantities that make it a particularly useful probe of its physical environment and related photochemistry. Most significant among these are (1) the triplet state electronic energy relative to the ground state, (2) the zero-field splitting parameters, (3) hyperfine interactions with magnetic nuclei on the Chl macrocycle, (4) rate constants for the population and depopulation of the spin sublevels, and (5) rate constants for relaxation among the spin sublevels.

In general, optical spectroscopy, particularly studies of Chl luminescence, is most useful for determining the first of these quantities, whereas magnetic resonance methods are required to measure the other triplet state properties, which are more closely related to the detailed structure of the Chl and its environment. Because so many triplet state properties can usefully be probed by magnetic resonance, this review will treat optical studies relatively briefly and concentrate more closely on the magnetic resonance methods that have been applied in the experimental characterization of the Chl triplet state.

Magnetic resonance is particularly useful in the investigation of Chl triplets because of the phenomenon of electron spin polarization (ESP). ESP is simply a deviation of the spin state populations from a Boltzmann equilibrium distribution. In general, all mechanisms of both triplet state formation and decay are selective with respect to spin states; moreover, they may be selective with respect to either the high-field or the zero-field spin states. Provided that spin relaxation is relatively slow, all triplet states will therefore have non-Boltzmann spin sublevel populations and exhibit magnetic resonance spectra with some transitions appearing in absorption and others in emission. Thus, not only does the position of a resonance peak furnish structural information about the triplet state, its polarization also reflects the triplet state dynamics. Finally, magnetic resonance techniques can often be time-resolved to provide a direct measurement of photochemical kinetics.

Two main types of magnetic resonance experiment have been employed in Chl triplet research: optically detected magnetic resonance (ODMR), which is usually but not necessarily [88] performed at zero magnetic field, and EPR and related multiple resonance techniques, which require a magnetic field. Both methods measure structural parameters such as the ZFS, both exhibit ESP that is sensitive to triplet state dynamics, and both may be time-resolved. We will briefly describe these main methods and their application to Chl triplets.

The role of nuclear magnetic resonance (NMR) in investigations of ^{3}Chl deserves a brief note. Triplet energy transfer between Chls in solution produces an NMR line broadening from which nuclear HFI in ^{3}Chl can be estimated [89]. NMR has also been used to study the chemically induced nuclear polarization (CIDNP) resulting from ^{3}Chl electron transfer to a quinone acceptor [90]. Such results suggest similar effects should be observable in photosynthetic systems; however, despite some recent experimental evidence for CIDNP specifically associated with the triplet photochemistry of the bacterial RC [91–93], no NMR observation of the phenomenon have been reported.

II-C.1. Optical spectroscopy of the chlorophyll triplet state

The experimental methodology is well established for measuring the transient triplet-triplet absorption spectrum [94–97], delayed Chl fluorescence via back-population of S_1 from T_1 [98], and triplet state phosphorescence [99–103]. The methods used for emission and absorption spectroscopy are quite similar, and differ mainly in that absorption measurements utilize a continuous weak probing beam on the sample, while emission measurements require stricter precautions to eliminate scattered light and adventitious emission from sources other than the sample. In one method, the excitation light is modulated, often by mechanical chopping, and the absorption or emission spectrum recorded using a lock-in amplifier to filter the modulated photodetector output. The second, more frequently employed method is a simple flash experiment in which the sam-

ple is photoexcited by a laser or flashlamp pulse, and the signal collected in the time domain using some form of a transient digitizer.

The applicability of optical methods to ^{3}Chl is somewhat limited by several factors, including spectral resolution and sensitivity. The triplet-triplet absorption spectrum of the T_1 state of Chls is relatively broad and featureless, so that identifying specific transitions with spectral components is difficult. Phosphorescence studies of ^{3}Chl have historically been hampered both by the relatively long wavelength (about 1000 nm) and the extremely low quantum yield of ^{3}Chl phosphorescence (10^{-4} to 10^{-5}). In the case of BChls and bacterial systems, these two factors have prohibited the detection of phosphorescence until the recent application of high sensitivity GaAs detectors at long IR wavelengths [104,105].

Luminescence can be used to estimate the $T_1 - S_0$ energy gap directly by phosphorescence measurements, or indirectly by observing the temperature dependence of the intensity of delayed fluorescence that results from thermally activated repopulation of S_1 from the triplet state [98]. The triplet lifetime may also be measured from the delayed fluorescence, but the extremely low quantum yield and adventitious fluorescence from impurities complicate such measurements. In most cases, direct measurements by phosphorescence and transient absorption are preferable.

Optical measurements of the overall triplet decay rate have provided an important standard for comparison with less direct kinetic measurements by magnetic resonance methods. Furthermore, because optical methods afford a way to measure both the $T_1 - S_0$ energy gap and the overall decay rate of the T_1 state, the combination of phosphorescence and transient absorption spectroscopy has been used to demonstrate the validity of the 'energy-gap law' for radiationless transitions of the triplet state, which relates the triplet decay rate to the triplet-singlet energy difference [106–108]. In turn, the energy-gap law has proved useful for estimating the $T_1 - S_0$ energy gap from the experimental triplet decay rate for samples in which the former quantity cannot be measured directly.

II-C.2. Optically detected magnetic resonance

A comprehensive treatise on optically detected magnetic resonance (ODMR) methods and their various applications to biophysical systems is the book edited by Clarke [37]; more recent reviews can be found in references [109] and [110]. As their name implies, ODMR techniques rely upon differences in the optical properties of singlet and triplet species to obtain a magnetic resonance spectrum. Such methods also depend on at least one spin state-dependent reaction pathway in the course of triplet formation or decay. The basic kinetic scheme for a typical ODMR experiment is

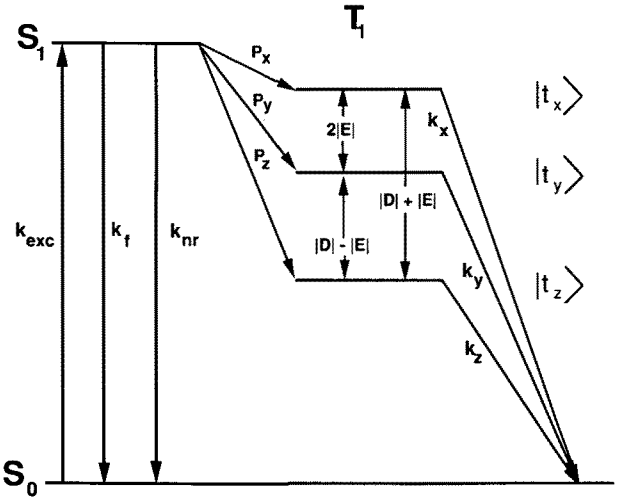

Fig. 5. Simple kinetic scheme describing a typical ODMR experiment for a chlorophyll. Double-headed vertical arrows indicate microwave-induced transitions. Pathways not shown are phosphorescence of T_1 (negligible for chlorophylls) and kinetic processes involving higher S and T states.

shown in Fig. 5. A Chl molecule in its ground state S_0 is photoexcited by weak, continuous illumination (pathway k_{exc}) into its first excited singlet state, S_1, which may fluoresce (k_f), decay to S_0 nonradiatively (k_{nr}) or undergo intersystem crossing ($P_{x,y,z}$) to the first excited triplet state, T_1. T_1 then phosphoresces (a negligible process for ODMR of chlorophylls) or decays nonradiatively to the ground state ($k_{x,y,z}$). Because the rate constants for formation and decay are different for each of the triplet sublevels, a microwave-induced change in their populations may change the overall T_1 decay rate, provided that the microwave transitions are faster than relaxation among the spin sublevels. The ODMR spectrum is obtained by sweeping the frequency of applied cw microwaves. At resonance, the steady state populations of T_1, S_0, and S_1 all change, and the resonance can be detected by monitoring any of their optical properties. It is also possible to measure optical properties of nearby molecules that depend upon the presence of T_1, S_0, or S_1.

ODMR has been applied to photosynthetic pigments by monitoring $T_n \leftarrow T_1$ absorption [111,112], S_1 fluorescence [113–115] and $S_1 \leftarrow S_0$ absorption [116]; these methods are frequently known as fluorescence- or absorption-detected magnetic resonance (FDMR or ADMR). Most recently, resonance Raman detected ODMR has been applied to photosynthetic pigments [117]. By proper choice of experimental conditions, for example low temperature (~ 4.2 K) and weak probe light intensity, complications from spin relaxation and $T_n \leftarrow T_1$ absorption [115] can be minimized.

ODMR techniques present some particularly desirable features. Because optical detection is extremely sensitive, FDMR techniques are useful for in vivo systems

such as whole cells, where the species of interest is present only at low concentrations. Zero-field ODMR also provides a direct and accurate measurement of the ZFS parameters; in principle, three ODMR peaks are observable, corresponding to the zero-field transitions $|t_x\rangle \leftrightarrow |t_z\rangle$, $|t_y\rangle \leftrightarrow |t_z\rangle$ and $|t_x\rangle \leftrightarrow |t_y\rangle$, with energies $|D+E|$, $|D-E|$, and $|2E|$, as shown in Fig. 5. Because the anisotropy of the electron spin-spin dipolar interaction does not contribute to the magnetic resonance linewidth in the absence of a field, the ODMR lines are much narrower than the standard EPR; moreover, the ODMR peaks are not broadened by nuclear HFI at zero field [118]. Furthermore, differences in the relative decay rates of the zero field spin states will be reflected directly in the polarization of the observed transitions. Thus, the $|2E|$ transition is usually not observed in Chl triplets because the populations of $|t_x\rangle$ and $|t_y\rangle$ are nearly equal.

Perhaps more importantly, ODMR provides a means of correlating optical and magnetic properties of the sample. For example, the magnetic resonance spectrum of a selected optical species may be measured using narrow-band excitation [119–122]. Alternatively, an emission or absorbance spectrum selected with respect to triplet ZFS may be obtained by modulating resonant microwaves and measuring the optical signal using phase-sensitive detection [123].

Finally, optical detection schemes afford good time resolution, a feature which until recently made ODMR the method of choice for determining rate constants for zero-field spin state dynamics. There are two basic methods for kinetic measurements by ODMR: the first measures the response of the steady-state system to a microwave pulse and its subsequent return to steady-state [113], and the second measures the equilibrium concentrations of S_1, S_0, or T_1 in the presence and absence of microwaves [124]. Details of these methods may be found in several chapters of reference [37]. Pulsed microwave ODMR has also been used to detect electron spin echoes and measure the phase memory decay time for the zero-field states [125,126].

II-C.3. EPR

Fig. 6 shows the appearance of a typical X-band (9.5 GHz, $\mathbf{B}_0 \sim 3200$ G) EPR spectrum for a randomly oriented distribution of rigidly fixed ^{3}Chl molecules. At a single orientation in the field, a triplet EPR spectrum would consist of two $\Delta m_s = 1$ peaks corresponding to the $|t_{-1}\rangle \leftrightarrow |t_0\rangle$ and $|t_0\rangle \leftrightarrow |t_{+1}\rangle$ transitions (called transition I and II, respectively). For ^{3}Chl at X-band, the splitting between peaks I and II is well approximated by the difference in first-order transition energies, $3D_{zz}$ (cf. Eqn. 6). For a static distribution of triplet orientations, a given transition appears as a broad structure with three peaks in the first derivative spectrum, corresponding to the three 'canonical orienta-

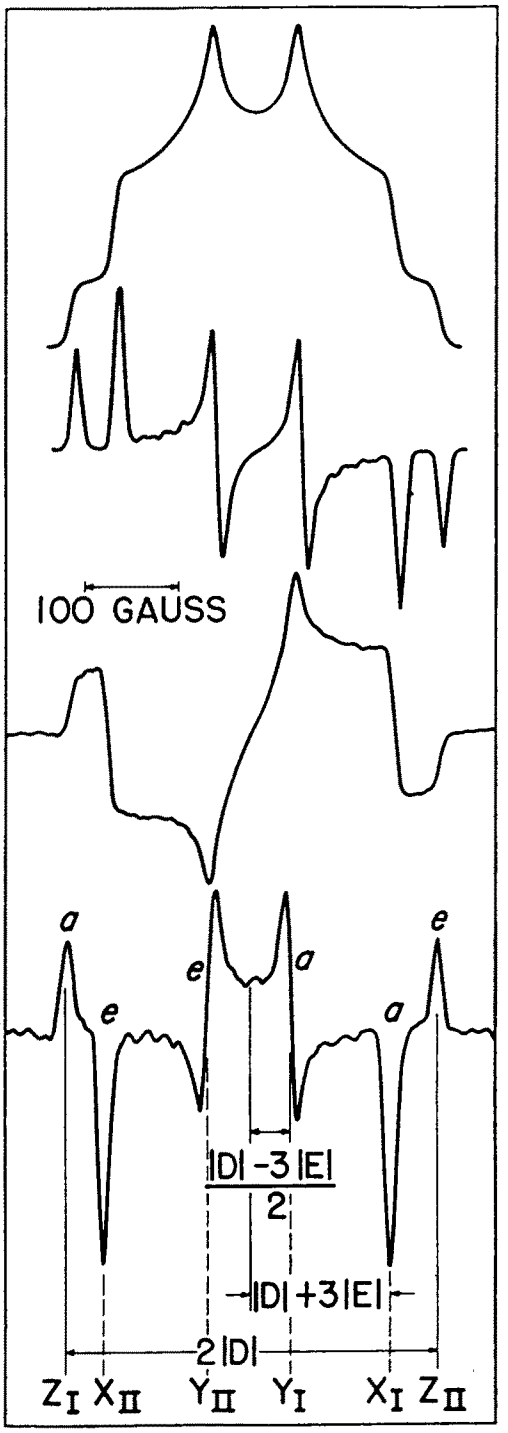

Fig. 6. Triplet EPR spectra, showing an ideal, unpolarized spectrum of a randomly oriented triplet molecule in (A) absorption mode and (B) first derivative mode, the more usual presentation for EPR spectra. A spectrum with the same ZFS and a spin polarization corresponding to that of the bacterial primary donor triplet, is shown in (C) absorption mode and (D) first derivative mode for comparison. The peaks in (D) are marked '*a*' for absorption and '*e*' for emission (cf. spectrum B). The labelling of the peaks in (D) is appropriate for the case $D > 0$, $E < 0$; for $D < 0$, the labels 'I' and 'II' should be interchanged and for $E > 0$, the labels 'X' and 'Y' should be interchanged.

tions' where $\mathbf{B}_0$ is aligned with a zero-field axis (labeled X, Y, and Z in Fig. 6). As Fig. 6 indicates, $|D|$ and $|E|$ may be determined directly from the EPR spectrum: the I/II splittings given for the X, Y, and Z orientations in Fig. 6 are obtained by setting the appropriate direction cosine in Eqn. 6 to unity, and the other two to zero.

Because the $\mathbf{B}_0$ field of an EPR spectrometer provides a unique axis of quantization for the electron spins, EPR can be used to obtain structural information from the magnetic anisotropy of ^{3}Chl. There are a variety of methods that rely upon some means of imposing a preferential orientation on the triplet molecule relative to the $\mathbf{B}_0$ direction. Chlorophylls in vitro have been aligned by dissolving them in a liquid crystalline solvent [127–130]; whole cells have been oriented in a magnetic field [131]; photosynthetic membranes may be aligned by drying them on a slide [132], or sedimenting them onto a sheet of Mylar [133]; isolated proteins may be embedded in a polymer film that can be stretched [134,135], or in a gel that can be compressed [136] to provide a preferred alignment direction. Another widely employed method is magnetophotoselection [59,137–141] which uses polarized excitation light to create an anisotropic distribution of photoexcited ^{3}Chl molecules. By rotating the direction of preferred orientation relative to the field, the zero-field axes of the ^{3}Chl molecule can be partially determined relative to macroscopically defined directions. A general theoretical treatment for the EPR spectrum of partially aligned triplet molecules has been given [142].

Detailed information about electron-nuclear interactions in ^{3}Chl is not available from EPR; the numerous small HFI interactions cannot be resolved from the EPR lineshape. However, such resolution is possible using electron nuclear double resonance (ENDOR), in which the EPR microwave transition is monitored and nuclear resonances induced by an applied radio-frequency are detected as a change in the EPR intensity. ENDOR played an important role in establishing the dimeric nature of P, since it clearly demonstrated that HFI interactions were halved in P^+ relative to those of in vitro $BChl^+$ [143,144]. Such a comparison is also possible for the triplet states of P and BChl, although triplet state ENDOR spectra has only recently been applied to such systems [145–147]. A particular advantage of triplet ENDOR is that specific molecular orientations may be selected, providing an ENDOR spectrum similar to that from a single crystal [145–147]. One potential limitation is that the triplet lifetime may be short relative to the electronic and nuclear spin relaxation rates; however, ENDOR spectra are obtainable even in this case provided the triplet is strongly polarized [145–147].

Although most of the EPR methods described here are used to obtain structural information from rigidly fixed triplets in the solid state, the triplet state magnetic anisotropy may also be used to study the dynamics of molecular motion [148], as has been demonstrated in a recent study of ^{3}Chl rotational diffusion in a liquid crystalline solvent [149].

II-C.4. New EPR methods in chlorophyll triplet research

Early EPR studies of Chl and porphyrin triplets in frozen solution used continuous light excitation [150–154]; however, most in vitro systems yield only very weak triplet EPR signals under such conditions. More usually, the excitation light is modulated and the EPR signal enhanced using phase-sensitive detection. This method, and the related single light pulse experiment [155–157], suppress the dark signals and signals with slow kinetics (ms range) that are typically found in vivo; in addition, their crude time resolution often permits a qualitative ordering of triplet sublevel population and decay rates [35]. Because of its relative simplicity, the light modulation technique has received perhaps the widest application to photosynthetic systems.

Recent improvements in the sensitivity and time resolution of EPR techniques have permitted much more detailed investigations into the kinetics of the short-lived species in photosynthetic reactions. Commercial continuous wave (CW) EPR spectrometers have been modified in three basic ways to enhance their time resolution. The first, a simple modification of the lock-in amplifier [158,159], can provide a time resolution of about ~ 20 μs while retaining the standard 100 kHz field modulation frequency. Recently [160], a spectrometer operating with 200 kHz modulation was modified to give about 1 μs time resolution. Since the field modulation rate ultimately limits the available time resolution, a second method of improving time resolution is to increase the modulation frequency to 1–2 MHz. However, the field amplitudes available at such frequencies are generally too small for the broad EPR lines associated with ^{3}Chl. For photosynthetic systems, the preferred approach has generally been the third method, called 'direct detection' [130,149,161–168], which eliminates field modulation altogether, and has a time resolution on the order of 50–200 ns. All three methods require digital averaging of the transient signal to maintain reasonable sensitivity; however, a recent critical comparison [160] suggests that the first method may provide the best signal-to-noise under certain circumstances. Further details of these techniques have been reviewed elsewhere [169,170].

EPR has also been time-resolved using pulsed microwaves. The electron spin echo (ESE) experiment and its application to photosynthetic systems has been described in detail [169]. ESE presents some advantages beyond its capability to time-resolve the EPR spectrum [169]. In the typical ESE experiment, the echo intensity is recorded as a function of τ, the delay between micro-

wave pulses. In addition to measuring the phase memory decay time (T_2) of the sample, this type of experiment may reveal modulation of the echo intensity as a function of τ (known as ESE envelope modulation, or ESEEM). The ESEEM frequencies contain information about the nuclear hyperfine and quadrupole coupling constants of the species being studied.

The most recent pulsed EPR method to appear is Fourier Transform (FT)-EPR, which is under development in several laboratories [171–175] and is now commercially available [176]. This technique requires microwave pulses powerful enough to cover a broad frequency range, as is done with radiofrequencies in the analogous and more common FT-NMR technique. FT-EPR is well suited to study transient magnetization created by a short laser pulse. Although it has not yet been applied to triplets in vivo, it has been used to study chemically induced dynamic electron polarization (CIDEP) in radical ions formed by electron transfer from porphyrin excited triplet states to duroquinone. The nature of the CIDEP gives information about the porphyrin triplet state dynamics [177–179].

III. Triplet state studies of monomeric chlorophyll

Investigations of in vitro ^{3}Chl have been aimed at understanding the effects of relatively controlled environmental changes on the spectroscopic properties of ^{3}Chl, with the eventual goal of characterizing the environment of in vivo ^{3}Chl by comparison. Detailed accounts of this work, with extensive tabulation of spectroscopic parameters for various types of ^{3}Chl have been given in previous reviews [34,35,38]. We will summarize some general results from these studies, with specific reference to the physical models presented in Section II.

III-A. In vitro chlorophylls

III-A.1. Structure

Environmental effects on the absorption and emission spectra of in vitro Chls have been studied in detail [180–184] and phosphorescence studies of the triplet states of Chl and photosynthetic systems have been reviewed by Krasnovskii [185]. Although the central Mg^{2+} ion does not participate to any significant extent in the Chl 'four orbitals', it still exerts a decisive effect on Chl's electronic structure. In addition to the four nitrogens of the pyrrole rings, the electrophilic Mg^{2+} can accommodate one or two additional ligands [186]. Thus, the Mg^{2+} can influence the spectroscopic properties of Chl by the number and type of ligands coordinated to it, and by the degree of Chl aggregation, which often occurs via direct or indirect interaction between the Mg^{2+} of one Chl and some electron-donating group of another. Both influences depend in turn upon the polarity and electron-donating capability of the solvent.

The wavelengths of the lowest energy (Q_x and Q_y) absorption maxima of Chl (659–671 nm) are rather sensitive to the ligation state of the Mg^{2+}. Evans and Katz [187] demonstrated that the biligated species of BChl absorbs to the red of the monoligated species, an assignment that was confirmed by resonance Raman studies [182]. This type of red shift is associated with a change in coordination number for other chlorophylls [188], and is accompanied by a corresponding shift in the fluorescence spectrum. In terms of the four-orbital model, the effect of an electron-donating ligand may be rationalized as a destablization of orbitals with electron density on the pyrrole nitrogens (b_1 and to a lesser extent c_1 and c_2, as can be seen from Fig. 3) resulting in increased interaction between the $|b_1c_1\rangle$ and $|b_2c_2\rangle$ configurations, and reduction of the Q_y energy.

In addition, solvent conditions may cause Chl to associate into dimers and higher polymers [189], which also exhibit large red shifts in the Q_y absorption maximum [180,190] due to singlet exciton interactions [190–192]. The most important example of this type of dimer [188–195] consists of plane-parallel Chls whose Mg^{2+} ions are linked via interstitial H_2O ligands to the ring V keto-carbonyl (or ester carbonyl [194,195]). In pheophytins, which have no Mg^{2+}, dimerization can still occur via π–π interactions at sufficiently high concentrations [196]. The self-aggregating properties of in vitro Chls and their possible connection with the dimeric Chl species observed in vivo have led to intensive investigations of synthetically linked Chl dimers. A discussion of the triplet state properties of these types of dimers will be postponed to our discussion of model systems in Section VII.

Theoretically, the ZFS parameters can be related to the spatial distribution of the unpaired electrons by integrating the difference of the electronic coordinates, the vector $\mathbf{r}_{12}$, over the spatial part of the triplet wave function, Ψ:

$$D = \tfrac{3}{4}(g\beta_e)^2\langle\Psi|\frac{r_{12}^2 - 3z_{12}^2}{r_{12}^5}|\Psi\rangle \tag{22}$$

$$E = \tfrac{3}{4}(g\beta_e)^2\langle\Psi|\frac{y_{12}^2 - x_{12}^2}{r_{12}^5}|\Psi\rangle \tag{23}$$

where x, y and z refer to the zero-field axis system. Since the zero-field z axis is taken to be normal to the molecular plane (Section 2), on average $\langle z_{12}^2\rangle \ll \langle x_{12}^2\rangle + \langle y_{12}^2\rangle \approx \langle r_{12}^2\rangle$ for a large flat molecule like Chl. Then Eqn. 22 predicts $D > 0$, and shows that D is inversely related to $\langle r_{12}^3\rangle$, the average distance between the electrons. Thus, D is an approximate measure of electronic delocalization in the triplet MO. According to Eqn. 23, the E parameter measures the degree of in-plane orbital

symmetry; for example, an electronic distribution with perfect fourfold symmetry would give $\langle x_{12}^2 \rangle = \langle y_{12}^2 \rangle$ and $E = 0$.

This simple 'electrons-in-a-box' picture often fails to account for the available experimental observations. For example, in the series Mg-TPP, Chl *a*, BChl *a*, one might expect successive ring reductions to restrict electronic delocalization and increase $|D|$, whereas the opposite is observed [34,35]. Similarly, since the conjugated systems of Chls are elongated in the **y** zero-field direction, $\langle y_{12}^2 \rangle > \langle x_{12}^2 \rangle$ and Eqn. 23 predicts $E > 0$. However, magnetophotoselection [59] experiments have show that $E > 0$ only for BChls, whereas $E < 0$ for Chls (assuming the **x** and **y** axes shown in Fig. 2).

In fact, systematic study of the ZFS of in vitro Chls under different experimental conditions [34,35] has demonstrated that they reflect a much wider range of structural and environmental effects including (1) the spatial extent and approximate symmetry of the MO's, (2) the presence and identity of the central metal ion, (3) the number of metal ligands (4) solvent polarity, and (5) nearby electrical charges, all of which affect configuration mixing within the Chl triplet manifold.

Eqns. 22 and 23 can in principle be used to calculate such effects rigorously if the appropriate triplet MOs are used. The calculations that have been carried out for selected porphyrins [57,58] are quite cumbersome for general application because they require the inclusion of extensive configuration interaction for reasonably reliable results. Most physical interpretations of environmental effects on the ZFS have instead used the simpler four-orbital model. Thus, for example, the trend of smaller $|D|$ with ring reduction may be interpreted in terms of a decrease of configuration interaction between $|b_1c_1\rangle$ and $|b_2c_2\rangle$ [107], which is strongly influenced by both electron delocalization and orbital symmetry.

The known red shift of Chl fluorescence with an additional Mg^{2+} ligand has permitted FDMR and EPR to identify ligand effects on the triplet state properties of Chl *a* [74,197–199], Chl *b* [74,199,200] and BChl *a* [201], based on the known effects of ligands on their absorption or fluorescence spectra. In general, the ZFS parameters are smaller for bi-ligated than for mono-ligated species. In the cases of Chl *a* and BChl *a*, the added ligand reduces $|D|$ by about $\sim 5\%$, and E by about 20%. A similar trend is apparent for Chl *b*, although the results are less straightforward because of its additional hydrogen-bonding functional groups [74,201].

The effect of an extra electron-donating ligand may be qualitatively understood as a reduction of electronic attraction to the Mg^{2+} that permits greater electron delocalization in the conjugated ring system of bi-ligated species, resulting in smaller ZFS [197]. However, quantitative interpretation of this effect using more sophisticated models has been somewhat unsatisfactory. According to the four-orbital model [57,107], the increase in configuration mixing of $|b_1c_1\rangle$ and $|b_2c_2\rangle$ that lowers the S_1 energy should also increase $|D|$ in T_1. It is possible to rationalize a decrease in $|D|$ using the four-orbital model [38], but it may not be valid to neglect configurations outside the four-orbital basis, since the contribution of $|b_1c_1\rangle$ to the T_1 states of Chl and BChl is quite small. Schaafsma [38] has discussed another mechanism for the reduction of $|D|$ based on an earlier suggestion by Dvornikov [100], in which the energies of the two lowest triplet configurations of monoligated Chl *a* are interchanged upon addition of the second ligand.

Correlation between the S_1 energy and the ZFS of the T_1 state has been observed using site-selected FDMR of monoligated Chl *a* in a low temperature glass [122]. As was the case in the ligand studies, smaller values of $|D|$ are associated with red-shifted fluorescence; in addition, the FDMR lines broaden slightly. These effects can be described using a perturbation treatment of the $\mathbf{H}_{ISC}$ matrix elements connecting T_1 with S_1 [202,203]. Since $|t_x\rangle$ and $|t_y\rangle$ have the largest matrix elements (cf. Section II), their energies shift closer to $|t_z\rangle$ as the $S_1 - T_1$ energy gap decreases, resulting in a smaller $|D|$. If the variations in the site energies of S_1 and T_1 are not perfectly correlated, this mechanism can also produce broadening of the ODMR transitions [202,203]. These results suggest that a second ligand could affect the magnitude of $|D|$ indirectly through the S_1 energy level.

Several groups have studied the ZFS of in vitro Chl dimers in an effort to characterize the effects of aggregation [74,199] with the eventual goal of determining the structure of in vivo dimers from their ZFS. Many of the dimers investigated exhibited only a very small reduction of the ZFS with respect to their constituent monomers [78,79]. A study of selected dimer triplets [204] showed that their $\Delta m_s = 2$ transition was appreciably narrower than that of the constituent monomers, demonstrating that the triplet state was actually delocalized over the dimer. Dimerization does not significantly reduce the ZFS in such cases because corresponding monomer zero-field axes are nearly parallel (or anti-parallel), consistent with dimer structures proposed earlier [188,195,205].

III-A.2. Kinetics

The zero-field sublevel decay rates for most relevant chlorophylls have been fairly well established by ODMR and EPR, and new methods have permitted the refinement of such measurements. However, some care is required to ascertain the correct values from the many measurements reported in the literature. For example, in the very important case of ^{3}BChl, the published values for the decay rates measured by ODMR methods

vary by a factor of about 5. ADMR kinetic studies give decay rates comparable to those of the bacterial primary donor triplet [206,207], but significantly faster than those previously determined by FDMR [34,208]. More recent measurements by lineshape analysis of light-modulated cw EPR spectra [209] yielded intermediate values; however, optical measurements of the overall ^{3}BChl decay rate are much more consistent with the ADMR results, suggesting that the faster set of decay rates is correct.

Another recent refinement in analysis of time-resolved EPR for kinetic measurements makes use of the exact transformation from zero-field to high-field spin states to calculate the population and decay of $|t_{+1}\rangle$ and $|t_{-1}\rangle$ [210]. This approach provides a good fit to the kinetic traces at all three canonical orientations of ^{3}Chl *a*, in contrast to previous methods which only produced good agreement at two orientations using the high-field approximation (i.e., the transformation given in Eqn. [5]) [211].

The sublevel kinetics of monomeric ^{3}Chl are also quite sensitive to the presence of a central metal ion and its ligation state: the decay rates are consistently slower in Chls than in pheophytins. One possible explanation of this effect is that the metal removes N-H vibrations that serve to promote ISC in pheophytin [212]. Such vibrational modes have been directly implicated in a study of ^{2}H-substituted porphyrins [213], but their role in the more closely related chlorin molecule is less clear [214]. A somewhat different model has emerged from studies of the relative effects of metal substitution on each of the zero-field levels in triplet porphyrins [67,113] and ^{3}Chl [215,216]. The introduction of Mg^{2+} into the pheophytin ring specifically reduces the ISC rates from $|t_x\rangle$ and $|t_y\rangle$, suggesting that ISC from these sublevels involves all of the pyrrole nitrogens. Since, according to Eqn. 16, one-center spin-orbit coupling from $|t_x\rangle$ and $|t_y\rangle$ requires occupied MOs with appreciable $|p_x\rangle$ or $|p_y\rangle$ character, the states most likely to participate in this type of coupling are $n\pi^*$ or $\sigma\pi^*$ states involving the in-plane nitrogen p-electrons. Stabilization of the nitrogen n or σ orbitals by interaction with Mg^{2+} could raise the energy of the associated $n\pi^*$ or $\sigma\pi^*$ excited states, and reduce the efficiency of spin-orbit coupled ISC.

The effects of Mg^{2+} ligation have been explained using similar arguments. Clarke et al. [197,198] found that the average triplet lifetime of Chl *a* in *n*-octane at 2 K decreased from ~3 ms to ~1.4 ms with the addition of a second water ligand; similar effects have been measured for BChl *a* using optical flash photolysis [217]. The destabilization of nitrogen σ orbitals by electron donation from the ligand lowers the energy of spin-orbit coupled $\sigma\pi^*$ states, thus restoring some of the efficiency of ISC from the in-plane spin sublevels and reducing the triplet state lifetime.

In general, the introduction of heavier metals such as Zn^{2+} into the Chl ring dramatically increases ISC to and from $|t_z\rangle$ while leaving that from $|t_x\rangle$ and $|t_y\rangle$ relatively unchanged [215,216]. The $|d_{xz}\rangle$ and $|d_{yz}\rangle$ orbitals of such metals have nonvanishing L_z matrix elements (cf. Eqn. 14) and thus provide a new metal-centered spin-orbit coupling term linking $|t_z\rangle$ to nearby singlet $\pi\pi^*$ states. Because the $\pi\pi^*$ states are much closer in energy than the $\sigma\pi^*$ states that are coupled to $|t_x\rangle$ and $|t_y\rangle$, ISC via $|t_z\rangle$ becomes the dominant route in such Chls.

Kinetic measurements have also served to augment ZFS data for purposes of analyzing the triplet properties of Chl dimers using the exciton model. The ZFS alone cannot uniquely determine the relative orientation of the constituent monomers, especially in cases where the dimer ZFS differ substantially from those of the monomer. Moreover, since $|E|$ does not exhibit consistent trends with respect to molecular symmetry and the local environment of monomeric ^{3}Chl, it is not a reliable indication of molecular geometry. Instead, the ZFS data may be used to define a region of solution which may be further restricted by modeling the kinetic data. In light of the demonstrated ligand effects on the ZFS and kinetic behavior of ^{3}Chl, it is also important to consider ligation in all cases where the Chl monomer is used to suggest structural features of Chl aggregates [37,197].

III-B. In vivo chlorophylls

The known effects of Mg^{2+} ligation on ^{3}Chl have been compared to results obtained from in vivo antenna Chl and BChl [197,201]. In both cases it was concluded that the majority of the antenna Chl or BChl is bound to the protein via a single Mg^{2+} ligand [197,201]. These suggestions are consistent with resonance Raman results on antenna complexes involving Chl *a* [218,219] and BChl *a* [220]. In contrast, FDMR of various antenna complexes in photosynthetic bacteria has revealed two distinct triplet states [221]. The additional species may be an impurity of bi-ligated BChl [201] that is observable with the much greater sensitivity of the FDMR technique.

The nature of an in vivo protein environment has been studied most directly in a pyrochlorophyllide *a*-apomyoglobin complex [222]. This system exhibits two fluorescence peaks at 671 nm and 685 nm, in contrast to the single broad band of Chl *a* in solution, the exact maximum of which depends on the excitation wavelength. Two similar but distinct ZFS are associated with each fluorescence peak, supporting the notion that the peaks represent different pyrochlorophyllide species. The overall decay rates of the two species are similar and equal to approximately the average of mono- and bi-ligated Chl. The results, combined with a room tem-

perature NMR study [223], suggest two conformations of pyrochlorophyllide with slightly different electrostatic environments, but the same state of (probably mono-) ligation. The observation that the triplet decay kinetics are faster than expected for monoligated Chl is not completely understood, but it suggests that the electrostatic field of a protein environment may exert a large influence on the photophysics of ^{3}Chl in vivo.

IV. Triplet state studies of the bacterial RC

The unique photochemical properties of the bacterial RC and its ready availability in well-characterized preparations have made the bacterial primary donor a focus for triplet state investigations. The structural and kinetic parameters of ^{3}P for a variety of organisms and preparative methods have been comprehensively tabulated in previous reviews [34,35,39]; here, we will summarize the salient conclusions of the early studies that have provided the foundation on which more recent work has been developed.

Although ^{3}P may reasonably be assigned to a BChl species on the basis of its magnetic properties, these differ in two very important respects from ^{3}BChl in vitro, as is immediately evident from Fig. 7. First, the ZFS of ^{3}P are reduced relative to those of monomeric ^{3}BChl: the reduction is appreciably larger than any of the solvent or ligand effects discussed in the previous section. Second, the ESP is significantly different from that of ^{3}BChl: it is much more intense and appears in a different absorption/emission pattern than any ^{3}BChl in vitro. These features indicate fundamental differences in both the structure and the photochemical function of the primary donor.

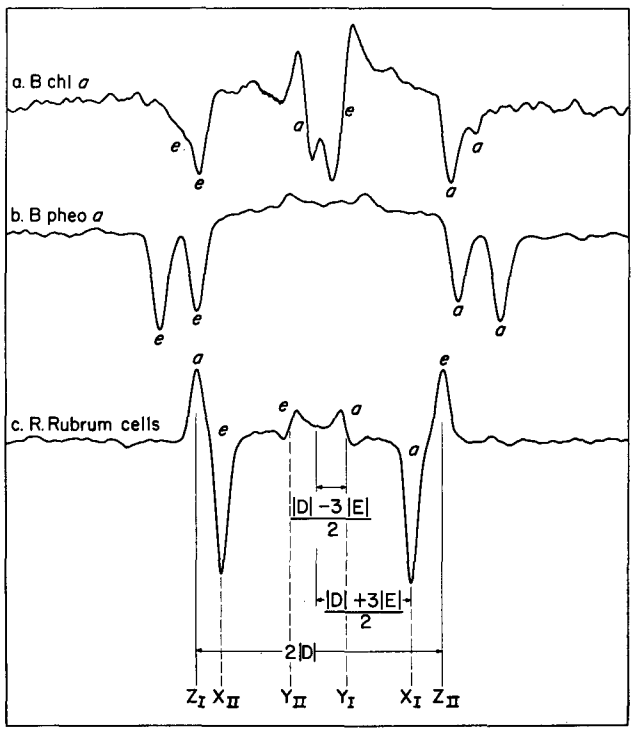

Fig. 7. EPR spectra of the triplet states of (a) bacteriochlorophyll *a* (b) bacteriopheophytin *a* and (c) the primary donor in the purple bacterium *Rhodospirillum rubrum*, demonstrating the differences in the zero-field splittings and electron spin polarization.

IV-A. Structure of the bacterial primary donor

IV-A.1. Early structural studies

According to the gross structural features defined by its ZFS, the primary donor of purple photosynthetic bacteria falls into two categories that correlate well with the type of BChl contained in the organism. The most apparent difference between primary donors in BChl *a*- and BChl *b*-containing organisms is the degree of reduction in its ZFS relative to the corresponding monomeric ^{3}BChl. In BChl *a*-containing organisms, $|D|$ is reduced by about 20% relative to monomeric ^{3}BChl *a*, whereas the reduction factor is higher, about 30%, in BChl *b*-containing organisms. Within each category, the ZFS of ^{3}P are quite consistent among different species compared with the variations observed for the ZFS of ^{3}Chl in vitro. This result suggests that the structure and environment of P, as probed by its triplet state, have been well conserved during the evolution of photosynthesis. Furthermore, the ZFS are the same in different preparations including whole cells, chromatophores, isolated RCs, and RC crystals, indicating that the structure is not significantly perturbed by the preparative procedure.

Early studies of ^{3}P sought to account for its reduced ZFS relative to ^{3}BChl in terms of its geometry. The first attempts to deduce the structure of P using an exciton model [72,74] assumed equal sharing of the excitation over a C_2-symmetric dimer and produced a geometry in which the normals of the two BChl planes formed an angle of about 45°. These results differ significantly from the X-ray crystallographic structure, which does possess approximate C_2 symmetry, but has a relative tilt angle of only 15° between the monomer planes [4]. In retrospect, it is clear that the major source of error was the omission of charge-transfer states from the exciton model used [224]. Since neither the geometry nor the charge-transfer character of ^{3}P was known prior to crystallization of the RC, the exciton model presented too many unknown parameter to be of significant value in assigning a structure to P.

Efforts to define the orientation of the ^{3}P zero-field axes relative to other physical features of the RC proved more successful. Studies of oriented whole cells [131] placed the *z* zero-field axis of ^{3}P in the plane of the photosynthetic membrane, a result confirmed by the X-ray structure. Magnetophotoselection studies measured the direction of optical transition dipoles of P [138,139], bacteriopheophytin [140] and a carotenoid

pigment [141] in the RC relative to the zero-field axes of ^{3}P.

IV-A.2. Structure from ENDOR and ESE studies

The electron spin distribution in ^{3}P has been studied by ENDOR and ESEEM with some initial success. In the first ^{1}H ENDOR study of ^{3}P, Lendzian *et al.* [147] demonstrated that single crystal-like ENDOR spectra could be obtained at the *z* orientation of ^{3}P. Although they could not compare their results directly to monomeric ^{3}BChl without knowledge of the ^{3}P zero-field axes, they concluded that the triplet excitation is delocalized over two BChls on an ENDOR timescale based on the almost isotropic HFI of the β-protons on rings II and IV.

ESEEM studies [225,226] of nitrogen HFI in randomly oriented samples of ^{3}BChl *a* and ^{3}P of *Rhodospirillum rubrum* have been less conclusive. Analysis of ESEEM frequencies from natural abundance ^{14}N (nuclear spin $I = 1$) is complicated by the comparable magnitudes of the nuclear hyperfine, quadrupolar, and Zeeman interactions. To separate these contributions, ESEEM was also performed on pigments and RCs enriched in ^{15}N ($I = \frac{1}{2}$) [225,226], which has a different magnetogyric ratio and no quadrupole moment. Neither study detected any orientation dependence of the ESEEM frequencies observed for ^{14}N or ^{15}N in either in vivo or in vitro pigments [225,226]. There have been initial reports of ESEEM from single RC crystals of both *Rb. sphaeroides* R-26 [227] and *R. viridis* [228], but detailed studies are not yet available.

At present, both ENDOR and ESEEM studies are hampered by the lack of experimental HFI values for ^{3}BChl. For comparison with ^{3}P data, the HFI in ^{3}BChl *a* has been estimated by averaging the measured values for BChl a^+ and BChl a^- [147,225] and any conclusions regarding the structure of ^{3}P have been based on this assumption.

IV-A.3. Single crystal EPR studies

The availability of single RC crystals for triplet EPR studies represented a significant advance towards understanding the electronic structure of the primary donor. With a single crystal, it became possible to impose a distinct orientation of the primary donor with respect to the spectrometer field, permitting systematic study of the magnetic anisotropies of the triplet state. Typically, each unique external crystal (morphological) axis is placed perpendicular to the magnetic field, the crystal is rotated around this axis, and the EPR spectrum recorded as a function of rotation angle. It is desirable to obtain a rotation pattern for all three axes if possible, since in this case, the **D** tensor may be completely determined from the single crystal data. The availability of rotations for all three axes may also permit unambiguous assignment of the crystal space group [229]. Fig. 8 shows typical crystal rotation patterns obtained by plotting the resonance peak positions as a function of rotation angle around each external axis of a single crystal from *Rb. sphaeroides* R-26.

Once the crystal rotations are accomplished for at least two morphological axes, a knowledge of the ^{3}P ZFS permits the determination of the ^{3}P **D** tensor relative to the morphological axes of the crystal. Since the orientation of the internal unit cell axes of the crystal are known relative to the external morphological axes (often the two systems are identical) the magnetic axes can be directly compared with the X-ray atomic coordinates of the RC. A detailed knowledge of the geometry of P greatly reduces the number of exciton model parameters (for example, the **R** matrices in Eqns. 18 and 21 are fully specified), allowing a more definitive assessment of configuration interactions in ^{3}P. Thus, single crystals have provided a powerful new means of correlating the dynamic states of the RC with its structural features.

Single crystal triplet studies have been carried out on RC crystals from *R. viridis* [60] and both the carotenoidless R-26 [60] and the carotenoid-containing 2.4.1 [63] strains of *Rb. sphaeroides*. Despite attempts to observe the carotenoid triplet in RC crystals from *Rb. sphaeroides* 2.4.1 at temperatures above 35 K, no rotation pattern could be measured for this species [63]. Instead, a faint set of absorption and emission peaks appeared at nearly constant field offset, similar to the **z** peaks of a randomly oriented triplet molecule, which suggests that the carotenoid triplet could be present, but disordered in the crystal [63].

There are eight molecules in the $P_{4_32_12}$ space group of the *R. viridis* crystal unit cell [2] and four in the $P_{2_12_12_1}$ space groups of the cystals from both strains of *Rb. sphaeroides* [13,229]. Therefore, since two peaks (the $|t_0\rangle \rightarrow |t_{-1}\rangle$ emission and the $|t_{+1}\rangle \leftarrow |t_0\rangle$ absorption) appear for each triplet molecule in the unit cell, as many as eight (four) absorption/emission pairs may appear at an arbitrary orientation of the crystal in the field. As few as one pair may be observed when B_0 is aligned with a crystal symmetry axis [60,61,229].

The peak positions for a given triplet molecule at a specified crystal orientation may be determined as follows. Let $\mathbf{R}(\phi,\theta,\psi)$ be the Euler rotation matrix where (ϕ,θ,ψ) define the orientation of the triplet magnetic axes with respect to the crystal unit cell axes [230] *. **R** may be rotated into the laboratory frame using the matrix $\mathbf{E}(\alpha,\beta,\gamma)$, where (α,β,γ) specify the orientation of the unit cell axes with respect to the laboratory frame, including the known orientation of the morphological axes relative to the EPR spectrometer, and any

* The Euler angle convention used is the *x*-convention given in the textbook of Goldstein (Ref. 230).

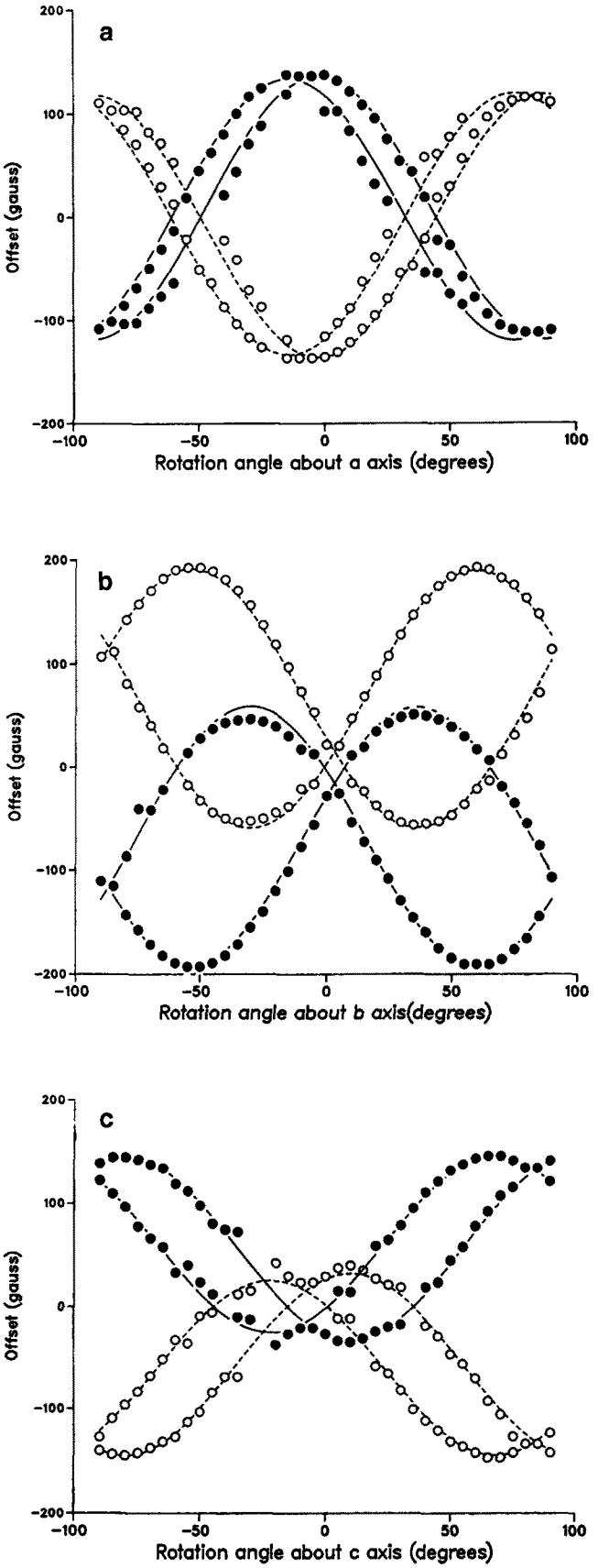

Fig. 8. Primary donor triplet EPR peak positions as a function of angle of rotation about the three unit cell axes (a,b,c) of a single RC protein crystal from *Rb. sphaeroides* R-26.

rotation between the unit cell and the morphological crystal axes. Then the product $\mathbf{E}(\alpha,\beta,\gamma)\mathbf{R}(\phi,\theta,\psi)$ produces a matrix whose columns are the direction cosines of the triplet magnetic axes with each of the laboratory axes. Assuming $\mathbf{B}_0$ is defined along the laboratory **z**, the third row of the resultant matrix gives the direction cosines (l_x,l_y,l_z) of $\mathbf{B}_0$ in the triplet magnetic frame, so that Eqn. [6] can be used to calculate the first order peak positions.

To produce a set of crystal rotation curves similar to Fig. 8, the calculation just described is repeated with a different **E** for each crystal orientation, and a different **R** for each of the symmetry-related RCs in the unit cell. The additional **R** matrices are generated from $\mathbf{R}(\phi,\theta,\psi)$ using the crystal space group symmetry operations. In practice, (ϕ,θ,ψ) are determined from the experimental data by a nonlinear least-squares procedure. After a starting (ϕ,θ,ψ) is chosen, the calculated crystal rotation curves are compared to the experimental curves and (ϕ,θ,ψ) are adjusted iteratively to minimize the differences. Further details of the method that has been applied to bacterial RC crystals are given in reference [63].

Because of crystal symmetry, there are eight or four sets of (ϕ,θ,ψ) that produce exactly the same set of rotation curves. The specific (ϕ,θ,ψ) found by the least squares procedure therefore corresponds to an arbitrary one of the crystal symmetry-related sites. Before a detailed comparison of the single crystal EPR results with the crystallographic structure is possible, it is necessary to identify which set of (ϕ,θ,ψ) corresponds to the particular RC in the unit cell for which the atomic coordinates have been specified.

In order to make this identification, Norris and coworkers [62] adopted the strategy of using the exciton model to calculate 'trial' magnetic axes from the atomic coordinates of the P dimer. Two limiting cases of the model (neglecting charge transfer states) were examined: (1) a monomeric triplet state, localized on either the L-side ($BChl_L$) or the M-side ($BChl_M$) of the dimer, and (2) a symmetric dimer triplet state, equally distributed between $BChl_L$ and $BChl_M$. The zero-field axes of $BChl_L$ and $BChl_M$ were derived by fitting a least squares plane to the coordinates of atoms in their conjugated ring systems and using the axis definitions given in section II. The trial axes were then compared to the experimental axes for each possible set of (ϕ,θ,ψ); a high degree of overlap between experimental and trial axes served to associate a specific set of (ϕ,θ,ψ) values with the atomic coordinates. In crystals from both *R. viridis* and *Rb. sphaeroides*, only one set of experimental (ϕ,θ,ψ) sets overlapped significantly with the trial axes, permitting an unambiguous assignment of zero-field axes to the crystal structure.

A surprising result from initial comparisons [231,232] was that the ^3P state of *R. viridis* is most closely

approximated as a triplet state localized on the $BChl_L$ half of the dimer, whereas that of *Rb. sphaeroides* is best approximated as a triplet symmetrically shared on the L and M halves of the dimer [62]. Fig. 9 illustrates the close correspondence between the experimental axes and the idealized 'trial' axes used in the comparisons for both species. Despite the closeness of the approach, however, the misalignment [62] still exceeded the experimental uncertainties of the measured axis directions [24,61]; moreover, none of the trial limiting cases produced the correct experimental ZFS. Much better agreement with the experimental measurements resulted when

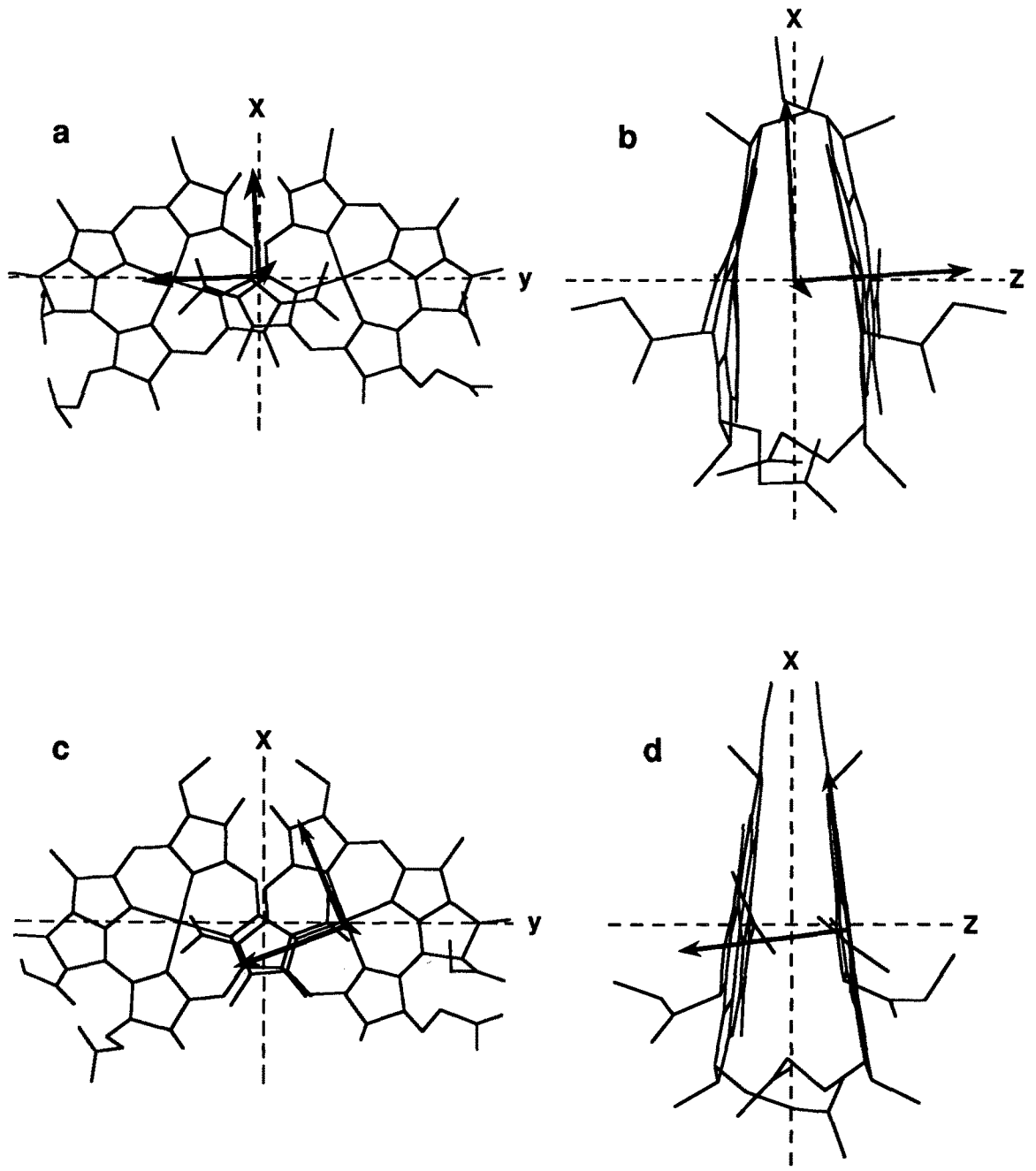

Fig. 9. Comparison of the experimentally measured zero-field axes (arrows) with the molecular structure of the primary donor dimers from *Rb. sphaeroides* R-26 (a and b) and *R. viridis* (c and d). Dashed lines represent the 'average' monomer x, y and z zero-field axes for a dimer triplet state equally shared on the two monomers. View is along the average zero-field z axis for (a) and (c) and along the average zero-field y axis for (b) and (d). The experimental axes measured for *R. viridis* are located at the Mg atom of $BChl_L$ to emphasize their overlap with the monomer zero-field axes.

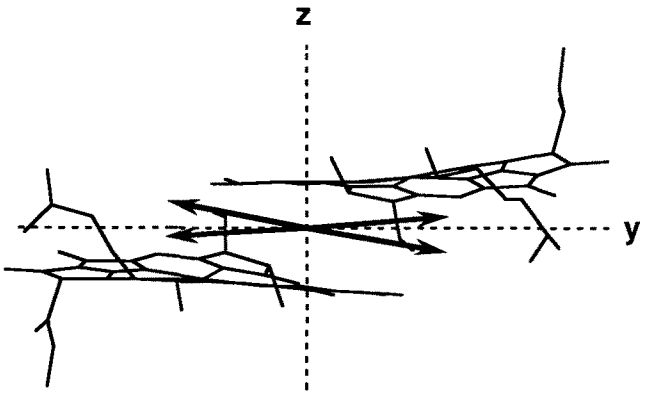

Fig. 10. Comparison of the transition dipole direction of the redmost absorption with the molecular structure of the primary donor. The two arrows represent the two possible orientations measured by magnetophotoselection experiments in reference [138] and the dashed lines indicate the 'average' z and y axes of the two monomers. The theoretical direction for the transition dipole is close to the average y axis [83,84,86].

a variable degree of triplet delocalization and charge-transfer contributions were introduced into the model [62]. Exciton model calculations for ^{3}P are discussed in greater detail below.

In addition to furnishing a clearer picture of the ^{3}P state, the single crystal EPR results may be used to relate the structure directly to spectroscopic features of the RC that had previously only been determined relative to the ^{3}P zero-field axes. As an example, we will project the 870 nm transition dipole moment of P determined by magnetophotoselection [138] onto the molecular structure of P, as shown in Fig. 10. This direction is given simply by the product $\mathbf{R}(\phi,\theta,\psi)\mathbf{L}$, where $\mathbf{L}$ is a column vector of the transition moment direction cosines (l_x,l_y,l_z) in the zero-field axis frame. Since magnetophotoselection determines only the absolute values of l_x, l_y, and l_z, in general four possible combinations of their relative signs must be considered. However, the experimental value for l_x is nearly zero *, leaving only the two vectors shown in Fig. 10. According to exciton calculations, the 870 nm transition consists almost entirely of equal contributions from the Q_y transitions of the P dimer BChls [83,84,86]; thus, its transition dipole should lie along the y symmetry axis of the dimer, very close to one of the experimental axes shown in Fig. 10.

IV-A.4. ODMR structural studies

The inherent high resolution of zero-field ODMR has permitted very detailed characterization of ^{3}P structure in both intact whole cells and isolated RCs. FDMR signals from whole cells are opposite in sign to those from RCs because the observed fluorescence arises from antenna BChl rather than P. Since energy transfer from the antenna BChl to P competes with fluorescence, the emission intensity will vary *inversely* as the concentration of ground state P according to the Vredenberg-Duysens relation [233]. Thus, in whole cells or chromatophores, a microwave-induced increase in the concentration of ground state P is observed as a decrease in fluorescence [234–237], with the exception of *R. viridis*, where the antenna fluoresces to the red of P and does not transfer energy at low temperature [238]. In isolated RCs, the observed fluorescence is directly proportional to the ground state P concentration [239,240]; however, negative FDMR signals have been detected in isolated RCs [239,240] and even RC crystals [241], indicating the presence of contaminating pigments bound to the RC which can transfer excitation energy to P.

In general, FDMR resonance lines of ^{3}P are much narrower than those of ^{3}Chl in a glassy matrix, demonstrating the relative homogeneity of the RC protein environment. Nevertheless, the Gaussian lineshape of the $|D|+|E|$ and $|D|-|E|$ lines suggests they are still inhomogeneously broadened. The inhomogeneous contribution to the linewidth has been estimated by hole-burning experiments [236] in which saturating microwaves are applied at the center frequency of a line and the line is scanned with a second microwave source. The homogeneous linewidth reflected by the width of the saturated 'hole' is generally about 10% of the total linewidth [236,240].

Typically, the $|D|+|E|$ line of ^{3}P is somewhat broader than the $|D|-|E|$ line, indicating a degree of positive correlation between the distributions in $|D|$ and $|E|$ which cancels in the $|D|-|E|$ line. The correlation is even more apparent in double resonance FDMR experiments [236,240,241] in which one of the $|D|+|E|$ or $|D|-|E|$ transitions is saturated and the $|2E|$ transition scanned with a second microwave source. With this increased selectivity, it has been possible to resolve distinct sets of $|D|$ and $|E|$ values; at least two separate forms of ^{3}P have been detected in RCs and intact whole cells of *Rb. sphaeroides* and *R. viridis* [236,240,241].

FDMR has been used to make inferences about the environment of the antenna BChl. Surprisingly, even at 1.5 K, the microwave-selected fluorescence band is nearly as broad as the unselected fluorescence spectrum from whole cells in a number of species [242]. Since the width of the fluorescence is assumed to arise from a distribution of local environments, this result means that the excitation energy must visit many sites before becoming trapped by P. Such widespread delocalization at 1.5 K requires either strong coupling among the antenna to permit long-range excitation transfer, or significant spectral overlap between nearest antenna neighbors. Hoff and de Vries [242] suggested the latter

* The definitions of zero-field x and y axes used here are reversed from Ref. 138 to conform to the labeling of the optical transitions.

of these possibilities as more likely, based on the relatively broad phonon wings observed in site-selected BChl absorption spectra [243].

ADMR studies of ^{3}P have offered still further insight into the structure of the RC [244,245]. Similar to FDMR results, double resonance ADMR studies have indicated inhomogeneous broadening of the ZFS [244] and revealed several distinct forms of ^{3}P in the RC [238,246]. Microwave- and wavelength-selected ADMR experiments have correlated $|D|$ with the redmost P absorption wavelength: lower $|D|$ values are associated with lower energies of the S_1 state [238,246], just as for ^{3}Chl in a glassy matrix [122]. The selection studies also indicate inhomogeneity in the red P absorption band, which shifts and narrows when specific values of $|D|$ and $|E|$ are selected [238,246]. This result may be compared with photochemical hole-burning studies [247–249], in which the P absorption also shifts and narrows slightly with different narrow-band excitation wavelengths, but which have been interpreted as reflecting a predominantly homogeneous linewidth in the P absorption band.

Among the most useful features of ADMR are the triplet minus ground state singlet (^{3}P – P) optical difference spectra that can be obtained using a lock-in amplifier and modulated microwave power [245,250]. Such spectra have been obtained from both RCs and whole cells from a number of different species, and they compare quite favorably with ^{3}P – P and P^+ – P difference spectra obtained by flash photolysis methods [98,251,252] in terms of both sensitivity and spectral resolution. Thus, ADMR permits detailed observation not only of the spectral properties of ^{3}P and P, but also those of the neighboring RC pigments that are associated with the presence of ^{3}P or P.

The main features of the low temperature ^{3}P – P spectrum in the vicinity of the BChl Q_y absorption are best exemplified in *R. viridis* [245,250]. They include (1) a bleaching of the 1000 nm absorption band of P; (2) the appearance of a BChl monomer band at 830 nm; (3) the appearance of a BChl monomer triplet-triplet absorption at 870 nm; and (4) a blue shift of the 830 and 855 nm absorption bands attributed to the accessory BChls in the RC ground state. The appearance of the 830 nm absorption is particularly significant because it appears to arise from one of the P dimer BChls in its ground state [245,250]. This indicates that the triplet excitation is localized on half of the dimer on an optical timescale, and it suggests that a comparision of features (2) and (3) above may indicate the extent of delocalization on longer timescales [250]. In addition, structure often appears on the long-wavelength bleaching as a red shoulder or separately resolved peak [238,246,250]; this feature has been ascribed either to a charge-transfer state [238,246] or to heterogeneity in the RC environment [250]. Recent photochemical hole-burning studies tend to support the first of these possibilities [249]. The ^{3}P – P spectra from other species exhibit similar trends to those just described, although some features are less clear because of spectral overlap between P and the accessory BChls, or different degrees of triplet delocalization [250].

Structural information from ADMR may be enhanced further by measuring the linear dichroism of the absorbance changes relative to the $\mathbf{B}_1$ field direction of linearly polarized microwaves (LD-ADMR) [253,254]. The microwaves select a $\cos^2\theta$ distribution of one of the zero-field axes with respect to the $\mathbf{B}_1$ direction. The specific axis chosen depends on the microwave frequency; for example, the $|D|+|E|$ and $|D|-|E|$ transition frequencies correspond to the **x** and **y** axes if $|D|-|E|>0$. Once linear dichroism measurements are obtained with respect to two zero-field axes, the orientation of the transition dipoles of the ^{3}P – P spectrum can be determined relative to the zero-field axes of ^{3}P with reasonable accuracy. Since the directions of the ground state transition dipoles have also been calculated relative to the crystal structure [83,84,86]. LD-ADMR in principle provides enough information to estimate the ^{3}P zero-field axes directions relative to the RC atomic coordinates [255–258]. The quantitative results from such studies are included with the model results discussed in the next section.

IV-A.5. Exciton models of primary donor triplet structure

Several applications of the exciton model presented in Section II to the bacterial primary donor have been reported, based on the ^{3}P zero-field axes measured directly by single crystal EPR [62] or calculated from LD-ADMR spectra [255–258]. For purposes of comparing these results, we will standardize the reported model parameters according to the convention of Scherer and Fischer [256]; they include the symmetry parameter ζ (which is -1 for localization on $BChl_M$, $+1$ for localization on $BChl_L$, and 0 for a fully delocalized triplet) and the fraction of charge transfer character, CT. With reference to the model presented in Eqns. 15 and 16, assuming $M_1 = BChl_L$, $M_2 = BChl_M$, and neglecting the index i, then $\zeta \equiv (c_2 - c_1)/(c_2 + c_1)$, and $CT = c_3$, c_4, or some undetermined combination of them. The **D** tensor can then be calculated from these coefficients and the known geometry of the P dimer according to Eqn. 17. The $\mathbf{D}^{(j)}$ tensors for the charge-transfer configurations are constructed by summing over the interactions of discrete point-dipoles [224] distributed at the atomic coordinates of the conjugated ring members, and weighted by spin densities calculated for the appropriate $BChl^+$ and $BChl^-$ [259].

The most critical experimental results to model are the direction cosines of the zero-field axes and the magnitude of D. The ζ and CT parameters affect these quantities in very different ways. The delocalization

TABLE I

Orientation of primary donor triplet zero-field axes in R. viridis and Rb. sphaeroides R-26 [a]

Axis	*R. viridis*					*Rb. sphaeroides* R-26					Ref.
	x	y	z	ζ	CT	x	y	z	ζ	CT	
C_2	50	55	59 [b]								
				−0.5	–						[255]
$P^{(-)}$	61	39	66 [b]								
C_2	40 [c]	50 [c]	85			15 [c]	90 [c]	75			
				−0.6	0.30				+0.4	0.18	[256]
$P^{(-)}$	60 [c]	40 [c]	65			90 [c]	5 [c]	82			
C_2	14 [d]	80 [d]	84 [d]								
				−1.0 [e]	–						[258]
$P^{(-)}$	80	11	82 [d]								
C_2	23	68	83			4	88	93			
				−1.0	0.23				−0.3	0.13	[62]
$P^{(-)}$	68	22	89			93	4	87			

[a] For comparison, angles are given as $\cos^{-1}|l|$, where l is the cosine of the angle between the indicated directions.
[b] Calculated from the other two angles shown.
[c] The x and y defined in Ref. [256] have been interchanged to correspond to $E > 0$.
[d] Calculated from data shown in Fig. 3 of Ref. [258].
[e] Assumed value.

introduced by small (< 25%) amounts of charge transfer reduces D, but exerts only a weak influence on the directions of the calculated ^{3}P zero-field axes; in contrast, ζ strongly influences the zero-field axes, but does not significantly affect D since the monomer **z** axes are within 15° of parallel. Thus, nearly independent determination of the two model parameters is possible.

Table I summarizes the various measurements of ^{3}P zero-field axis orientations, together with the ζ and CT parameters derived from them. The orientation angles are reported with respect to the directions of the C_2 symmetry axis and the redmost transition dipole of P (denoted $P^{(-)}$), which correspond closely to the **x** and **y** axes of a triplet symmetrically shared on P. As Table I shows, the calculations agree on the gross qualitative features of ^{3}P in *R. viridis* and *Rb. sphaeroides* R-26, and they all include a significant degree of charge transfer to account for the low D value in both species, with *R. viridis* requiring a somewhat greater contribution. Moreover, although only one of these studies took into account possible rotation of the monomeric ^{3}BChl **x** and **y** axes from the Q_x and Q_y directions [256], the good agreement between calculated and experimental axes, especially those from the single crystal EPR of *R. viridis*, suggests that the rotation is small.

The reported models diverge significantly in their details; in particular, the zero-field axes reported by Fischer and co-workers differ substantially from the EPR values. The differences result in some serious qualitative discrepancies: the ζ parameters derived from EPR fall outside the rather wide ranges of solution given by Scherer and Fischer for both organisms [256], and in the case of *Rb. sphaeroides*, these authors find slightly more localization on $BChl_M$ rather than $BChl_L$. Analysis of the same LD-ADMR data by Lous and Hoff [258], corrected for microwave saturation effects, yield results much closer to the EPR measurement for *R. viridis*.

These discrepancies point out the complications and ambiguities that may arise from the large number of parameters needed to model LD-ADMR spectra; however, the reasonable agreement between the results of references [258] and [62] demonstrates that LD-ADMR can provide a quite adequate picture of triplet state structure when properly interpreted. Although highly detailed triplet structural studies may require the greater accuracy of single crystal EPR, LD-ADMR promises to be an invaluable tool for investigating RCs not yet available in single crystals.

IV-A.6. Weaknesses of the exciton model

There is a mounting collection of evidence that the exciton model just discussed is at best an incomplete picture of ^{3}P structure. Shuvalov and Parson suggested that ^{3}P consists of an equilibrium mixture of the dimer triplet and the state $^3(P^+BChl^-)$ based on the temperature dependence of the 800 nm bleaching in the ^{3}P optical difference spectrum [98]. Evidence against this possibility has come from direct-detection EPR of ^{3}P at temperatures up to room temperature. Above 100 K, D gradually increases up to ~ 5% larger than its low temperature value [164,166]. This is contrary to the reduction in D one would expect from increased electronic separation in a thermally accessible charge-transfer state, and would appear to rule out the proposed equilibrium mixture. However, the results still admit a *coherent* inclusion of charge transfer in ^{3}P.

A major unanswered question is the identity of the putative charge transfer state inferred from exciton model calculations. Because small charge-transfer contributions do not significantly affect the zero-field axes of ^{3}P, such calculations cannot unambiguously identify the state, and most treatments tacitly assume the intradimer charge-transfer configurations discussed above. However, Stark spectroscopy [260,261] and detailed MO calculations of the RC [262] have shown that charge transfer configurations between $BChl_L$ and $BChl_M$ make significant contributions to the *singlet* excited state of P. This suggests that the analogous triplet configurations should also be close to ^{1}P in energy, too far from ^{3}P to account for the required amount of triplet charge transfer.

Additional evidence regarding charge-transfer contributions comes from phosphorescence studies, which have permitted accurate estimates of the energies of ^{3}P in *R. viridis, and Rb. sphaeroides* R-26 [104], and a

variety of BChls [105] relative to their ground states. These measurements have shown that the energy difference between the first excited singlet and triplet states is much smaller in P than in BChl. Although this difference probably reflects mainly the red shift of ^{1}P by singlet exciton interactions, it is superficially consistent with the notion of charge transfer character in both singlet and triplet P. However, other features of ^{3}P phosphorescence are less consistent with charge transfer character [104]. The ^{3}P phosphorescence peak is much narrower than the fluorescence and absorption bands of ^{1}P and P, and its wavelength is much more weakly dependent upon temperature. These features indicate that ^{3}P interacts less with its protein environment than ^{1}P, which suggests it has a smaller electric dipole moment and less charge transfer character.

The increase of D with temperature presents a different structural riddle. Within the framework of the exciton model, it is difficult to imagine a reasonable explanation without invoking a large-scale structural rearrangement. One suggestion, based on the closely spaced energies of ^{3}BChl and ^{3}P [105], is that D increases because of thermally activated hopping of the triplet excitation onto the M-side accessory BChl.

A further consideration is spin-orbit coupling, which has not yet been included in detailed theoretical models of ^{3}P. Even the spin-orbit coupled decay rates of ^{3}P and ^{3}BChl have so far been neglected in exciton calculations for ^{3}P. It has already been pointed out [39] that spin-orbit terms may be non-negligible in any consideration of the reduced ZFS of ^{3}P, by analogy with the metal-centered L_zS_z coupling between the two lowest triplet states that exerts a significant influence on the ZFS of Zn-porphin. Another way in which spin-orbit coupling could influence the ZFS of ^{3}P is via interaction with the lowest excited singlet (S_1) state [202,203], similar to that discussed for monomeric ^{3}Chl in Section III.

In both of these cases, the ZFS are changed by a second-order shift in the energies of selected spin sublevels as a result of spin-orbit mixing. It should be noted that a given spin sublevel is coupled to triplet and singlet states by different components of the $\mathbf{L}\cdot\mathbf{S}$ operator, since intersystem coupling requires the antisymmetric component of the $\mathbf{S}$ operator (cf. Eqn. [13]). Thus, the $|t_x\rangle$ and $|t_y\rangle$ sublevels of different triplet states are mixed by L_zS_z, whereas they are coupled to singlet states by L_xS_x and L_yS_y, respectively. Furthermore, triplet-triplet interactions will not be reflected directly in the rates of intersystem crossing, whereas mixing with the S_1 state will in general also affect the rates of spin sublevel population. This distinction does not apply in the special case of ^{3}P, which is not populated by spin-orbit coupled ISC.

While there is no definitive evidence with regard to either triplet-triplet or triplet-singlet spin-orbit coupling effects on the ZFS of ^{3}P, at present the latter type of interaction seems more likely to account for experimental observations. It is not clear that the L_zS_z-mediated triplet-triplet coupling observed in Zn-porphyrins will be significant in Mg-chlorophylls. This type of interaction requires appreciable contribution of the metal d-orbitals in the $\pi\pi^*$ MOs of the ring, whereas the contribution of the empty d-orbitals of Mg is expected to be quite small in BChl. Moreover, the heavy atom effect [64] would greatly attenuate any Mg-centered coupling relative to the heavier Zn atom. Finally, it seems unlikely that the large reduction of the ^{3}P ZFS relative to in vitro ^{3}BChl can be explained in terms of triplet-triplet interactions, since the triplet state energies of BChl appear to be only weakly affected by the protein environment [105].

Spin-orbit coupling between T_1 and S_1 remains an alternative possibility. The ZFS of both ^{3}BChl and ^{3}P are well correlated with the wavelength of their respective S_1 state energies, which are reflected by the wavelength of the redmost Q_y absorption [238,246,250]. This correlation appears to be maintained in the light-harvesting BChls of *Rb. sphaeroides* and *R. capsulatus* $A1a^+$, in which both the triplet D values and fluorescence wavelengths are intermediate to those of ^{3}P and ^{3}BChl in vitro [263]. In the simplest model, T_1 would be couipled to S_1 mainly through the L_xS_x and L_yS_y terms, so that a decrease in the $S_1 - T_1$ energy difference would shift $|t_x\rangle$ and $|t_y\rangle$ closer to $|t_z\rangle$ in energy, reducing the D ZFS of T_1. Thus, the red shift of the lower exciton state of ^{1}P relative to ^{1}BChl might account for the reduction in the ^{3}P ZFS relative to ^{3}BChl, including the different reduction factors for BChl *a*- and BChl *b*-containing organisms, without any need to invoke charge transfer character in ^{3}P. Such a mechanism could also explain the observed temperature dependence of D in terms of the known red shift of ^{1}P at lower temperatures [264]. Nevertheless, there are alternative mechanisms that might explain the correlation between D and S_1 energy (cf. Section III), and it is not clear that the L_xS_x and L_yS_y interactions are strong enough to account for the large observed changes in ZFS.

It is apparent that no one of these proposals can explain all the observed structural properties of ^{3}P, and further detailed investigations are needed to formulate a more comprehensive model. Temperature studies using ADMR and single-crystal EPR should be particularly helpful in evaluating the various possibilities.

IV-B. Kinetics of the primary donor triplet state

One of the most important results from early triplet state studies of in vivo systems was the elucidation of the triplet formation mechanism in the bacterial RC, which provided strong evidence for an intermediate radical pair (RP) as the essential step in the initial

photosynthetic light reaction. Since the RP model has provided the basis for numerous recent triplet state investigations of the bacterial RC, it is worthwhile to recapitulate its emergence from the early studies.

IV-B.1. The radical pair mechanism

The intense and distinctive spin polarization of the ^{3}P EPR spectrum provided the first evidence that more than one molecule was involved in ^{3}P formation [265]. The EPR signal from ^{3}P was over 20-times stronger than in vitro ^{3}Chl signals; more significantly, the six lines observed in the EPR spectrum of isotropically oriented ^{3}P exhibited a polarization pattern distinct from that observed for any ^{3}Chl in vitro [266]. From low to high field, the EPR peaks follow the pattern AEEAAE, where A represents an absorptive and E an emissive peak [26]. Such a pattern arises when peaks corresponding to a given $\Delta m_s = 1$ transition (I or II) all have the same polarization (cf. Fig. 6). Thus, the observed ESP of ^{3}P suggests an ISC mechanism selective with respect to the *high-field* spin states; indeed, there is no way that spin-orbit coupled ISC, which is selective with respect to the zero-field states, can produce the same relative high-field spin state populations at all orientations.

As Fig. 11 shows, the observed ^{3}P ESP pattern can arise in two cases: either (1) $D > 0$ with $|t_0\rangle$ overpopulated with respect to $|t_\pm\rangle$ at all orientations, or (2) $D < 0$ with $|t_\pm\rangle$ overpopulated with respect to $|t_0\rangle$. The sign of D was determined in a spin relaxation study [267] carried out at a light modulation frequency fast enough to 'freeze out' effects of $\Delta m_s = 1$ spin relaxation, but slow enough to observe $\Delta m_s = 2$ relaxation. No relaxation-induced asymmetry of the EPR intensities was observed at very low microwave powers; only at higher microwave powers, when significant population is transferred to $|t_\pm\rangle$ did such effects appear. Since relaxation effects would be discernable at all microwave powers if $|t_\pm\rangle$ were initially populated, this result established $|t_0\rangle$ as the preferentially populated high-field state. We will refer to this condition as 't_0-polarization' of ^{3}P.

The t_0 polarization led to the proposal [266] that ^{3}P is formed by a radical pair mechanism similar to that originally used to describe chemically induced dynamic nuclear polarization (CIDNP) [268,269]. The mechanism requires formation of a radical pair in which ISC occurs as a result of the different magnetic environments of the two radicals, followed by RP collapse to form ^{3}P and other reaction products. Since RP creation and annihilation are fast (i.e., nonadiabatic) relative to the electron spin motion, they do not affect the correlation of the two electron spins; thus the RP is formed with its spins correlated as in the precursor state, and the product spin states reflect the ISC that developed in the RP. Thus, the observed ESP of ^{3}P could be explained by $|s\rangle - |t_0\rangle$ ISC in the primary RP, which is typical of weakly interacting, correlated RPs at standard EPR fields.

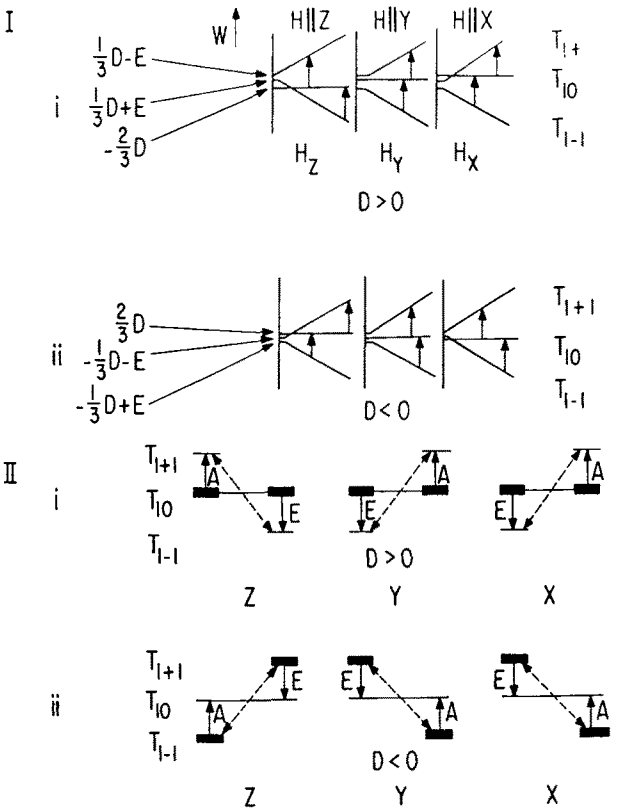

Fig. 11. Energy level diagram showing the two possible explanations for the electron spin polarization pattern observed in the bacterial primary donor (cf. Fig. 6). Vertical arrows indicate microwave transitions. (I) shows how the $|t_0\rangle \leftrightarrow |t_{+1}\rangle$ and the $|t_{-1}\rangle \leftrightarrow |t_0\rangle$ transitions are interchanged by a change in the sign of D. In (II), the heavy lines denote relative overpopulation of the indicated spin sublevel that produce absorption (A) and emission (E) EPR peaks. The dashed lines in (II) corresponds to $\Delta m_s = 2$ spin relaxation.

The components of the RP were identified by transient optical difference spectroscopy. At low redox potential Parson et al. [270] observed two transient states they called 'P^F' ('fast') and 'P^R' ('relaxed') and, noting a similarity between the spectra of P^R and ^{3}BChl in solution, suggested that P^R was the ^{3}P state observed by EPR. Subsequent picosecond spectroscopy on unblocked RCs showed P^F to be a short-lived intermediate in the primary light reaction, whereas the triplet did not appear [18]. The difference spectrum of P^F corresponded well with the spectrum of BPh^- in vitro [271], implicating the (P^+ BPh^-) radical ion pair as the intermediate in both triplet formation and charge separation.

Fig. 12 summarizes the sequence of events following photoexcitation of blocked RCs that was established on the basis of the t_0 polarization and flash photolysis experiments. The excited singlet state ^{1}P* transfers an electron to form ^{1}(P^+BPh^-), where the $|s\rangle$ and $|t_0\rangle$

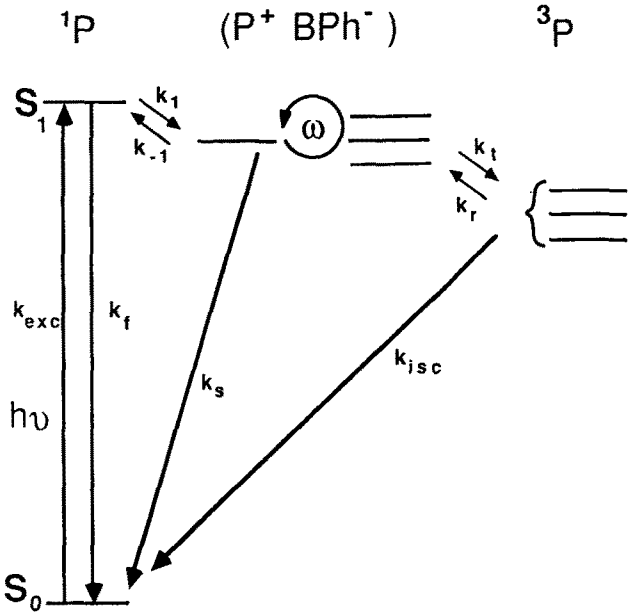

Fig. 12. Kinetic scheme for formation of the primary donor triplet by the radical pair mechanism in bacterial reaction centers where secondary electron transfer has been blocked by removal or prior reduction of the quinone.

RP spin states are mixed by differences in nuclear hyperfine interactions and, at higher fields [272] a difference in the electronic g-factors of P^+ and BPh^-. Since charge separation cannot proceed, the charges recombine to produce P (or ^1P) from the $^1(P^\ddagger BPh^{\bar{}})$ state, and ^3P from the $^3(P^\ddagger BPh^{\bar{}})$ states. The different free energies of the products dictate the different recombination rate constants for singlet and triplet RP states, represented by k_s and k_t in Fig. 12.

IV-B.2. Triplet state investigations of primary charge separation

One of the central problems in the study of photosynthetic light reactions has been to characterize those features of the RC that permit it to carry out fast, efficient charge separation. Many recent triplet studies of the bacterial RC have focused on this problem by exploiting the fact that the mechanisms of ^3P formation and primary charge separation share the intermediate RP state, $(P^\ddagger BPh^{\bar{}})$. Because of this intimate connection, ^3P has served as an invaluable probe into the energetics and mechanism of primary charge separation in photosynthesis.

Two related experimental techniques have been applied to study the magnetic interactions within the $(P^\ddagger BPh^{\bar{}})$ state that form ^3P. Both methods rely on the dependence of ^3P yield upon the strength of an applied magnetic field [273,274], by analogy with effects observed for radical reactions in solution [275–279]. Here we present a brief summary of results from such studies, highlighting those features most relevant to the rate and mechanism of ^3P formation in RC's; more detailed treatments may be found in several recent reviews [280–283].

The effect of an applied magnetic field can be qualitatively understood as follows. At zero field, the RP spin states are close in energy and mixed together by nuclear HFI in a complicated way, so that ISC occurs to all three RP triplet states. As the triplet states become quantized along the direction of an applied magnetic field $\mathbf{B}_0$ $|t_+\rangle$ and $|t_-\rangle$ are removed by the Zeeman energy, and only $|t_0\rangle$ is close enough to interact appreciably with the initially populated $|s\rangle$ state. Thus, in general ISC is slowed by the application of a magnetic field, which results in a decreased yield of ^3P. However, in special cases, spin-spin interactions within the radical pair can result in a resolvable 'level crossing' between $|s\rangle$ and $|t_+\rangle$ or $|t_-\rangle$, which results in an initial increase in the ^3P yield as the $\mathbf{B}_0$ field is applied. One important such interaction is electron spin exchange, which results in a $|s\rangle - |t_0\rangle$ energy gap of $2J$. Under favorable conditions, it is sometimes possible to observe a 'peak' at $B_0 = |2J|/g_e\beta_e$ in the B_0 profile of radical pair ISC-induced triplet yield [232,274,284]. Finally, ^3P yield also increases at very high fields (greater than 1 T) because of the g-factor difference between $P^\ddagger$ and $BPh^{\bar{}}$, Δg. For sufficiently large $\mathbf{B}_0$, radical pair ISC becomes dominated by $\Delta g\beta_e\mathbf{B}_0$ mixing, and it can be much faster than the ISC at lower $\mathbf{B}_0$ fields, which is governed mainly by nuclear hyperfine interactions [272].

A related experiment is reaction yield detected magnetic resonance (RYDMR) [285], where microwaves are applied during the $(P^\ddagger BPh^{\bar{}})$ lifetime and the ^3P yield monitored optically as the static field $\mathbf{B}_0$ is swept through resonance. At low microwave powers, a microwave resonance causes transitions between the $|t_0\rangle$ and the $|t_\pm\rangle$ RP spin states, which transfers population to the $|t_\pm\rangle$ levels and increases the ^3P yield. Thus, two RYDMR peaks, corresponding to the $|t_+\rangle$ and $|t_-\rangle$ transitions, should in principle be observable; however, only one peak is resolved for $(P^\ddagger BPh^{\bar{}})$ because the spin-spin interactions and Δg in this radical pair are smaller than the EPR linewidths of the individual $P^\ddagger$ and $BPh^{\bar{}}$ radicals.

At high microwave powers, when the microwave field $\mathbf{B}_1$ dominates the other magnetic interactions within $(P^\ddagger BPh^{\bar{}})$, the RYDMR spectrum is 'inverted' (i.e., the resonance is observed as a *decrease* in the ^3P yield) [286–288]. This behavior cannot adequately be explained in terms of simple microwave transition probabilities; instead, for the special case of $(P^\ddagger BPh^{\bar{}})$ it is most convenient to consider the RP spins in a new basis set, $|s\rangle$, $|t'_+\rangle$, $|t'_0\rangle$, and $|t'_-\rangle$, defined in a rotating reference frame with **z** along the $\mathbf{B}_1$ field [287,289,290]. This picture makes clear the analogy between the $\mathbf{B}_1$ dependence of the ^3P yield measured at the center of the RYDMR peak and the static $\mathbf{B}_0$ field effect discussed above: as $\mathbf{B}_1$ is increased, the electron spins

become quantized along **z** in this frame, thus removing $|t'_+\rangle$, and $|t'_-\rangle$ from $|s\rangle$ in energy and reducing the ^{3}P yield. (This corresponds to an inhibition of ISC between $|s\rangle$ and the laboratory-frame $|t_0\rangle$ state.) A 'peak' may also be resolved in the $\mathbf{B}_1$ profile; that is, the ^{3}P yield increases until $B_1 = |2J|/g_e\beta_e$, [289–291] and then decreases at higher B_1, leading eventually to the inverted RYDMR spectrum.

In addition to affording an accurate measurement of the spin exchange energy $|2J|$ in (P^+ BPh^-), both magnetic field and RYDMR effects are quite sensitive to the rate constant k_t for ^{3}P formation (cf. Fig. 12) [274,292,293]. The temperature dependence of k_t measured from such effects shows that this electron transfer is activationless [294], or only weakly activated [289]. This result, together with the temperature-independent $|2J|$ measured in (P^+ BPh^-) [232,295,296] and careful measurements of the ^{3}P energy level (discussed below), has provided new insights into the detailed mechanism of primary electron transfer [297–300]. In particular, these features suggest that electron transfer from P to BPh_L does not proceed via a two-step mechanism involving $BChl_L$ as a short-lived intermediate acceptor [301,302], but rather via a concerted 'superexchange' mechanism [297–300] in which $BChl_L$ enhances the electronic coupling between P and BPh_L.

EPR studies of ^{3}P have recently been used to investigate a different type of magnetic interaction in the precursor (P^+ BPh^-) radical pair. In Q (menaquinone)-reduced RCs of *R. viridis* and *C. vinosum*, ^{3}P exhibits the standard t_0 ESP at low temperature, but a remarkable inversion occurs in the polarization of the two central peaks above 20 K [303]. This effect is abolished when Q is doubly reduced [304], or when Q or the associated Fe^{2+} ion are removed from the RC [305]. Furthermore, the effect is enhanced in RCs of *Rb. sphaeroides* R-26 when the native ubiquinone is replaced with menaquinone, which is known to have a larger magnetic interaction with BPh^- [306]. These results suggest that the observed ESP reflects spin-spin interaction between the (P^+ BPh^-) RP and the singly reduced Q^- radical, combined with the large *g*-anisotropy and fast spin relaxation of Q^- due to its interaction with the Fe^{2+}. Time-resolved EPR of ^{3}P in *R. viridis* RCs [307] has verified that the polarization arises in the precursor RP state, and also revealed spin lattice relaxation in ^{3}P that most likely arises from activated repopulation of (P^+ BPh^-) from ^{3}P (discussed below). The strong orientation dependence of the ESP inversion has been attributed to large magnetic anisotropy of the Q^-Fe^{2+} complex on the basis of model calculations [308].

IV-B.3. Decay mechanism of the primary donor triplet

Although ^{3}P is populated by radical pair ISC, its decay mechanism at low temperatures is similar to the spin-orbit ISC of ^{3}BChl in vitro. Initial measurements of the zero-field spin state decay rates gave disparate results, depending upon the experimental technique used. The values reported by Clarke and co-workers [234,235] using the equilibrium method gave consistently smaller rate constants than the pulsed microwave studies of Hoff [236]. These discrepancies have been exhaustively explored by Hoff [39,207], who concluded that the equilibrium measurements were in error, probably because insufficient microwave power was used. One interesting feature of low temperature ^{3}P decay is the large isotope effect observed in deuterium-substituted bacteria [237]. The decay rates are decreased by nearly a factor of two, much larger than the 20% reduction observed in deuterated ^{3}Chl [212].

At higher temperatures, ^{3}P decay is remarkably different from in vitro ^{3}BChl. Chidsey et al. [91] first observed that the overall decay rate of ^{3}P near room temperature depends upon the strength of an applied magnetic field. Since the field dependence was similar to that of ^{3}P yield formed via (P^+ BPh^-), they proposed that (P^+ BPh^-) was also an intermediate in the *decay* of ^{3}P. Thus, at high temperatures, ^{3}P decay proceeds by thermal repopulation of the (P^+ BPh^-) state (indicated by k_r in Fig. 12), ISC from the $|t_0\rangle$ to the $|s\rangle$ RP state, and subsequent decay via the k_s pathway. As the temperature is reduced, the (P^+ BPh^-) state becomes thermally inaccessible, and ISC proceeds by the usual spin-orbit mechanism. The temperature dependence of the ^{3}P decay rate was used to estimate the free energy difference between the ^{3}P and (P^+ BPh^-) states [91]. The field profile of the ^{3}P decay rate also appears to depend on the redox state of Q: in the presence of diamagnetic Q^{2-}, it resembles that of Q-depleted RCs, but becomes much broader (i.e. requires higher fields to reduce the triplet decay rate) in the Q^- state [309]. This is analogous to changes in the magnetic field dependence of ^{3}P yield with respect to the Q redox state [280].

Subsequent analysis of ^{3}P decay rates at high magnetic fields has refined this estimate [93]. For the simple kinetic scheme shown in Fig. 12, Chidsey et al. [91] showed that the triplet decay rate should vary linearly with the triplet yield at at a given temperature. Deviations from a linear relationship have been explained by nuclear spin polarization (CIDNP) of P and BPh.[92,93] Immediately after (P^+ BPh^-) decay, the RCs in the ^{3}P and ground states will have nuclear spin state populations corresponding to relatively fast and slow $|s\rangle - |t_0\rangle$ ISC, respectively. Thus, radical pairs repopulated from ^{3}P will undergo $|t_0\rangle - |s\rangle$ ISC faster than than the initial $|s\rangle - |t_0\rangle$ ISC that formed ^{3}P at an equilibrium nuclear spin distribution, and ^{3}P lifetime will not be strictly linear with ^{3}P yield. This effect disappears at very high fields, where ISC depends upon $\Delta g\beta_e\mathbf{B}_0$ rather than the nuclear spin distribution. Thus,

the $^3P - (P^+ BPh^-)$ free energy difference may be accurately estimated by the temperature dependence of ^3P decay at high fields, without complicating CIDNP effects [93]. This result, combined with measurement of ^3P phosphorescence [104], has provided perhaps the most accurate estimate of enthalpy and entropy differences between $(P^+ BPh^-)$ and the ground state, permitting more detailed analysis of primary electron transfer.

A number of anomalies in ^3P decay have been reported that may indicate extra states or pathways in the reaction scheme. Chidsey et al. [310], noting that the experimental ^3P quantum yield is significantly lower than the theoretical value, postulated additional triplet state decay pathways to account for the difference. Specifically, they proposed a charge-transfer triplet state involving radicals with non-parallel π-electron systems that could introduce fast spin-orbit coupling to the ground state [80,81], and they discussed several reaction schemes that could accommodate such an intermediate. No direct spectroscopic evidence for such intermediates has been reported; in light of the high temperature ^3P decay mechanism just discussed, it may be necessary to re-evaluate the theoretical ^3P yield, including spin-lattice relaxation effects.

Other ^3P decay mechanisms have been suggested. RYDMR spectra of the $(P^+ BPh^-)$ state [286,311] exhibit a broad background signal that has been attributed at least in part to ^3P; corresponding broad features have also been reported in some magnetic field studies [312]. It has been suggested that this signal could arise from microwave saturation of the high-field spin states of ^3P, which would reduce the ^3P decay rate via repopulation of $(P^+ BPh^-)$ and $|t_0\rangle - |s\rangle$ ISC [91]. However, the signal only appears at high actinic light intensity [311], suggesting instead that it arises from triplet decay mechanisms requiring multiply excited RCs, for example, triplet-triplet annihilation.

V. Triplet state studies of higher plants

Although triplet state investigations of higher plant photosystems have not yet attained the detail of bacterial studies, much of what has been learned about the bacterial primary donor is directly applicable in higher photosynthetic organisms. (An excellent reference for recent work on plant photosystems, including comparative studies with bacterial photosynthesis is the book edited by Staehelin and Arntzen [313].) Indeed, Chl triplet states from plant Photosystems I and II exhibit some notable similarities to ^3P in bacteria. Under conditions where normal electron transport is blocked, t_0-polarized triplets have been observed in Photosystems I [27] and II [28] and also in green photosynthetic bacteria [314], providing important verification that this ESP is uniquely associated with primary charge separation. Although there are obvious differences between the photosystems of plants and purple photosynthetic bacteria, this shared characteristic indicates underlying fundamental structural requirements for efficient charge separation. Thus, the triplet states found in plant photosystems also furnish internal spin probes of the structure and dynamics of their primary photochemical apparatus. On the other hand, the relatively well-characterized properties of the bacterial primary donor offer convenient standards by which to assess differences in the behavior of triplets from the plant photosystems.

V-A. Photosystem I

The PS I RC has a number of antenna pigments which apparently share the protein environment of the primary reactants [315]. This makes it possible to detect more than one triplet state by EPR depending on the preparation studied and its redox state. In principle, then, triplet state studies of PS I not only provide details of RC structure and function, but also information about energy transfer and structure in the closely associated antenna pigments.

The current model for the sequence of the PS I primary reactants (for reviews see Refs. 316–319) can be specified as $P_{700}A_0A_1XAB$, where P_{700}, the primary electron donor, is believed to be a Chl species, the primary electron acceptor A_0 is possibly a Chl monomer, the secondary acceptor A_1 is possibly a quinone species, and X, A, and B are iron-sulfur (Fe-S) centers. P_{700} resides in a protein complex known as CP-1 or CC1 (core complex 1) [315,320] that consists of one or more polypeptides coded by the genes *psI-A1* and *psI-A2* [321,322]. A_0 is most probably located close to P_{700} in the same complex; its identification as a Chl species was made primarily on the basis of the absorption difference spectrum of $(P_{700}A_0^-)$ in flash experiments [323–326] and that of photoaccumulated $(P_{700}A_0^-)$ [327,328], which corresponds approximately to the spectrum of Chl a^- in vitro [329]. The A_1 acceptor was tentatively identified as a quinone based on its EPR [330–332] and absorption difference [333] spectra; this assignment has been verified by recent observations that reconstitution of A_1-extracted PS I particles with various menaquinones suppresses charge recombination from $(P_{700}^+A_0^-)$ and restores photochemical turnover of the Fe-S centers [334–336].

There are a number of unresolved questions about the reaction sequence given above, several of which concern the nature and number of the acceptors preceding the Fe-S acceptors and possible deviations from the linear pathway shown. The triplet state characteristics of the PS I RC and their sensitive dependence on the mechanism and kinetics of its photochemistry have

proven useful in elucidating the reaction sequence in PS I.

Triplet state studies immediately provided evidence for at least one intermediate acceptor between P_{700} and X. A t_0-polarized triplet EPR signal with ZFS comparable to monomeric ^{3}Chl *a* was first observed by Frank *et al.* in chloroplasts and PS I particles prepared with the X, A, and B acceptors in their reduced states [27]. The signal was assigned to the triplet state of a Chl species formed via recombination of a radical pair consisting of P_{700}^+ and a reduced acceptor preceding X. By analogy with bacterial RCs, it has generally been assumed that this t_0-polarized PS I triplet resides on the primary donor P_{700} [316], an assignment consistent with results from subsequent absorption difference spectroscopy [336–338].

The P_{700} triplet was also observable in PS I particles in which the X, A, and B acceptors had been removed by detergent treatment [339,340]. Reduction of such particles abolished the $^3P_{700}$ signal, producing instead an EPR signal near $g = 2.00$ that was assigned to the intermediate acceptor radical anion. However, subsequent investigation of PS I particles that did contain A, B, and X revealed two components in the $g = 2.00$ signal, which were attributed to two intermediate acceptors, named A_0 and A_1 [341,342]. Reduction of A_1 produced an increase in $^3P_{700}$ yield, which subsequently decreased upon reduction of A_0 [341]. The conclusion from these studies was that A_0 and A_1 function sequentially as electron acceptors, suggesting that $(P_{700}^+A_0^-)$ is the precursor RP of the t_0-polarized triplet in PS I.

The properties of $^3P_{700}$ formed by this reaction pathway are analogous to those of ^{3}P in the bacterial system in several other important respects. Flash absorption studies of CP1 particles lacking A_1 and the Fe-S centers [336,343,344] have shown the room-temperature lifetime of $(P_{700}^+A_0^-)$ to be 30–50 ns, comparable to the bacterial (P^+BPh^-) lifetime of 10–20 ns. In light of the similar kinetics, one might expect that the yield of $^3P_{700}$ formed by back-reaction from $(P_{700}^+A_0^-)$ would exhibit a magnetic field effect, by analogy with the bacterial RC (cf. Section IV-B.1). Such effects have been observed, first indirectly by monitoring the fluorescence from antenna Chl in preparations enriched in PS I [345,346], and more recently by directly measuring the triplet yield using absorption difference spectroscopy [344,347]. Both fluorescence [345] and triplet absorbance [347] experiments reveal a substantially larger magnetic interaction between the primary donor and acceptor radicals than is present in the bacterial system ($J/g_e\beta_e = 40$–60 G). Finally, a spin-polarized radical pair spectrum has been observed in PS I [342,348–350] that is similar to a spectrum observed in Fe-depleted bacterial RCs at low temperature [159]. By analogy with the bacterial signal, which can be assigned to (P^+Q^-), this spectrum has has been attributed to $(P_{700}^+A_1^-)$ (for a review, see Ref. 351). Thus, based upon the known reaction sequence in the bacterial RC, this similarity suggests that A_0 and A_1 could function analogously to BPh and Q in bacteria. Such results are not conclusive, since both the bacterial [352] and PS I [353] radical pair spectra can be modeled without requiring a precursor radical pair: instead, the observed ESP may be explained by assuming a small spin-dipolar interaction in the (P^+Q^-) and $(P_{700}^+A_1^-)$ radical pairs. Nevertheless, the small magnitude of the interaction that is required to model the experimental spectra from both bacterial RCs and PS I suggests that the radicals are widely spaced, consistent with the presence of an intermediate radical pair that may give rise to the t_0 polarization of the donor triplet state.

Studies of Sétif and co-workers [354,355] suggest that at room temperature $^3P_{700}$ may also be formed by recombination of the $(P_{700}^+A_1^-)$ radical pair. Under conditions where X is present but has been photochemically pre-reduced by weak illumination, flash absorption spectroscopy revealed two decay phases: a faster decay attributable to $(P_{700}^+A_1^-)$ recombination, and a slower phase that was assigned to $^3P_{700}$ decay on the basis of its absorption difference spectrum. Given that this pathway for $^3P_{700}$ formation involves radical pair ISC, one might expect the slow component to exhibit a magnetic field effect; however, none is observed [355]. It may be that the spin relaxation in $(P_{700}^+A_1^-)$, perhaps enhanced by a nearby Fe-S center, 'short-circuits' the spin state selectivity imposed by a magnetic field by destroying coherence during the radical pair lifetime. In this case the EPR spectrum of $^3P_{700}$ formed via $(P_{700}^+A_1^-)$ should not exhibit the strong t_0 polarization observed under other conditions, which may provide an experimental test for this mechanism.

The spin sublevel decay kinetics of $^3P_{700}$ have been measured by EPR [342,356] FDMR [357–359] and ADMR [360]. The EPR and ADMR values for k_x, k_y, and k_z all correspond quite well, but are significantly larger than the values determined by FDMR. The discrepancy has been attributed to the equilibrium method used in the FDMR measurements [360] (cf. section IV-B.3). Thus, accepting the ADMR values, the low temperature zero-field decay rates for $^3P_{700}$ are very close to those of monomeric ^{3}Chl in vitro [207]. The lifetime of $^3P_{700}$, like that of ^{3}P in bacterial RCs, is highly temperature-dependent, ranging from 10μs at 294 K to about 800μs below 80 K [361]. This analogy suggests that $^3P_{700}$ might decay via repopulation of a precursor radical pair as has been demonstrated in bacterial RCs; however, there is no reported experimental evidence for this mechanism in PS I.

The $^3P_{700}$ state has frequently served as a diagnostic for distinguishing photochemistry in different PS I preparations. A comparison of PS I preparations with and without the X, A, and B acceptors [316] showed that A_1 did not always act as an electron acceptor below -30°C

when X, A, and B were uncoupled. Further confirmation of these results came from experiments in which the $^3P_{700}$ yield was determined as a function of inactivation of X, A, and B by urea-ferricyanide treatment of subchloroplast particles [362]. No evidence for the participation of A_1 in PS I electron transport was apparent following the destruction of X, suggesting that A_1 is associated in some way with the X Fe-S center. This is consistent with the conclusion from ^{35}S labeling studies that the protein complex containing P_{700} is also an Fe-S protein [363].

Depending on the redox state of the RC, other triplet states are observable in PS I particles that obviously differ from the $^3P_{700}$ state. When samples are prepared in a dark redox state in which no acceptors, or only A and B, are reduced, or in which P_{700} is oxidized, then different light-induced triplet EPR signals are observed in both light modulation EPR [27,167,339,364,365] and ODMR [366] experiments. The signals show ESP characteristic of spin orbit ISC, and ZFS parameters different from those of the t_0-polarized $^3P_{700}$. The signals have been variously assigned to the triplet state of antenna Chl or carotenoid pigments [364–366], or even to the triplet state of the Chl electron acceptor, A_0 [364]. In a recent study, Regev, Nechushtai, and Levanon [167] demonstrated how one can discriminate among these different signals and the different dynamic processes of the antenna pigments using more than one EPR technique with different time responses while at the same time varying sample conditions such as temperature and redox state.

In particular, they resolved EPR signals from $^3P_{700}$, antenna ^{3}Chl, and $^3\beta$-carotene and identified the antenna ^{3}Chl as the precursor of $^3\beta$-carotene. Comparison of light-modulated and direct-detection EPR signals suggested that ^{3}Chl and $^3\beta$-carotene may decay via mutual triplet-triplet annihilation under conditions of high light flux. These experiments illustrate how new EPR methods can be used to probe the details of triplet photochemistry in vivo.

V-B. Photosystem II

Despite the current intense research focus on PS II (for recent reviews, see Refs. 318 and 367–369), published triplet state studies of PS II are ar present far less numerous than those of the bacterial RC or even PS I. There are two main reasons for this lag. First, purified, well-characterized, and photochemically active preparations of the PS II RC have been obtained only relatively recently [370], limiting their availability for detailed triplet state investigations of the sort that have been applied to the bacterial RC. More significantly, much evidence has accumulated to suggest that the primary reactants of plant PS II are quite similar to those of purple photosynthetic bacteria, so that many of the initial triplet state studies carried out on bacterial RCs need not be repeated in PS II. Nevertheless, significant differences do exist between the two systems, as some of the initial triplet state studies of PS II have indicated.

As in the bacterial RC, the primary reactants in PS II consist of a primary electron donor, P_{680}, that is some sort of a Chl species (possibly a dimer) followed by a pheophytin acceptor [371,371] and two quinone molecules [373] (plastoquinones) magnetically coupled to a non-heme Fe [374,375]. The resemblance between PS II and the bacterial RC is perhaps most evident in its protein structure and amino acid sequence. The RC 'core' that has been identified as the site of the primary light reactions contains (among others) two polypeptides now commonly known as D_1 and D_2 [376–378] that exhibit considerable sequence homology with each other and with the L and M subunits of several bacterial RCs [20–23]. Significantly, the amino acid residues thought to be responsible for binding of the chromophores and the location of transmembrane α-helices as indicated by hydropathy plots [379] and antibody binding studies [380], are conserved among these proteins. This has led to the proposal [381,382] that the three-dimensional structure of the PS II RC is roughly the same as that of the bacterial RC.

Flash absorption-difference spectroscopy in various PS II preparations has shown that the photochemical behavior of PS II is also quite similar to that deduced for bacteria [383–386]. The lifetime of the primary radical pair ($P_{680}^+Ph^-$) in blocked PS II RCs has been measured to be from 3 to about 50 ns, depending on the preparation; apparently removal of antenna and other accessory proteins lengthens the lifetime [387].

Given the host of similarities between PS II and the bacterial RC, it would be somewhat surprising if it did not exhibit a t_0-polarized donor triplet state as well. Indeed, some of the evidence for the reaction sequence given above has come from triplet state studies. Rutherford et al. [28] first observed a t_0-polarized triplet EPR signal in PS II preparations in which the quinone acceptor was reduced. As in photosynthetic bacteria, the intensity of the PS II triplet EPR signal diminishes as the intermediate Ph acceptor is reduced [388]. Thus, by analogy with $^3P_{870}$, the triplet signal was attributed to population of $^3P_{680}$ by charge recombination from the ($P_{680}^+Ph^-$) radical pair [28]; however, in contrast to $^3P_{870}$, its ZFS parameters were more comparable to those of monomeric ^{3}Chl species or $^3P_{700}$. Subsequently, a t_0-polarized triplet EPR signal with the same ZFS parameters has been observed in the recently isolated D_1/D_2/cytochrome b-559 'core complex' which do not contain the quinone acceptors [389,390]. Titration of the $^3P_{680}$ EPR signal has shown that Ph is the only electron acceptor in this smaller RC unit, [390,391], except at very high oxidation potentials when the non-heme iron

in the +3 oxidation state may function as an acceptor [390].

Most recently, EPR spectroscopy of $^3P_{680}$ has been used to demonstrate the stability of an improved preparation of the PS II core complex [392]. The ZFS of $^3P_{680}$ in such preparations are slightly smaller than previously published values, but still do not exhibit the large reduction relative to in vitro pigments that is characteristic of bacterial RCs. Two groups have also recently reported a low-yield triplet state other than $^3P_{680}$ in the PS II core complex [391,393] which is most likely attributable to ^{3}Ph in damaged RCs. Under conditions where $^3P_{680}$ yield is attenuated by prior photoreduction of Ph^-, the same two groups report observing an EPR spectrum corresponding to a pair of radicals, in one case strongly interacting [393], that may correspond to Ph^- and the cation radical of a species on the donor side of P_{680} [391,393].

The influence of a magnetic field on the yield of $^3P_{680}$ has been observed indirectly as a magnetic field effect on fluorescence intensity from chloroplasts and algae [394–396]. By analogy with magnetic field effects on fluorescence in bacteria [280,397], taken together with the other similarities between PS II and bacterial RCs, this suggests that such effects should be detectable using direct spectroscopic observation of $^3P_{680}$. No such experiments have yet been reported. It would be interesting to determine how closely the magnetic interactions in $(P_{680}^+Ph^-)$ correspond to those in the bacterial primary radical pair, and future triplet studies of the magnetic field and RYDMR effects in PS II are warranted.

V-C. Relative structures of plant and bacterial primary donor triplets

In some sense, efforts to determine the structures of P_{700} and P_{680} from their triplet state properties are at the same stage as similar efforts for the bacterial primary donor prior to crystallization of the bacterial RC. The fact that EPR signals attributed to $^3P_{700}$ and $^3P_{680}$ exhibit ZFS parameters similar to monomeric ^{3}Chl values is insufficient evidence to suggest that P_{700} and P_{680} are monomeric Chl species. This point has been discussed in a number of reports [27,28,339,398] As noted by Den Blanken et al. [360], attempts to deduce the primary donor structure solely from its ZFS parameters may have limited validity because variation of the ligands to the central Mg of Chl *a*, or a change in the local electrostatic environment (for example, a change in solvent) can alter the monomeric ZFS parameters considerably (by as much as 10%) [214,360,399]. Also, as may be the case in the $^3P_{870}$ dimer, small charge transfer contributions to the triplet state may strongly affect the magnitude of the ZFS parameters. ADMR experiments on both PS I [360] and PS II [399] indicate that both P_{700} and P_{680} are dimeric Chl *a* species with strong interactions between the two monomers in the singlet state and weak interactions in the triplet state. The work further suggests that the general structure of P_{700} resembles that of P_{870} in the bacterial RC.

As was the case for the bacterial primary donor, the triplet state kinetic parameters provide insufficient information to define the structures of the species giving rise to the t_0-polarized triplet states found in PS I and PS II. Some kinetic information has been obtained by EPR, ADMR, flash absorption, and magnetic field studies of PS I [347,364,360,337]: the parameters are similar to those found for ^{3}Chl *a* in vitro [34]. Likewise, the kinetic parameters of the triplet state in PS II [206,340] are not very different from ^{3}Chl *a* in vitro. These observations may or may not correspond to the situation in bacterial RCs, depending on what kinetic parameters are assumed for ^{3}BChl *a* in vitro [34,206–209]

The triplets found in PS I and PS II differ from the bacterial primary donor in some other important respects. For instance, the quantum yields of the plant triplets are not as high as the ~ 100% found for $^3P_{870}$ at liquid helium temperatures [342,337,343,400]. In the case of PS I, relatively large $^3P_{700}$ yields ($\phi = 0.6$–0.8 at 20 K) have been measured by flash absorption techniques [337,343]; however, the $^3P_{700}$ yield measured by EPR is on the order of 0.05–0.10 [342], similar to the estimated $^3P_{680}$ yield in PS II [398,400,401]. Apparently this low yield can be increased by addition of certain detergents [398,400]. The triplet yield is also affected by detergent concentration and/or addition of exogenous quinones. It is interesting that these two factors also affect the overall lineshape, specifically the ratio of the intensities of the outer to inner peaks of the continuous light triplet EPR spectrum [402]. Several recent optical emission and absorption studies of PS II have shown that the yield of the initial charge separation is strongly affected by the redox state of Q_A [403–405].

Rutherford has pointed out that differences between PS II and bacterial RCs such as those just discussed can be rationalized and still accommodate the bacterial RC as a model for PS II [398]. On the other hand, Rutherford et al. have studied the orientation of the $^3P_{680}$ zero-field axes with respect to the membrane plane [406,407]. They find that the plane of the Chl *a* PS II primary donor (assuming it is a monomeric triplet) is parallel to the plane of the membrane, in sharp contrast to the orientation of $^3P_{870}$ in bacterial RCs. The suggestion has been made that the triplet which is observed in PS II may not reside on P_{680} but on another Chl molecule, perhaps an antenna Chl or one of the so-called accessory Chls of the RC [400]. The first of these possibilities could account for the observation of two sets of triplets with slightly different ZFS parameters in ADMR experiments on PS II [399].

VI. Triplet state studies of model systems

Even with the bacterial RC structure now known, duplicating its photophysical properties in synthetic compounds has proved to be an extraordinary challenge. The triplet state observed in vivo is the result of a highly ordered system that can carry out efficient charge separation, and its spectroscopic properties are correspondingly unique. Thus, triplet state spectroscopy has been employed in much recent research on model compounds as a rigorous criterion for a working electron transfer system. Another equally important component of recent in vitro work has been directed towards extending our current understanding of the effects of molecular interactions upon chlorophyll triplet state properties in general.

There has been considerable interest in developing organized assemblies of chlorophylls and porphyrins as artificial photochemical devices. An essential step in this effort is to impose some sort of macroscopic organization on such assemblies. Thus, the triplet state properties of chlorophylls and porphyrins have been studied in a number of relatively ordered environments, including liposomes, [408,409] graphite surfaces [410], a synthetic polypeptide [411] and liquid crystalline solvents [149, 130] Chlorophylls exhibit interesting triplet-triplet energy transfer properties in liposomes and on graphite surfaces, and more detailed work on such systems is warranted. The relatively high degree of molecular order imposed by liquid crystal environments provides more structural and dynamic information about the chlorophyll triplet state than is available in completely randomly ordered environments. Much of the recent work in this area has been detailed in a review [130].

For detailed study of intermolecular electron and energy transfer processes, it is often necessary to impose a higher degree of ordering by synthesizing specific molecular linkages. Many model compounds have been based on the special pair concept for the bacterial primary electron donor, which was proposed and substantiated in a number of ways [143,144] before the RC crystal structure became available. In light of other evidence that a dimeric primary donor may be a universal feature of photosynthetic systems, the prospect of constructing a dimeric Chl species in vitro that exhibits in vivo triplet properties has intrigued chemists for a number of years. The literature in this area is extensive, including studies of non-covalently bound dimers (discussed briefly in Section III) along with studies of numerous covalently linked dimers of porphyrins and chlorophylls (including pyrochlorophyll). This work has been reviewed [412,413], and we will summarize here some of the results from triplet state studies of these model dimer systems.

The application of the exciton model as described in Section II.B (although generally without inclusion of charge transfer states) to describe the triplet state properties of the chlorophyll and porphyrin dimer models in terms of the monomer precursors has been discussed [79]. When charge transfer terms contribute, then the triplet ZFS parameters and decay rates are not sufficient to obtain information about the dimer geometry [414].

Initial ODMR and triplet EPR results on non-covalently linked low temperature chlorophyll dimers and covalently linked folded pyrochlorophyll dimers gave ZFS and triplet kinetics which were similar to that found for the respective monomers [78]. Since symmetric structures had been proposed for these two model dimer cases [195,205] in which the molecules are plane parallel and the in-plane Q_y transition moments aligned antiparallel, no change in the triplet state properties of the dimers compared to the monomers were expected if the proposed structures were correct and if the simple exciton model applied. One exception was the Zn-substituted Chl dimer investigated by Clarke et al. [78]: despite the all-axes-parallel configuration imposed by the covalent linkage in this dimer, the dimer ISC rates were significantly faster than would be predicted for this geometry. The authors suggested that this may indicate the importance of the $j \neq j'$ cross terms in the coherent exciton model (cf. Eqn. 22) which could be introduced by metal-centered SOC interactions.

It has been suggested, on the basis of the good agreement between the theoretical predictions and experimental results for symmetric dimers, that the triplet exciton model is applicable to chlorophyll dimers in general [78]. However, recent model studies have provided abundant evidence that one cannot conclude from the ZFS parameters and kinetics alone if the triplet state is delocalized over the two macrocycles or localized on one of the macrocycles [415]. For example, flash photolysis experiments on low temperature non-covalently linked dimers [416] and on covalently linked dimers [417] suggest that the latter is true, at least on the optical timescale.

Several doubly linked porphyrins and pyrochlorophyll dimers have been synthesized [412–414]. The simple exciton model was successfully applied to obtain the geometry of a pair of bis-Zn porphyrin dimers [414]. These molecules are separated by four and five atom bridges (CH_2-CO-NH-CH_2- and CH_2-CH_2-CO-NH-CH_2-). In this case, weak π-electron interactions between the porphyrin subunits were found. This is in contrast to a doubly linked pyrochlorophyll dimer (cyclophane 6) in which the two macrocycles are held together by six atom linkages (CH_2-CH_2-O-CO-CH_2-CH_2-) so that the two Q_y transition dipoles form an angle of 90°. The ZFS parameters of the triplet state of this cyclophane are identical to those of monomeric pyrochlorophyllide *a* [418]. Thus, on the timescale of the EPR experiment the triplet excitation is localized on

one macrocycle; otherwise, the ZFS parameter E would be zero [413,418]. When a similar cyclophane of non-metallated pyrochlorophyll with two five atom linkages (cyclophane 5) was studied the ZFS parameter D was smaller by about 9% compared to the monomer and E increased by about 50%. This result was interpreted as localization of the triplet excitation on one macrocycle with concomitant electron delocalization onto the oxygen linkages [418]. The results illustrate once more the difficulties with using ZFS parameters to distinguish between monomers or dimers or to make conclusions about dimeric structures.

Energy transfer has been studied in mixed dimers of porphyrin and of pyrochlorophyll in which one of the chromophores contains a metal and the other does not [130,418,419]. Two such studies have demonstrated the dependence of energy transfer on the mutual orientation of the two chromophores.

The triplet state formed from photoexcitation of dimers of Zn-TPP linked by methylene bridges (2–6 carbons) to free base TPP in liquid crystalline matrices were studied by EPR [130]. The use of liquid crystalline matrices made it possible to determine the orientation of the zero-field axes within the dimer. In general, the triplet state due to the lower-energy free base porphyrin was observed. However, at lower temperatures or at short times after excitation, a superposition of the free base and Zn-TPP EPR spectra was observed. The results were interpreted as a competition between (1) singlet energy transfer from Zn-TPP to TPP followed by ISC to the TPP triplet state and (2) ISC directly from the excited singlet state of Zn-TPP to its triplet state. Approximate values for singlet energy transfer were derived from the triplet spectra; the singlet energy transfer rates depended on the dimer conformation which was reflected in the zero-field axis directions.

The mixed case (one Mg-containing and one free base chromophore) of cyclophane 6 described above showed different triplet EPR spectra depending on the degree of ligation of the Mg [418]. The hexacoordinate cyclophane gave the spectrum expected for a localized triplet on the metallated half. The pentacoordinated cyclophane gave a spectrum which was a superposition of the triplet spectra of the two halves. In the latter case, it was not possible to distinguish between localized triplet states or a slow rate of energy transfer between the two halves, whereas energy transfer from the free base to the metallated half was demonstrated in the hexacoordinated case. The results suggested that triplet rather than singlet energy transfer was taking place. Again, the energy transfer was dependent on the geometry of the macrocycle, and this probably explains why it was observed in the hexacoordinate case where the increased ligation forced the cyclophane geometry.

Recently there have been several studies of the triplet state properties of water-soluble porphyrins which dimerize in aqueous solution [420–425]. These include tetrakis(4-sulfonatophenyl)porphyrin which forms dimers upon the addition of cations or cation-crown ethers, [420–422] crown porphyrins [424] which dimerize upon the addition of cations, and mixtures of cationic and anionic porphyrins which become electrostatically linked [423,425]. These studies provide another illustration of the diverse properties exhibited by the dimer triplet states. In several cases reductions in the ZFS parameter D of the dimers were found relative to monomer values. The reduced ZFS in the dimers were attributed to a combination of excitation transfer and charge transfer [420–422]. However, a similar relative reduction in ZFS was attributed to a triplet state localization in the electrostatically linked dimers [423]. On the other hand, the changes in ZFS upon dimerization of the Zn crown porphyrins could be interpreted in terms of the triplet excition theory whereas its free base dimer appears to give a localized triplet state [423,424].

Two very active areas of research which make use of the triplet state are in experiments designed to study electron and energy transfer in model systems. We briefly mention some of this work here.

A large number of experiments are underway to study synthetically linked donor-acceptor molecules such as porphyrins or chlorophylls linked to quinone molecules with fixed relative orientations. An important observation in this work would be to observe a triplet state of the donor after photoexcitation which exhibits electron spin polarization indicative of radical pair intersystem crossing. However, most of the model systems fail to undergo high quantum efficiency photoinitiated charge separation in the solid state at low temperatures [426,427]. Recently, Wasielewski et al. [428] have shown that this is primarily due to destabilization of the ion pair state in low-temperature solids relative to polar liquids. They have prepared two fixed-distance donor-acceptor molecules, made up of a Zn porphyrin donor and a tetracyanonaphthoquinonodimethane derivative acceptor. Both model compounds undergo high quantum efficiency photo-induced charge separation at low temperatures. In one molecule the charge separated state decays to the porphyrin triplet state. Although this triplet state does not exhibit the t_0 electron spin polarization indicative of radical pair intersystem crossing, the triplet state is not formed via the usual intersystem crossing mechanism for Zn porphyrins. The in-plane intersystem crossing is explained by an enhancement of spin-orbit interaction due to the orientation of the donor HOMO and acceptor LUMO.

Triplet formation has been studied in a diphenyletioporphyrin covalently linked to an anthraquinone via a sulfonyloxy bridge [429]. In one of these systems where the center to center distance between the porphyrin and anthraquinone is 3.2 Å, the porphyrin triplet state was found to lie below the charge-transfer

state. Although the electron spin polarization for this triplet state is different from that of unsubstituted diphenyletioporphyrin, the t_0 electron spin polarization is not observed for the triplet state of the model compound. The explanation for this observation is that the exchange interaction between the unpaired electrons in the charge separated state is much larger than the hyperfine interactions.

Recently, several carotenoporphyrins [430–433] and carotenopyropheophorbides [434,435] have been synthesized in order to study the structural requirements for the antenna and protective functions of carotenoids in the photosynthetic unit. The photoprotective function (i.e., quenching of the porphyrin triplet by energy transfer to carotenoid) was demonstrated in a number of model systems where the two moieties were in close proximity [430,431] or where molecular motion could bring the two parts of the molecule into close proximity [433]. The triplet EPR spectra of a number of these model systems having different donor structures, different carotenoid acceptors and different relative orientations between donor and acceptor have been studied [436]. The different systems all produced a carotenoid triplet state with the same electron spin polarization pattern, independent of the porphyrin donor triplet ESP, interchromophore distance (i.e., coupling strength), and relative orientation of the molecules. A structural alteration of the carotene triplet state which gives a redistribution of its spin sublevel populations was proposed to explain these results.

VII. Outlook

Although our current understanding about the initial light reactions of photosynthetic systems has been considerably advanced by the crystallization and characterization of the bacterial RC ground state, the subtleties of the interactions that shape its dynamic states remain poorly understood. Future investigation of single crystals of RCs from bacteria and higher plants will focus on the structure and dynamics of the photoexcited, working states of the RC. Chlorophyll triplet state studies will continue to be a critical tool in such efforts, furnishing a highly sensitive probe of the specific influences of the in vivo protein environment. The full potential of single crystals for magnetic resonance studies, especially time-resolved techniques and multiple resonance methods such as ENDOR, has yet to be fully realized.

The triplet state of the bacterial primary donor is the best characterized of the in vivo systems; nevertheless, several weaknesses remain in the picture that has emerged from recent studies based on the X-ray crystal structure. The long-standing effort to describe the dimeric donor triplet state in terms of its constituent monomers leaves many unanswered questions about its precise nature. Detailed ODMR investigations of site inhomogeneities in the singlet and triplet manifolds of the RC could serve to identify specific environmental effects on the structure of the primary donor. The possible participation of the closely spaced accessory pigments in the primary donor triplet state warrants further investigation; future studies will also need to identify any charge-transfer configurations in the triplet state and relate them to the photochemical function of the RC. Towards this end, studies of linear electric field effects on triplet spectroscopic properties such as phosphorescence (Stark effects), ZFS, and spin sublevel kinetics may be useful.

Two major approaches to making a detailed probe of the protein surrounding the primary donor appear promising. First, comparative triplet state studies among different species can reveal specific environmental influences. Already it has been suggested that the triplet state structure of the bacterial primary donor may have taxonomic significance [250]; this might be verified by studying the correlation of triplet properties with amino acid sequences in cases where the primary structure of the RC proteins are known, although single RC crystals from different bacteria and plant photosystems would be the most useful. The availability of new crystals from bacteria [437], light harvesting chlorophyll proteins [438,439], PS I reaction centers [440–442] and the isolation of the D_1/D_2/cyt *b*-559 complex from PS II [370] promise to make direct comparisons between bacteria and higher plants feasible in the near future. A second avenue of pursuit will be direct genetic manipulation of the bacterial reaction center itself [443]. Interesting mutant reaction centers from *Rb. capsulatus*, in which $BChl_M$ has been converted to pheophytin by replacement of the histidine that acts as its axial ligand, have recently been obtained for spectroscopic studies [444]. These RCs retain their photochemical activity, but give rise to triplet states quite different from those in native RCs (Kolaczkowski, S.V., Bylina, E.J. and Norris, J.R., unpublished data). It seems clear that such possibilities will guide the course of photosynthetic triplet state studies in the future, and experimental methods that were once exclusively the domain of physical chemists will increasingly find use at the hands of the molecular biologist.

Acknowledgements

We are grateful to many of our colleagues for their advice, criticisms, and many useful discussions, including Prof. P.L. Dutton, Prof. H. Levanon, Prof. A.J. Hoff, Prof. D. Stehlik, Dr. A.W. Rutherford, Dr. M.R. Wasielewski, Dr. D.M. Tiede, Dr. P. Gast, and espe-

cially Prof. James R. Norris for his continual encouragement and support. D.E.B. acknowledges the support of NIH NRSA GM-12924 during part of the completion of the manuscript. This work was supported by the Division of Chemical Sciences, Office of Basic Energy Sciences, U.S. Department of Energy, under contract W-31-109-ENG-38.

References

1 Hutchison, Jr., C.A. and Mangum, B.W. (1958) J. Chem. Phys. 29, 952–953.
2 Michel H. (1982) J. Mol. Biol. 152, 562–567.
3 Allen, J.P. and Feher, G. (1984) Proc. Natl. Acad. Sci. USA 81, 4795–4799.
4 Deisenhofer, J., Epp, O., Miki, K., Huber, R. and Michel, H. (1984) J. Mol. Biol. 180, 385–398.
5 Deisenhofer, J., Epp, O., Miki, K., Huber, R. and Michel, H. (1985) Nature 318, 618–624.
6 Michel, H., Epp, O. and Deisenhofer, J. (1986) EMBO J. 5, 2445–2451.
7 Chang, C.H., Tiede, D.M., Tang, J., Smith, U., Norris, J.R. and Schiffer, M. (1986) FEBS Lett. 205, 82–86.
8 Allen, J.P., Feher, G., Yeates, T.O., Rees, D.C., Deisenhofer, J., Michel, H. and Huber, R. (1986) Proc. Natl. Acad. Sci. USA 83,8589–8593.
9 Allen, J.P., Feher, G., Yeates, T.O., Komiya, H. and Rees, D.C. (1987) Proc. Natl. Acad. Sci. USA 84, 5730–5734.
10 Reed, D.W. and Clayton, R.K. (1968) Biochem. Biophys. Res. Commun. 30,471–475.
11 Clayton, R.K. and Wang, R.T. (1971) Methods Enzymol. 23, 696–704.
12 Feher, G. and Okamura, M.Y. (1978) in The Photosynthetic Bacteria (Clayton, R.K. and Sistrom, W.R., eds.), pp. 349–386, Plenum Press, New York.
13 Frank, H.A., Taremi, S.S. and Knox, J.R. (1987) J. Mol. Biol. 198, 139–141.
14 Allen, J.P., Feher, G., Yeates, T.O., Komiya, H. and Rees, D.C. (1988) in The Photosynthetic Bacterial Reaction Center, NATO ASI Series A: Life Science (Breton, J. and Vermeglio, A., eds.), pp. 5–12, Plenum Press, New York.
15 Woodbury, N.W.T., Becker, M., Middendorf, D. and Parson, W.W. (1985) Biochem. 24, 7516–7521.
16 Wasielewski, M.R. and Tiede, D.M. (1986) FEBS Lett. 204, 368–372.
17 Fleming, G.R., Martin, J.-L. and Breton, J. (1988) Nature 333, 190–192.
18 Rockley, M.B., Windsor, M.W., Cogdell, R.J. and Parson, W.W. (1975) Proc. Natl. Acad. Sci. USA 72, 2251–2255.
19 Kirmaier, C., Holten, D. and Parson, W.W. (1985) Biochim. Biophys. Acta 810, 33–48.
20 Williams, J.C., Steiner, L.A., Ogden, R.C., Simon M.I., and Feher, G. (1983) Proc. Natl. Acad. Sci. USA 80, 6505–6509.
21 Williams, J.C., Steiner, L.A., Ogden, R.C., Simon, M.I., and Feher, G. (1984) Proc. Natl. Acad. Sci. USA 81, 7303–7307.
22 Youvan, D.C., Byelina, E.J., Alberti, M., Begusch, H. and Hearst, J.E. (1984) Cell 37, 949–959.
23 Michel, H., Weyer, K.A., Grünberg, H., Dunger, I., Österhelt, D. et al. (1986) EMBO J. 5, 1149–1158.
24 Gast, P., Michalski, T., Hunt, J.E. and Norris, J.R. (1985) FEBS Lett. 179, 325–328.
25 Budil, D.E., Gast, P., Chang, C.H., Schiffer, M. and Norris, J.R. (1987) Annu. Rev. Phys. Chem. 38, 561–583.
26 Dutton, P.L., Leigh, J.S. and Seibert, M. (1972) Biochem. Biophys. Res. Commun. 46, 406–413.
27 Frank, H.A., McClean, M.B. and K. Sauer (1979) Proc. Natl. Acad. Sci. USA 76, 5124–5128.
28 Rutherford, A.W., Paterson, D.R. and Mullet, J.E. (1981) Biochim. Biophys. Acta 635, 205–214.
29 Franck, J.C. (1957) in Photosynthesis (Gaffron, H., Brown, A.H. and French, C.S., eds.), pp. 19–30, Wiley-Interscience, New York.
30 Franck, J.C. (1959) Science 130, 1416.
31 Robinson, G.W. (1963) Proc. Natl. Acad. Sci. USA 49, 521–529.
32 Robinson, G.W. (1966) Brookhaven Symp. Biol. 19, 16–48.
33 Fong, F.K. (1976) J. Am. Chem. Soc. 98, 7840–7843.
34 Levanon, H. and Norris, J.R. (1978) Chem. Rev. 78, 185–198.
35 Thurnauer, M.C. (1979) Rev. Chem. Int. 1, 197–230.
36 Levanon, H. and Norris, J.R. (1982) in Light Reaction Path of Photosynthesis (Fong, F.K., ed.), pp. 152–195, Springer, Berlin.
37 Clarke, R.H. (ed.) (1982) ODMR Spectroscopy: Techniques and Applications to Biophysical Systems, Wiley-Interscience, New York, 1982.
38 Schaafsma, T.J. (1982) in ODMR Spectroscopy: Techniques and Applications to Biophysical Systems (Clarke, R.H., ed.), Ch. 8, Wiley-Interscience, New York.
39 Hoff, A.J. (1982) in ODMR Spectroscopy: Techniques and Applications to Biophysical Systems (Clarke, R.H., ed.), Ch. 9, Wiley-Interscience, New York.
40 Hoff, A.J. (1986) in Light Emission by Plants and Bacteria (Govindjee, Amesz, J. and Fork, D.C., eds.), pp. 225–264, Academic Press, Orlando.
41 Katz, J.J. and Norris, J.R. (1973) Curr. Top. Bioenerg. 5, 41–75.
42 Weiss, C. (1972) J. Mol. Spectrosc. 44, 37–80.
43 Weiss, C. (1972) in The Porphyrins, Vol. III: Physical Chemistry, Part A (Dolphin, D., ed.), pp. 211–223, Academic Press, New York.
44 Christoffersen, R.E. (1979) Int. J. Quantum Chem. 16, 573–604.
45 Song, P.-S. (1978) Ultraviolet and Visible Spectroscopy of Bioorganic Molecules., Chemical Society Annual Reports (B), Vol. 74, pp. 18–40.
46 Gouterman, M. (1961) J. Mol. Spectrosc. 6, 138–163.
47 Longuet-Higgins, H.C., Rector, C.W. and Platt, J.R. (1950) J. Chem. Phys. 18, 1174–1181.
48 Weiss, C., Kobayashi H. and Gouterman, M. (1965) J. Mol. Spectrosc. 16, 415–450.
49 Song, P.-S., Moore, T.A. and Sun, M. (1972) in The Chemistry of Plant Pigments (Chichester, C.O., ed.), pp. 33–74, Academic Press, New York.
50 Spangler, D., McKinney, R., Christoffersen, R.E., Maggiora, G.M. and Shipman, L.L. (1975) Chem. Phys. Lett. 36, 427–431.
51 Petke, J.D., Maggiora, G.M., Shipman, L.L. and Christofferson, R.E. (1979) Photochem. Photobiol. 30, 203–223.
52 Petke, J.D., Maggiora, G.M., Shipman, L.L. and Christofferson, R.E. (1980) Photochem. Photobiol. 31, 243–257.
53 Chang, J.C. (1977) J. Chem. Phys. 67, 3901–3909.
54 Kuki, A. and Boxer, S.G. (1983) Biochem. 22, 2923–2933.
55 Van der Waals, J.H. and De Groot, M.S. (1967), in The Triplet State (Zahlan, A.B., ed.), pp. 101–132, Cambridge University Press, London.
56 Hutchison, Jr., C.A. (1967) in The Triplet State (Zahlan, A.B., ed.), pp. 63–99, Cambridge University Press.
57 Langhoff, S.R., Davidson, E.R., Gouterman, M., Leenstra, W.R. and Kwiram, A.L. (1975) J. Chem. Phys. 62, 169–176.
58 Kooter, J.A., Van der Waals J.H. and Knop, J.V. (1979) Mol. Phys. 37, 1015–1036.
59 Thurnauer, M.C. and Norris, J.R. (1977) Chem. Phys. Lett. 47, 100–105.

60 Gast, P., Wasielewski, M.R., Schiffer, M. and Norris, J.R. (1983) Nature 305, 451–452.
61 Gast, P. and Norris, J.R. (1984) FEBS Lett. 177, 277–280.
62 Norris, J.R., Budil, D.E., Gast, P., Chang, C.H., El-Kabbani, O. and Schiffer, M. (1989) Proc. Natl. Acad. Sci. USA 86, 4335–4339.
63 Budil, D.E., Taremi, S.S, Gast, P., Norris, J.R. and Frank, H.A. (1988) Isr. J. Chem. 28, 59–66.
64 McGlynn, S.P., Azumi, T. and Kinoshita, M. (1969) Molecular Spectroscopy of the Triplet State, Ch. 5, Prentice-Hall, Englewood Cliffs.
65 Antheunis, D.A., Schmidt, J. and Van der Waals, J.H. (1974) Mol. Phys. 27, 1521–1541.
66 Henry, B.R. and Siebrand, W. (1971) J. Chem. Phys. 54, 1072–1085.
67 Metz, F., Friedrich, S. and Hohlneicher, G. (1972) Chem. Phys. Lett. 16, 353–358.
68 Clarke, R.H. and Frank, H.A. (1976) J. Chem. Phys. 65, 39–47.
69 Albrecht, A.C. (1963) J. Chem. Phys. 38, 354–365.
70 Sternlicht, H. and McConnell, H.M. (1961) J. Chem. Phys. 35, 1793–1800.
71 Hochstrasser, R.M. and Lin, T.-S. (1968) J. Chem. Phys. 49, 4929–4945.
72 Clarke, R.H., Connors, R.E., Frank, H.A. and Hoch, J.C. (1977) Chem. Phys. Lett. 45, 523–528.
73 Bowman, M.K. and Norris, J.R. (1977) Chem. Phys. Lett. 54, 45–48.
74 Hägele, W., Schmid, D. and Wolf, H.C. (1978) Z. Naturforsch. 33a, 94–97.
75 Nagakura, S. (1975) in Excited States, Vol. 2, (Lim, E.C., ed.), pp. 321–383, Academic Press, New York.
76 Lim, E.C. (1987) Acc. Chem. Res. 20, 8–17.
77 Bowman, M.K. and Norris, J.R. (1978) Chem. Phys. Lett. 54, 45–58.
78 Clarke, R.H., Hobart, D. and Leenstra, W.K. (1979) J. Am. Chem. Soc. 101, 2416–2423.
79 Clarke, R.H. (1982) in Light Reaction Path of Photosynthesis (Fong, F.K., ed.), Ch. 6, Springer, Berlin.
80 Shaik, S.S. and Epiotis, N.D. (1980) J. Am. Chem. Soc. 102, 122–131.
81 Epiotis, N.D. (1978) Theory of Organic Reactions, p. 226, Springer, Berlin.
82 Schadee, R.A., Schmidt, J. and VanderWaals, J.H. (1976) Chem. Phys. Lett. 41, 435–439.
83 Zinth, W., Knapp, E.W., Fischer, S.F., Kaiser, W., Deisenhofer, J. and Michel, H. (1985) Chem. Phys. Lett. 119, 1–4.
84 Knapp, E.W., Fischer, S.F., Kaiser, W., Deisenhofer, J., and Michel, H. (1985) Proc. Natl. Acad. Sci. USA 82, 8463–8467.
85 Knapp, E.W. and Fischer, S.F. (1985) in Antennas and Reaction Centers of Photosynthetic Bacteria, Springer Series in Chemical Physics, Vol. 42 (Michel-Beyerle, M.E., ed.), pp. 103–108, Springer, Berlin.
86 Breton, J. (1985) Biochim. Biophys. Acta 810, 235–245.
87 Vasmel, H., Amesz, J. and Hoff, A.J. (1986) Biochim. Biophys. Acta 852, 159–168.
88 Mushlin, R.A., Gast, P. and Hoff, A.J. (1980) FEBS Lett. 76, 542–546.
89 Boxer, S.G. and Closs, G.L. (1975) J. Am. Chem. Soc. 97, 3268–3270.
90 Lamola, A.A., Manion, M.L., Roth, H.D. and Tollin, G. (1975) Proc. Natl. Acad. Sci. USA 72, 3265–3269.
91 Chidsey, C.E.D., Takiff, L., Goldstein, R.A. and Boxer, S.G. (1985) Proc. Natl. Acad. Sci. USA 82, 6850–6854.
92 Goldstein, R.A. and Boxer, S.G. (1987) Biophys. J. 51, 937–946.
93 Goldstein, R.A., Takiff, L. and Boxer, S.G. (1988) Biochim. Biophys. Acta 934, 253–263.
94 Linschitz, H. and Sarkanen, K. (1958) Photochem. Photobiol. 36, 733–741.
95 Pekkarinen, L. and Linschitz, H. (1960) J. Am. Chem. Soc. 80, 4826–4832.
96 Chibisov, A.K. (1969) Photochem. Photobiol. 10, 331–347.
97 Holten, D., Gouterman, M., Parson, W.W., Windsor, M.W., and Rockley, M.G. (1976) Photochem. Photobiol. 23, 415–423.
98 Shuvalov, V.A. and Parson, W.W. (1981) Proc. Natl. Acad. Sci. USA 78, 957–961.
99 Mau, A.W.H. and Puza, M. (1977) Photochem. Photobiol. 23, 601–603.
100 Dvornikov, S.S., Knyukshto, V.N., Sevchenko, A.N., Solov'ev, K.N. and Tsvirko, M.P. (1978) Dokl. Akad. Nauk SSSR 240, 1457–1460.
101 Dvornikov, S.S., Knyukshto, V.N., Solov'ev, K.N., Tsvirko, L.M.P. (1979) J. Lumin. 18/19, 491–494.
102 Lebedev, N.N. and Krasnovskii, A.A., Jr. (1979) Biophysics 23, 1115–1117.
103 Mauring, K.Kh., Suisala, A.P., Avarmaa, R.A., Krasnovskii, A.A., Jr. (1980) Dokl. Akad. Nauk. SSSR 251, 729–731.
104 Takiff, L. and Boxer, S.G. (1988) Biochim. Biophys. Acta 932, 325–334.
105 Takiff, L. and Boxer, S.G. (1988) J. Am. Chem. Soc. 110, 4425–4426.
106 Englman, R. and Jortner, J. (1970) Mol. Phys. 18, 145–164.
107 Kleibeuker, J.F., Platenkamp, R.J. and Schaafsma, T.J. (1978) Chem. Phys. 27, 51–64.
108 Lebedev, N.N. and Krasnovskii, A.A., Jr. (1978) Biofizika 23, 1095–1096.
109 Maki, A.H. (1984) in Biological Magnetic Resonance, Vol. 6 (Berliner, L. and Reuben, J., eds.), pp. 187–294, Plenum Press, New York.
110 Hoff, A.J. (1989) in Advanced EPR: Applications in Biology and Biochemistry (Hoff, A.J., ed.), pp. 633–684, Elsevier, Amsterdam.
111 Clarke, R.H. and Hayes, J.M. (1972) J. Chem. Phys. 57, 569–570.
112 Clarke, R.H. and Hayes, J.M. (1973) J. Chem. Phys. 59, 3113–3118.
113 Van Dorp, W.G., Schaafsma, T.J., Soma, M. and Van der Waals, J.H. (1973) Chem. Phys. Lett. 21, 221–225.
114 Van Dorp, W.G., Schömaker, W.H., Soma, M. and Van der Waals, J.H. (1975) Mol. Phys. 30, 1701–1721.
115 Clarke, R.H. and Hofeldt, R.H. (1974) J. Chem. Phys. 61, 4582–4587.
116 Clarke, R.H. and Connors, R.E. (1975) Chem. Phys. Lett. 33, 365–368.
117 Clarke, R.H., Graham, D.J., Hanlon, E.B. and Mitra, P. (1983) J. Chem. Phys. 79, 149–150.
118 Hutchison, C.A., Nicholas, J.V. and Scott, G.W. (1970) J. Chem. Phys. 53, 1906–1917.
119 Shpol'skii, E.V. (1960) Sov. Phys. Usp. 3, 372–389.
120 Shpol'skii, E.V. (1962) Sov. Phys. Usp. 5, 522–531.
121 Shpol'skii, E.V. (1963) Sov. Phys. Usp. 6, 411–427.
122 Avarmaa, R. and Schaafsma, T.J. (1980) Chem. Phys. Lett. 71, 339–344.
123 El-Sayed, M.A. (1972) MTP Int. Rev. Sci. Phys. Chem., Ser. One (Ramsey, D.A., ed.), 3, 119–153 Butterworth, London.
124 Chiha, P.A. and Clarke, R.H. (1978) J. Magn. Reson. 29, 535–543.
125 Nishi, N., Schmidt, J., Hoff A.J. and Van der Waals, J.H. (1978) Chem. Phys. Lett. 56, 205–207.
126 Lous, E.J. and Hoff, A.J. (1987) Chem. Phys. Lett. 140, 620–625.
127 Grebel, V. and Levanon, H. (1980) Chem. Phys. Lett. 72, 218–224.
128 Gonen, O. and Levanon, H. (1987) J. Phys. Chem. 88, 4223–4228.
129 Ofir, H., Regev, A., Levanon, H., Vogel, E., Köcher, M. and Balci, M. (1987) J. Phys. Chem. 91, 2686–2688.
130 Levanon, H. (1987) Rev. Chem. Inst. 8, 287–320.

131 Frank, H.A., Friesner, R., Nairn, J.A., Dismukes, G.C., and Sauer, K. (1979) Biochim. Biophys. Acta 547, 484–501.
132 Vermeglio, A. and Clayton, R.K. (1976) Biochim. Biophys. Acta 449, 500–515.
133 Tiede, D.M. and Dutton, P.L. (1981) Biochim. Biophys. Acta 637, 278–290.
134 Rafferty, C.N. and Clayton, R.K. (1978) Biochim. Biophys. Acta 502, 51–60.
135 Bolt, J. and Sauer, K. (1979) Biochim. Biophys. Acta 546, 54–63.
136 Abdourakmanov, I.A., Ganago, A.V., Erokhin, Yu.E., Salov'ev, A.A. and Chuganov, V.A. (1979) Biochim. Biophys. Acta 546, 183–186.
137 El-Sayed, M.A. and Siegel, S. (1966) J. Chem. Phys. 44, 1416–1423.
138 Frank, H.A., Bolt, J., Friesner, R. and Sauer, K. (1979) Biochim. Biophys. Acta 547, 502–511.
139 Trosper, T.L., Frank, H.A., Norris, J.R. and Thurnauer, M.C. (1982) Biochim. Biophys. Acta 679, 44–50.
140 Boxer, S.G. and Roelofs, M.G. (1979) Proc. Natl. Acad. Sci. USA 76, 5636–5640.
141 Frank, H.A., Machnicki, J. and Toppo, P. (1984) Photochem. Photobiol. 39, 429–432.
142 Friesner, R., Nairn, J.A. and Sauer, K. (1979) J. Chem. Phys. 71, 358–365.
143 Norris, J.R., Scheer, H. and Katz, J.J. (1975) Ann. N.Y. Acad. Sci. 244, 260–280.
144 Feher, G., Hoff, A.J., Isaacson, R.A and Ackerson, L.C. (1975) Ann. N.Y. Acad. Sci. 244, 239–259.
145 Kirste, B. and Van Willigen, H. (1982) Chem. Phys. Lett. 92, 339–342.
146 Van Willigen, H. and Chandreshekar, T.K. (1983) J. Chem. Phys. 78, 7093–7098.
147 Lendzian, F., van Willigen, H., Sastry, S., Möbius, K., Schewer, H. and Feick, R. (1985) Chem. Phys. Lett. 118, 145–150.
148 Freed, J.H., Bruno, G.V. and Polnaszek, C.F. (1971) J. Chem. Phys. 55, 5270–5281.
149 Fessmann, J., Rösch, N., Ohmes, E. and Kothe, G. (1988) Chem. Phys. Lett. 152, 491–496.
150 Gradyushko, A.T., Sevchenko, A.N., Solovyov, K.N. and Tsvirko, M.P. (1968) Photochem. Photobiol. 11, 387–400.
151 Kleibeuker, J.F. and Schaafsma, T.J. (1974) Chem. Phys. Lett. 29, 116–122.
152 Rikhireva, G.T., Gribova, Z.B., Kayushin, L.P., Umrikhina, A.V. and Krasnovskii, A.A. (1964) Dokl. Acad. Nauk SSSR 159, 196–197.
153 Rikhireva, G.T., Sibel'dina, L.A., Grivoba, Z.P., Marihov, B.S., Kayushin, L.P. and Krasnovskii, A.A. (1968) Dokl. Akad. Nauk SSSR 181, 1485–1488.
154 Lhoste, J.M. (1968) C.R. Acad. Sci. (Paris) Ser D 226, 1059–1062.
155 Levanon, H. and Weissman, S.I. (1971) J. Am. Chem. Soc. 93, 4309–4310.
156 Lhoste, J.M. and Grivet, J.P. (1973) Adv. in Rad. Res., pp. 327–337, Gordon and Breach, New York.
157 Levanon, H. (1979) in Multiple Electronic Resonance (Dorio, M. and Freed, J.H., eds.), p. 437, Plenum Press, New York.
158 Norris, J.R. and Warden, J.T. (1980) EPR Lett. 1, 2–3.
159 Hoff, A.J., Gast, P. and Romijn, J.C. (1977) FEBS Lett. 73, 185–190.
160 de Jager, P.A. and Van Wijk, F.G.H. (1987) Rev. Sci. Instrum. 58, 735–741.
161 Gonen, O. and Levanon, H. (1985) J. Phys. Chem. 89, 1637–1643.
162 Gonen, O. and Levanon, H. (1986) J. Chem. Phys. 84, 4132–4141.
163 Regev, A., Galilili, T., Levanon, H. and Harriman, A. (1986) Chem. Phys. Lett. 131, 140–146.
164 Hoff, A.J. and Proskuryakov, I.I. (1985) Chem. Phys. Lett. 115, 303–310.
165 Proskuryakov, I.I. (1987) Proceedings Ampere Summer School, Novosibirsk.
166 Budil, D.E., Feezel, L.L., Bock, C., Thurnauer, M.C., and Stehlik, D. (1988) unpublished.
167 Regev, A., Nechushtai, R., Levanon, H. and Thornber, J.P. (1988) J. Phys. Chem. 93, 2421–2426.
168 Gunner, M.R., Robertson, D.E., LoBrutto, R.C., McLaughlin, A.C. and Dutton, P.L. (1987) in Progress in Photosyn. Res., Vol. 1 (Biggins, J., ed.), pp. 217–220, M. Nijhoff, Dordrecht.
169 Norris, J.R., Thurnauer, M.C. and Bowman, M.K. (1980) Adv. Biol. Med. Phys. 17, 365–416.
170 Trifunac, A.D., Lawler, R.G., Bartels, D.M. and Thurnauer, M.C. (1986) Prog. Reaction Kinetics 14, 43–156.
171 Gorcester, J. and Freed, J.H. (1986) J. Chem. Phys. 85, 5375–5377.
172 Gorcester, J. and Freed, J.H. (1988) J. Chem. Phys. 88, 4678–4693.
173 Bowman, M.K. (1986) Bull. Am. Phys. Soc. 31, 524.
174 Massoth, R.J. (1988) Ph. D. Dissertation, University of Kansas.
175 Dobbert, O., Prisner, T. and Dinse, K.P. (1986) J. Magn. Reson. 70, 173–175.
176 Bruker Instruments, Inc., Billerica, MA, U.S.A., Technical Infomation Sheet ESP380.
177 Prisner, T., Dobbert, O., Dinse, K.P. and van Willigen, H. (1988) J. Am. Chem. Soc. 110, 1623–1624.
178 Angerhofer, A., Toporowicz, M., Bowman, M.K., Norris, J.R. and Levanon, H. (1988) J. Phys. Chem. 92, 7164–7166.
179 Bowman, M.K., Toporowicz, M., Norris, J.R., Michalski, T.J., Angerhofer, A. and Levanon, H. (1988) Isr. J. Chem. 28, 215–222.
180 Katz, J.J., Norris, J.R., Shipman, L.L. and Thurnauer, M.C. (1978) Annu. Rev. Biophys. Bioeng. 7, 393–434.
181 Katz, J.J., Shipman, L.L., Cotton, T.M. and Janson, T.R. (1978) in The Porphyrins (Dolphin, D. ed.), Vol. V, Part C, pp. 401–458, Academic Press, New York.
182 Cotton, T.M. and VanDuyne, R.P.J (1981) J. Am. Chem. Soc. 103, 6020–6026.
183 Cotton, T.M., Loach, P.A., Katz, J.J. and Ballschmitter, K. (1978) Photochem. Photobiol. 27, 735–749.
184 Katz, J.J. Shipman, L.L. and Norris, J.R. (1979) in CIBA Foundation Symposium, Vol. 61, pp. 1–40, Excerpta Medica, Amsterdam.
185 Krasnovskii, A.A., Jr. (1982) Photochem. Photobiol. 36, 733–741.
186 Closs, G.L., Katz, J.J., Pennington, F.C., Thomas, M.R., and Strain, H.H. (1963) J. Am. Chem. Soc. 85, 3809–3821.
187 Evans, T.A. and Katz, J.J. (1975) Biochim. Biophys. Acta 396, 414–426.
188 Shipman, L.L., Cotton, T.M., Norris, J.R. and Katz, J.J. (1976) J. Am. Chem. Soc. 98, 8222–8230.
189 Brown, J.S. (1977) Photochem. Photobiol. 26, 319–326.
190 Shipman, L.L., Cotton, T.M., Norris, J.R. and Katz, J.J. (1976) Proc. Natl. Acad. Sci. USA 73, 1791–1794.
191 Warshel, A. (1979) J. Am. Chem. Soc. 101, 744–746.
192 Scherz, A. and Parson, W.W. (1984) Biochim. Biophys. Acta 766, 666–678.
193 Katz, J.J., Norris, J.R. and Shipman, L.L. (1976) Brookhaven Symp. Biol. 28, 16–55.
194 Fong, F.K. and Koester, V.J. (1976) Biochim. Biophys. Acta 423, 52–64.
195 Fong, F.K., Koester, V.J. and Galloway, L. (1977) J. Am. Chem. Soc. 99, 2372–2375.

196 Kooyman, R.P.H., Schaafsma, T.J., Jansen, G., Clarke, R.H., Hobart, D.R. and Leenstra, W.R. (1979) Chem. Phys. Lett. 68, 65–70.
197 Clarke, R.H., Hotchandani, S., Jagannathan, S.P. and Leblanc, R.M. (1982) Chem. Phys. Lett. 89, 37–40.
198 Clarke, R.H., Hotchandani, S., Jagannathan, S.P. and Leblanc, R.M. (1982) Photochem. Photobiol. 36, 575–579.
199 Kooyman, R.P.H., Schaafsma, T.J. and Kleibeuker, R.J. (1977) Photochem. Photobiol. 26, 235–240.
200 Hotchandani, S., Clarke, R.H. and Leblanc, R.M. (1986) Can. J. Chem. 64, 188–191.
201 Angerhofer, A., Schütz, J.U., Wolf, H.C. (1988) Chem. Phys. Lett. 151, 195–198.
202 Lemaistre, J.P. and Zewail A.H. (1979) Chem. Phys. Lett. 68, 296–301.
203 Lemaistre, J.P. and Zewail A.H. (1979) Chem. Phys. Lett. 68, 302–308.
204 Clark, R.F. and Clarke, R.H. (1980) J. Chem. Phys. 73, 5386–5388.
205 Boxer, S.G. and Closs, G.L. (1976) J. Am. Chem. Soc. 98, 5406–5408.
206 Den Blanken, H.J. and Hoff, A.J. (1983) Chem. Phys. Lett. 96, 343–347.
207 Hoff, A.J. and Cornelissen, B. (1982) Mol. Phys. 45, 413–425.
208 Hoff, A.J. (1979) Phys. Rep. 54, 75–200.
209 Gonen, O., Levanon, H., Thurnauer, M.C., Norris, J.R., and Closs, G.L. (1985) Chem. Phys. Lett. 113, 117–122.
210 Hiromitsu, I. and Kevan, L. (1988) J. Chem. Phys. 88, 691–695.
211 Levanon, H. and Vega, S. (1974) J. Chem. Phys. 61, 2265–2274.
212 Bowman, M.K. (1977) Chem. Phys. Lett. 48, 17–21.
213 Ponte-Goncalves, A.M. and Burgner, R.P. (1977) Chem. Phys. Lett. 46, 488–492.
214 Connors, R.E., Durand, Jr., R.R. and Borowski, K.J. (1980) Chem. Phys. Lett. 69, 559–562.
215 Clarke, R.H., Connors, R.E., Schaafsma, T.J., Kleibeuker, J.F. and Platenkamp, R.J. (1976) J. Am. Chem. Soc. 98, 3674–3677.
216 Clarke, R.H. and Frank, H.A. (1977) Chem. Phys. Lett. 51, 13–17.
217 Tait, C.D. and Holten, D. (1983) Photobiochem. Photobiophys. 6, 201–209.
218 Lutz, M. (1977) Biochim. Biophys. Acta 460, 408–430.
219 Lutz, M., Brown, J.S. and Remy, R. (1979) CIBA Foundation Symposium 61, pp. 105–125 Excerpta Medica, Amsterdam.
220 Robert, B. and Lutz, M. (1985) Biochim. Biophys. Acta 807, 10–23.
221 Angerhofer, A., Von Schütz, J.U. and Wolf, H.C. (1987) in Progress in Photosynthesis Research (Biggins, J., ed.) Vol 1, pp. 4.427–4.430, Nijhoff, Dordrecht.
222 Clarke, R.H., Hanlon, E.B. and Boxer, S.G. (1982) Chem. Phys. Lett. 89, 41–44.
223 Wright, K.A. and Boxer, S.G. (1980) Biochem. 20, 7546–7556.
224 Kooyman, R.P.H. and Schaafsma, T.J. (1980) J. Mol. Struct. 60, 373–380.
225 DeGroot, A., Evelo, R., Hoff, A.J., DeBeer, R. and Scheer, H. (1985) Chem. Phys. Lett. 118, 48–54.
226 Lin, C.P. (1986) Ph.D. Dissertation, The University of Chicago.
227 Buma, W.J., Evelo, R.G., Groenen, E.J.J., Hoff, A.J., Nan, H.M. and Schmidt, J.S. (1987) Chem. Phys. Lett. 142, 231–236.
228 Lin, C.P., Bowman, M.K. and Norris, J.R. (1985) J. Magn. Reson. 65, 369–374.
229 Norris, J.R. and Gast, P. (1985) J. Photochem. 29, 185–194.
230 Goldstein, H. (1980) Classical Mechanics 2nd ed., p. 147, Addison Wesley, Cambridge, Mass.
231 Norris, J.R., Budil, D.E., Crespi, H.L., Bowman, M.K., Gast, P., Lin, C.P., Chang, C.H. and Schiffer, M. (1985) in Antennas and Reaction Centers of Photosynthetic Bacteria, (Michel-Beyerle, M.E., ed.), p. 147–149, Springer, Berlin.
232 Norris, J.R., Lin, C.P. and Budil, D.E. (1987) J. Chem. Soc, Faraday Trans. I, 83, 13–27.
233 Vredenberg, W.J. and Duysens, L.N.M. (1963) Nature 197, 355–357.
234 Clarke, R.H., Connors, R.E., Norris, J.R. and Thurnauer, M.C. (1975) J. Am. Chem. Soc. 97, 7178–7179.
235 Clarke, R.H. and Connors, R.E. (1976) Chem. Phys. Lett. 42, 69–72.
236 Hoff, A.J. (1976) Biochim. Biophys. Acta 440, 765–771.
237 Hoff, A.J. and H.G. De Vries (1978) Biochim. Biophys. Acta 503, 94–106.
238 den Blanken, H.J., Jongenelis, A.P.J.M. and Hoff, A.J. (1983) Biochim. Biophys. Acta, 725, 472–482.
239 Den Blanken, H.J., Van der Zwet, G.P. and Hoff, A.J. (1982) Biochim. Biophys. Acta 681, 375–382.
240 Beck, J., Von Schütz, J.U. and Wolf, H.C. (1983) Chem. Phys. Lett. 94, 141–146.
241 Angerhofer, A., Von Schütz, J.U. and Wolf, H.C. (1984) Z. Naturforsch. 39c, 1085–1090.
242 Hoff, A.J. and De Vries, H.G. (1981) Isr. J. Chem. 21, 277–282.
243 Platenkamp, R.J., Den Blanken, H.J. and Hoff, A.J. (1980) Chem. Phys. Lett. 76, 35–41.
244 Den Blanken, H.J., Van der Zwet, G.P. and Hoff, A.J. (1982) Chem. Phys. Lett. 85, 335–338.
245 Den Blanken, H.J. and Hoff, A.J. (1982) Biochim. Biophys. Acta 681, 365–374.
246 Den Blanken, H.J. and Hoff, A.J. (1983) Chem. Phys. Lett. 98, 255–262.
247 Boxer, S.G., Middendorf, T.R. and Lockhart, D.J. (1986) FEBS Lett. 200, 237–241.
248 Meech, S.R., Hoff, A.J. and Wiersma, D.A. (1986) Proc. Natl. Acad. Sci. USA 83, 9464–9468.
249 Tang, D., Jankowiak, R., Gillie, J.K., Small, G.J. and Tiede, D.M. (1988) J. Chem. Phys. 92, 4012–4015.
250 Dijkman, J.A., DenBlanken, H.J. and Hoff, A.J. (1988) Isr. J. Chem. 28, 141–148.
251 Shuvalov, V.A. and Parson, W.W. (1981) Biochim. Biophys. Acta 638, 50–59.
252 Mathis, P. and Setif, P. (1981) Isr. J. Chem. 21, 316–320.
253 Den Blanken, H.J., Meiburg, R.F. and Hoff, A.J. (1984) Chem. Phys. Lett. 105, 336–342.
254 Hoff, A.J., Den Blanken, H.J., Vasmel, H. and Meiburg, R.F. (1985) Biochim. Biophys. Acta 806, 389–397.
255 Knapp, E.W., Scherer, P.O.J. and Fischer, S.F. (1986) Biochim. Biophys. Acta 852, 295–305.
256 Scherer, P.O.J. and Fischer, S.F. (1987) Chem. Phys. Lett. 136, 431–435.
257 Scherer, P.O.J. and Fischer, S.F. (1987) Biochim. Biophys. Acta 891, 157–164.
258 Lous, E.J. and Hoff, A.J. (1987) Proc. Natl. Acad. Sci. USA 84, 6147–6151.
259 Davis, M.S., Forman, A., Hanson, L.K., Thornber, J.P., and Fajer, J. (1979) J. Chem. Phys. 83, 3325–3332.
260 Lockhart, D.J. and Boxer, S.G. (1988) Proc. Natl. Acad. Sci. USA 85, 107–111.
261 Lösche, M., Feher, G. and Okamura, M.Y. (1987) Proc. Natl. Acad. Sci. USA 84, 7537–7541.
262 Parson, W.W. and Warschel, A. (1987) J. Am. Chem. Soc. 109, 6152–6163.
263 Angerhofer, A., Von Schütz, J.U. and Wolf, H.C. (1985) Z. Naturforsch. 40c, 379–387.
264 Woodbury, N.T.W. and Parson, W.W. (1984) Biochim. Biophys. Acta 767, 345–361.

265 Schaafsma, T.J., Kleibeuker, J.F., Platenkamp, R.J. and Geese, P. (1975) in Proc. 12th Eur. Congr. on Molecular Spectroscopy, Strasbourg, p. 491–494.
266 Thurnauer, M.C., Katz, J.J. and Norris, J.R. (1975) Proc. Natl. Acad. Sci. USA 79, 3270–3274.
267 Norris, J.R. and Thurnauer, M.C. (1976) Biophys. J. 16a, 224.
268 Closs, G.L. (1969) J. Am. Chem. Soc. 91, 4552–4554.
269 Kaptein, R. and Oosterhoff J.L. (1969) Chem. Phys. Lett. 4, 195–197.
270 Parson, W.W., Clayton, R.K. and Cogdell, R.J. (1975) Biochim. Biophys. Acta 387, 265–278.
271 Fajer, J., Brune, D.C., Davis, M.S., Forman, A. and Spaulding, L.D. (1975) Proc. Natl. Acad. Sci. USA 72, 4956–4960.
272 Boxer, S.G., Chidsey, C.E.D. and Roelofs, M.G. (1982) J. Am. Chem. Soc. 104, 1452–1454.
273 Blankenship, R.E., Schaafsma, T.J. and Parson, W.W. (1977) Biochim. Biophys. Acta 461, 297–305.
274 Werner, H.-J., Schulten, K. and Weller, A. (1978) Biochim. Biophys. Acta 502, 255–268.
275 Brocklehurst, B., Dixon, R.S., Gardy, E.M., Lopata, V.J., Quinn, M.J, Singh, A. and Sargent, F.P. (1974) Chem. Phys. Lett. 28, 361–363.
276 Schulten, K., Staerk, H., Weller, A., Werner, H.-J., Nickel, B. (1976) Z. Phys. Chem. (NF) 101, 371–390.
277 Haberkorn, R. (1977) Chem. Phys. 19, 165–179.
278 Haberkorn, R. (1977) Chem. Phys. 24, 111–117.
279 Salikov, K.M., Buchachenko, A.L., Molin, Yu.N., Sagdeev, R.Z. (1984) Spin Polarization and Magnetic Effects in Radical Reactions (Molin, Yu., ed.) Elsevier, Amsterdam (Akademiai Kiado, Budapest).
280 Hoff, A.J. (1981) Quart. Rev. Biophys. 14, 599–665.
281 Boxer, S.G., Chidsey, C.E.D. and Roelofs, M.G. (1983) Annu. Rev. Phys. Chem. 34, 389–417.
282 Hoff, A.J. (1986) Photochem. Photobiol. 43, 727–745.
283 Lersch, W. and Michel-Beyerle, M.E. (1989) in Advanced EPR in Biology and Biochemistry (Hoff, A.J., ed.), pp. 685–705, Elsevier, Amsterdam.
284 Weller, A., Staerk, H. and Treichel, R. (1984) Farad. Discuss. Chem. Soc. 78, 271–278.
285 Frankevich, E.L. and Kubarev, S.I. (1982) ODMR Spectroscopy: Techniques and Applications to Biophysical Systems (Clarke, R.H., ed.), Ch. 5, Wiley-Interscience, New York.
286 Bowman, M.K., Budil, D.E., Closs, G.L., Kostka, A.G., Wraight, C.A. and Norris, J.R. (1981) Proc. Natl. Acad. Sci. USA 78, 3305–3307.
287 Norris, J.R., Bowman, M.K., Budil, D.E., Tang, J., Wraight, C.A. and Closs, G.L. (1982) Proc. Natl. Acad. Sci. USA 79, 5532–5536.
288 Lersch, W., Lendzian, F., Lang, E., Feick, R., Möbius,, K. and Michel-Beyerle, M.E. (1989) J. Magn. Reson. 82, 143–149.
289 Budil, D.E. (1986) Ph.D. Dissertation, The University of Chicago.
290 Lersch, W. and Michel-Beyerle, M.E. (1983) Chem. Phys. 78, 115–126.
291 Tang, J. and Norris, J.R. (1983) Chem. Phys. Lett. 94, 77–80.
292 Ogrodnik, A., Krüger, H.W., Orthuber, H., Haberkorn, R. and Michel-Beyerle, M.E. (1982) Biophys. J. 39, 91–99.
293 Tang, J. and Norris, J.R. (1982) Chem. Phys. Lett. 92, 136–140.
294 Ogrodnik, A., Remy-Richter, N. and Michel-Beyerle, M.E. (1987) Chem. Phys. Lett. 135, 576–581.
295 Moehl, K.W., Lous, E.J. and Hoff, A.J. (1985) Chem. Phys. Lett. 121, 22–27.
296 Hunter, D.A., Hoff, A.J. and Hore, P.J. (1987) Chem. Phys. Lett. 134, 6–11.
297 Bixon, M., Jortner, J., Michel-Beyerle, M.E., Ogrodnik, A. and Lersch, W. (1987) Chem. Phys. Lett. 140, 626–630.
298 Michel-Beyerle, M.E., Bixon, M. and Jortner, J. (1988) Chem. Phys. Lett. 151, 188–194.
299 Michel-Beyerle, M.E., Plato, M., Deisenhofer, J., Michel, H., Bixon, M. and Jortner, J. (1988) Biochim. Biophys. Acta 932, 52–70.
300 Bixon, M., Michel-Beyerle, M.E. and Jortner, J. (1988) Isr. J. Chem. 28, 155–168.
301 Haberkorn, R., Michel-Beyerle, M.E. and Marcus, R. (1979) Proc. Natl. Acad. Sci. USA 76, 4185–4188.
302 Marcus, R.A. (1987) Chem. Phys. Lett. 133, 471–477.
303 Van Wijk, F.G.H., Gast, P. and Schaafsma, T.J. (1986) Photobiochem. Photobiophys. 11, 95–100.
304 Van Wijk, F.G.H., Gast, P. and Schaafsma, T.J. (1986) FEBS Lett. 206, 238–242.
305 Van Wijk, F.G.H., Beijer, C.B., Gast, P. and Schaafsma, T.J. (1987) Photochem. Photobiol. 46, 1015–1019.
306 Okamura, M.Y., Isaacson, R.A. and Feher, G. (1979) Biochim. Biophys. Acta 546, 394–417.
307 VanWijk, F.G.H. and Schaafsma T.J. (1988) Biochim. Biophys. Acta 936, 236–248.
308 Hore, P.J., Hunter, D.A., Van Wijk,, F.G.H., Schaafsma, T.J. and Hoff, A.J. (1988) Biochim. Biophys. Acta 936, 249–258.
309 Videl, M.H., Sétif, P. and Mathis, P. (1986) Photosynth. Res. 10, 347–354.
310 Chidsey, C.E.D., Kirmaier, C., Holten, D. and Boxer, S.G. (1984) Biochim. Biophys. Acta 766, 424–437.
311 Norris, J.R., Budil, D.E., Kolaczkowski, S.V., Tang, J.H. and Bowman, M.K. (1985) in Antennas and Reaction Centers of Photosynthetic Bacteria (Michel-Beyerle, M.E., ed.), pp. 190–197, Springer, Berlin.
312 Lersch, W., Ogrodnik, A. and Michel-Beyerle, M.E. (1982) Z. Naturforsch. 37a, 1454–1456.
313 Staehelin, L.A. and Arntzen, C.J., Encyclopedia of Plant Physiology: Photosynthesis III, Photosynthetic Membranes and Light Harvesting Systems, Springer, Berlin.
314 Swarthoff, T., Gast, P. and Hoff, A.J. (1981) FEBS Lett. 127, 83–86.
315 Thornber, J.P. (1986) in Encyclopedia of Plant Physiology: Photosynthesis III, Photosynthetic Membranes and Light Harvesting Systems (Staehelin, L.A. and Arntzen, C.J. eds.), pp. 98–142, Springer, Berlin.
316 Rutherford, A.W. and Heathcote, P. (1985) Photosyn. Res. 6, 295–316.
317 Sétif, P. and Rutherford A.W. (1987) in Photosynthesis (Amesz, J., ed.) pp. 63–96, Elsevier, Amsterdam.
318 Andréasson, A.W. and Vänngård, T. (1988) Annu. Rev. Plant Physiol. 39,379–411.
319 Golbeck, J.H. (1989) Biochim. Biophys. Acta 895, 167–204.
320 Wollman, F.-A. (1986) in Encyclopedia of Plant Physiology: Photosynthesis III, Photosynthetic Membranes and Light Harvesting Systems (Staehelin, L.A. and Arntzen, C.J. eds.), pp. 487–495, Springer, Berlin.
321 Fish, L.E., Kuck, U. and Bogorad, L. (1985) J. Biol. Chem. 260, 1413–1421.
322 Shinozaki, K., Ohine, M., Tanaka, M., Wakagusi, T., Hayashida, N. et al. (1986) EMBO J. 5, 2043–2049.
323 Shuvalov, V.A., Ke, B. and Dolan, E. (1979) FEBS Lett. 100, 5–8.
324 Shuvalov, V.A., Dolan, E. and Ke, B. (1979) Proc. Natl. Acad. Sci. USA 76, 770–773.
325 Baltimore, B. and Malkin, R. (1981) Photochem. Photobiol. 31, 485–490.
326 Nuijs, A.M., Shuvalov, V.A., Van Gorkom, H.J., Plijtken, J.J. and Duysens, L.N.M (1986) Biochim. Biophys. Acta 850, 310–318.
327 Swarthoff, T., Gast, P., Amesz, J. and Buisman, H.P. (1982) FEBS Lett. 146, 129–132.
328 Mansfield, R.W. and Evans, M.C.W. (1985) FEBS Lett. 190, 237–241.
329 Fujita, I., Davis, M.S. and Fajer, J. (1978) J. Am. Chem. Soc. 100, 280–282.

330 Furrer, R. and Thurnauer, M.C (1983) FEBS Lett. 153,399–403.
331 Thurnauer, M.C. and Gast, P. (1985) Photobiochem. Photobiophys. 9, 29–38.
332 Thurnauer, M.C., Gast, P., Petersen, J. and Stehlik, D. (1987) in Progress in Photosynthesis Research (Biggins, J., ed.) Vol 1, pp. 4.237–4.240, Nijhoff, Dordrecht.
333 Mansfield, R.W. and Evans, M.C.W (1986) FEBS Lett. 203, 225–229.
334 Iwaki, M. and Itoh, S. (1989) FEBS Lett. 256, 11–19.
335 Itoh, S., Iwaki, M. and Ikagami, I. (1987) Biochim. Biophys. Acta 893, 508–516.
336 Biggins, J. and Mathis, P. (1988) Biochemistry 27, 1494–1500.
337 Sétif, P., Hervo, G. and Mathis, P. (1981) Biochim. Biophys. Acta 638, 257–267.
338 Takahashi, Y., Katoh, S. (1984) Plant Cell Physiol. 25, 785–794.
339 Rutherford, A.W. and Mullet, J.E. (1981) Biochim. Biophys. Acta 635, 225–235.
340 Rutherford, A.W., Mullet, J.E., Paterson, D.R., Robinson, H.H., Arntzen, C.J. and Crofts, A.K. (1981) in Photosynthesis III (Akoyunoglu, G., ed.), pp. 919–928, Balaban Science Service, Philadelphia.
341 Bonnerjea, J. and Evans, M.C.W. (1982) FEBS Lett. 148, 313–316.
342 Gast, P., Swarthoff, T., Ebskamp, F.C.R. and Hoff, A.J. (1983) Biochim. Biophys. Acta 722, 168–175.
343 Sétif, P., Bottin, H. and Mathis, P. (1985) Biochim. Biophys. Acta 808, 112–122.
344 Ikegami, I., Sétif, P. and Mathis, P. (1987) Biochim. Biophys. Acta 894, 414–422.
345 Voznyak, V.M., Ganago, I.B., Moskalenko, A.A. and Elfimov (1980) Biochim. Biophys. Acta 592, 364–368.
346 Sonneveld, A., Duysens, L.N.M. and Moerdijk, A. (1981) Biochim. Biophys. Acta 636, 39–49.
347 Brettel, K. and Sétif, P. (1987) Biochim. Biophys. Acta 893, 109–114.
348 Thurnauer, M.C., Bowman, M.K. and Norris, J. (1979) FEBS Lett. 100, 309–312.
349 McIntosh, A.R., Bolton, J.R., Manikowski, H., Wons, S.K. and Taylor, C.P.S. (1979) Biochem. Biophys. Res. Commun. 87, 605–612.
350 McCracken, J.L., Frank, H.A. and Sauer, K. (1982) Biochim. Biophys. Acta 679, 156–168.
351 Hoff, A.J. (1984) Quart. Rev. Biophys. 17, 153–282.
352 Hore, P.J., Hunter, D.A., McKie, C.D. and Hoff, A.J. (1987) Chem. Phys. Lett. 137, 495–500.
353 Stehlik, D., Bock, C.H. and Petersen, J. (1989) J. Phys. Chem. 93, 1612–1619.
354 Sétif, P., Mathis, P. and Vänngård, T. (1984) Biochim. Biophys. Acta 767, 404–414.
355 Sétif, P. and Bottin, H. (1989) Biochem. 28, 2689–2697.
356 Sétif, P., Quaegenbeur, J.P. and Mathis, P. (1982) Biochim. Biophys. Acta 681, 345–353.
357 Hoff, A.J. and van der Waals, J.H. (1976) Biochim. Biophys. Acta 423, 615–620.
358 Clarke, R.H., Jagannathan, S.P. and Leenstra, W.R. (1980) Photochem. Photobiol. 32, 805–808.
359 Schaafsma, T.J., Searle, G.F.W. and Koehorst, R.B.M. (1982) J. Mol. Struct. 79, 461–464.
360 Den Blanken, H.J. and Hoff, A.J. (1983) Biochim. Biophys. Acta 724, 52–61.
361 Mathis, P., Saar, K. and Remy, R. (1978) FEBS Lett. 88, 275–278.
362 Warden, J.T. and Golbeck, J.H. (1987) Biochim. Biophys. Acta 891, 286–292.
363 Høj, P.B. and Møller, B.L. (1986) J. Biol. Chem. 261, 14292–14300.
364 Nechushtai, R., Nelson, N., Gonen, O. and Levanon, H. (1985) Biochim. Biophys. Acta 807, 35–43.
365 McClean, M.B. and Sauer, K. (1982) Biochim. Biophys. Acta 679, 384–392.
366 Van Brakel, G.H. (1982) Ph.D. Thesis, Agricultural University of the Netherlands, Wageningen.
367 Hearst, J.E. (1986), in Ref. 313, pp. 381–389.
368 Michel, H. and Deisenhofer, J. (1986) in Ref. 313, pp. 371–381.
369 Diner, B.A. (1986) in Ref. 313, pp. 422–436.
370 Nanba, O. and Satoh, K. (1987) Proc. Natl. Acad. Sci. USA 84, 109–112.
371 Klimov, V.V., Klevanik, A.V. and Shuvalov, V.A. (1977) FEBS Lett. 82, 183–186.
372 Klimov, V.V., Dolan, E., Shaw, E.R. and Ke, B. (1980) Proc. Natl. Acad. Sci. USA 77, 7227–7231.
373 Bouges-Bocquet, B. (1980) Biochim. Biophys. Acta 594, 85–103.
374 Rutherford, A.W. and Zimmerman, J.L. (1984) Biochim. Biophys. Acta 767, 168–175.
375 Rutherford, A.W. (1987) in Progress in Photosynthesis Research (Biggins, J., ed.) Vol 1, pp. 4.277–4.283, Nijhoff, Dordrecht.
376 Zurawski, G., Bohnert, H.J., Whitfeld, P.R. and Bottomley W. (1982) Proc. Natl. Acad. Sci. USA 79, 7699–7703.
377 Rochaix, J.-D., Dron, M., Rahire, M., Malnoe, P. (1984) Plant Mol. Biol. 3, 363–370.
378 Rasmussen, O.F., Bookjans, G., Stremmann, B.M., Henningsen, K.W. (1984) Plant Mol. Biol. 3, 363–370.
379 Trebst., A. and Draber, W. (1986) Photosynth. Res. 10, 381–392.
380 Sayre, R.T., Andersson, B. and Bogorad, L. (1986) Cell 47, 601–608.
381 Deisenhofer, J., Michel, H. and Huber, R. (1985) Trends Biochem. Sci. 10, 243–248.
382 Trebst, A. (1986) Z. Naturforsch. 41c, 240–245.
383 Nuijs, A.M., van Gorkom, H.J., Plijter, J.J., Duysens, L.N.M (1986) Biochim. Biophys. Acta 848, 167–175.
384 Danielius, V.R., Satoh, K., van Kan, P.J., Plijter, J.J., Nuijs, A.M. and van Gorkom, H.J. (1987) FEBS Lett. 213, 214–4.
385 Takahashi, Y., Hansson, Ö., Mathis, P., Satoh, K. (1987) Biochim. Biophys. Acta 893, 49–59.
386 Wasielewski, M.R., Johnson, D.G., Siebert, M. and Govindjee (1989) Proc. Natl. Acad. Sci. USA 86, 528–524.
387 Hansson, Ö., Duranton, J., Mathis, P. (1988) Biochim. Biophys. Acta 932, 91–96.
388 Rutherford, A.W., Mullet, J.E. and Crofts, A.R. (1981) FEBS Lett. 123, 235–237.
389 Okamura, M.Y., Satoh, K., Isaacson, R.A. and Feher, G. (1987) in Progress in Photosynthesis Research, Vol. I (Biggins, J., ed.) p. 4.379, Nijhoff, Dordrecht.
390 Telfer, A., Barber, J. and Evans, M.C.W. (1988) 232, 209–213.
391 Frank, H.A., Hansson, Ö. and Mathis, P. (1989) Photosynth. Res. 26, 279–289.
392 Ghanotakis, D.F., De Paula, J.C., Demetriou, D.M., Bowlley, N.R., Petersen, J., Babcock, G.T. and Yocum, C.F. (1989) Biochim. Biophys. Acta 974,44–53.
393 Demetriou, C., Lockett, C.J. and Nugent, J.H.A. (1988) Biochem. J. 252, 921–4.
394 Rademaker, H., Hoff, A.J. and Duysens, L.N.M (1979) Biochim. Biophys. Acta 546, 249–255.
395 Sonneveld, A., Duysens, L.N.M and Moerdijk, A. (1980) Proc. Natl. Acad. Sci. USA 77, 5889–5893.
396 Kolesnikova, L., Triebel, M.M. and Frankevich, Yu. L. (1982) Biophysics 27, 581–589.
397 Hoff, A.J., Rademaker, H., Van Grondelle. R. and Duysens, L.N.M. (1977) Biochim. Biophys. Acta 460, 547–554.
398 Rutherford, A.W. (1986) Biochem. Soc. Trans. 14, 15–17.
399 Den Blanken, H.J., Hoff, A.J., Jongenelis, A.P.J.H. and Diner, B.A. (1983) FEBS Lett. 157, 21–27.
400 Rutherford, A.W., Satoh, K. and Mathis, P. (1983) Biophys. J. 41, 40a.

401 Rutherford, A.W. (1983) in The Oxygen Evolving System of Photosynthesis (Inoue, Y., Crofts, A.R., Govindjee, Morata, N., Renger, G. and Satoh, K., eds.), pp. 63–69, Academic Press, Tokyo.
402 Demetriou, C., Lockett, C.J., Bowden, S.J. and Nugent, J.H.A. (1989) Proc. Intl. Congress Photosynthesis, Stockholm.
403 Schatz, G.H., Brock, H. and Holzwarth, A.R. (1987) Proc. Natl. Acad. Sci. USA 84, 8414–8418.
404 Schatz, G.H., Brock, H. and Holzwarth, A.R. (1988) Biophys. J. 54, 397–405.
405 Schlodder, E. and Brettel, K. (1988) Biochim. Biophys. Acta 933, 22–34.
406 Rutherford, A.W. (1985) Biochim. Biophys. Acta 807, 189–201.
407 Rutherford, A.W. and Acker, S. (1986) Biophys. J. 49, 101–102.
408 Krasnovsky, Jr., A.A. and Semenova, A.N. (1981) Photobiochem. Photobiophys. 3, 11–18.
409 Hiromitsu, I. and Kevan, L. (1988) J. Phys. Chem. 92, 2770–2773.
410 Clarke, R.H. and Hanlon, E.B. (1985) J. Chem. Phys. 82, 5275–5282.
411 Hala, J., Searle, G.F.W., Schaafsma, T.J., VanHoek, A., Pancoska, P., Blaha, K. and Vacek, K. (1986) Photochem. Photobiol. 44, 527–534.
412 Kaufmann, K.J. and Wasielewski, M.R. (1981) Advan. Chem. Phys. 47, 579–626.
413 Wasielewski, M.R. (1982) in Molecular Biology, Biochemistry and Biophysics, Vol. 35 (Fong, F.K., ed.), pp. 234–276, Springer, Berlin.
414 Gückel, F., Schweitzer, D., Collman, J.P., Bencosme, S., Evitt, E and Sessler, J. (1984) Chem. Phys. 86, 161–172.
415 Bucks, R.R. and Boxer, S.G. (1982) J. Am. Chem. Soc. 104, 340–343.
416 Periasamy, N. and Linschitz, H. (1979) J. Am. Chem. Soc. 101, 1056–1057.
417 Periasamy, N., Linschitz, H., Closs, G.L. and Boxer, S.G. (1978) Proc. Natl. Acad. Sci. USA 75, 2563–2566.
418 Litteken, S.R. (1983) Ph. D. Dissertation, University of Illinois at Urbana-Champaign.
419 Benthem, L., Koehorst, R.B.M. and Schaafsma, T.J. (1982) J. Mol. Struct. 79, 455–460.
420 Chandrashekar, T.K. and Van Willigen, H. (1983) J. Am. Chem. Soc. 105, 6323–6324.
421 Chandrashekar, T.K. and Van Willigen, H. (1984) Chem. Phys. Lett. 106, 237–241.
422 Chandrashekar, T.K., Van Willigen, H. and Ebersole, M.H. (1984) J. Phys. Chem. 88, 4326–4332.
423 Van Willigen, H., Das, U., Ojadi, E. and Linschitz, H. (1985) J. Am. Chem. Soc. 107, 7784–7785.
424 Chandrashekar, T.K., Van Willigen, H. and Ebersole, M.H. (1985) J. Phys. Chem. 89, 3453–3459.
425 Hofstra, U., Koehorst, R.B.M. and Schaafsma, T.J. (1986) Chem. Phys. Lett. 130, 555–559.
426 Leland, B.A., Joran, A.D., Felker, P.M., Hopfield, J.J., Zewail, A.H. and Dervan, P.B. (1985) J. Phys. Chem. 89, 5571–5573.
427 Harrison, R.J., Pearce, B., Beddard, G.S., Cowan, J.A., and Sanders, J.K.M. (1987) Chem. Phys. 116, 429–448.
428 Wasielewski, M.R., Johnson, D.G., Svec, W.A., Kersey, K.M. and Minsek, D.W. (1988) J. Am. Chem. Soc. 110, 7219–7221.
429 Hofstra, U., Schaafsma, T.J., Sanders, G.M., Van Dijk, M., Van der Plas, H.C., Johnson, D.G. and Wasielewski, M.R. (1988) Chem. Phys. Lett. 151, 169–175.
430 Dirks, G., Moore, A.L., Moore, T.A. and Gust, D. (1980) Photochem. Photobiol. 32, 277–280.
431 Moore, A.L., Dirks, G., Gust, D. and Moore, T.A. (1980) Photochem. Photobiol. 32, 691–695.
432 Moore, A.L., Joy, A., Tom, R., Gust, D., Moore, T.A., Bensasson, R.V. and Land, E.J. (1982) Science 216, 982–984.
433 Gust, D., Moore, T.A., Bensasson, R.V., Mathis, P., Land, E.J., Chachaty, C., Moore, A.L., Liddell, P.A. and Nemeth, G.A. (1985) J. Am. Chem. Soc. 107, 3631–3640.
434 Liddell, P.A., Nemeth, G.A., Lehman, W.R., Joy, A.M., Moore, A.L., Bensasson, R.V., Moore, T.A. and Gust, D. (1982) Photochem. Photobiol. 36, 641–645.
435 Wasielewski, M.R., Liddell, P.A., Barrett, D., Moore, T.A. and Gust, D. (1986) Nature 322, 570–572.
436 Frank, H.A., Chadwick, B.W., Oh, J.J., Gust, D., Moore, T.A., Liddell, P.A., Moore, A.L., Makings, L.R. and Cogdell, R.J. (1987) Biochim. Biophys. Acta 892, 253–263.
437 Wacker, T., Gad'on, N., Becker, A., Maentele, W., Kreutz, W., Drews, G. and Welte, W. (1986) FEBS Lett. 197, 267–273.
438 Allen, J.P., Theiler, R. and Feher, G. (1985) in Antennas and Reaction Centers of Photosynthetic Bacteria, (Michel-Beyerle, M.E., ed.), pp. 82–84, Springer, Berlin.
439 Cogdell, R.J., Wooley, K., Mackenzie, R.C., Lindsay, J.G. and Michel, H. (1985) in Antennas and Reaction Centers of Photosynthetic Bacteria (Michel-Beyerle, M.E., ed.), pp. 85–87, Springer, Berlin.
440 Ford, R.C., Picot, D. and Garavito, R.M. (1987) EMBO J. 6, 1581–1586.
441 Witt, I., Witt, H.T., Gerken, S., Saenger, W., Dekker, J.P. and Rögner, M. (1987) FEBS Lett. 221, 260–264.
442 Ford, R.C., Pauptit, R.A. and Holzenberg, A. (1988) FEBS Lett. 197, 385–389.
443 Bylina, E.J., Ismail, S. and Youvan, D.C. (1986) Plasmid, 16, 175–181.
444 Bylina, E.J. and Youvan, D.C. (1988) Proc. Natl. Acad. Sci. USA 85, 7226–7230.